LAND COVER CLASSIFICATION ACCURACY FROM ELECTRO-OPTICAL, X, C, AND L-BAND SYNTHETIC APERTURE RADAR DATA FUSION

by

Mark Gregory Hammann

A Dissertation
Submitted to the
Graduate Faculty
of
George Mason University
in Partial Fulfillment of
The Requirements for the Degree
of
Doctor of Philosophy
Earth Systems and Geoinformation Science

Committee:

_____	Dr. Barry Haack, Dissertation Director
_____	Dr. Donglian Sun, Committee Member
_____	Dr. Paul L. Delamater, Committee Member
_____	Dr. Michael Gilmore, Committee Member
_____	Dr. Anthony Stefanidis, Department Chair
_____	Dr. Donna M. Fox, Associate Dean, Office of Student Affairs & Special Programs, College of Science
_____	Dr. Peggy Agouris, Dean, College of Science
Date: _____	Fall Semester 2016 George Mason University Fairfax, VA

Land Cover Classification Accuracy from Electro-Optical, X, C, and L-Band Synthetic Aperture Radar Data Fusion

A Dissertation submitted in partial fulfillment of the requirements for the degree of Doctor of Philosophy at George Mason University

by

Mark Gregory Hammann
Master of Science
Oregon State University, 1981
Bachelor of Art
Whittier College, 1978

Director: Barry Haack, Professor
Department of Geography and Geoinformation Science

Fall Semester 2016
George Mason University
Fairfax, VA

DEDICATION

This dissertation is dedicated to my loving wife and best friend, Maria Elena, and my children: Mariana, Mark Christian, Teresa Marie, and William Gregory, who gave me the love and support to find the time and effort to take on and complete this endevour.

To my parents, Dr. William C. Hammann, Ph.D. and Mrs. Audrey K. Hammann who taught me the value of hard work and perseverance.

ACKNOWLEDGEMENTS

I would like to thank my dissertation chairman, Dr. Barry Haack, for his excellent instruction, guidance, patience, and for introducing me to SAR, data fusion, and land cover classification. I thank my committee members who were of invaluable assistance: Dr. Donglian Sun, Dr. Paul Delamater, Dr. Michael Gilmore, Dr. Richard Diecchio (retired), and Dr. Allan Falconer (retired). Special thanks goes to the Fenwick Library and their staff for their outstanding service and online resources which I still find amazing compared to the days of manual catelogue searches. The department of Geography and Geoinformation Science is thanked for the availability of the software licenses for ENVI/IDL and ArcGIS used in this dissertation. The support by ESA of the NEST project is appeciated. The USDA and GMU are thanked for the CropScape WWW project, as is Dr. Claire Boryan for her assistance. I acknowledge the excellent calibre of the GMU-GSS faculty who supported my coursework. Tuition support from GeoEye Inc., DigitalGlobe Inc., and EarthSightful Solutions LLC is acknowledged and appreciated.

DATA ACKNOWLEDGEMENTS

GeoEye-1 – Provided by GeoEye Inc. (now DigitalGlobe Inc.).

PALSAR - The Alaska Space Facility, under sponsorship from NASA, provided the PALSAR Imagery through grants awarded to Dr. Barry Haack (Brazil and California, CA) and Greg Hammann (Sudan).

RADARSAT-2 - Data over Wad Medani, Sudan were provided to Dr. B. Haack by the Canadian Space Agency under project 3126 of the Science and Operational Application Research (SOAR) for the RADARSAT-2 program.

Data over Campinas, Brazil and California were graciously provided to the author for purposes of this dissertation by MDA Geospatial Services Inc. Special thanks go to Mr. Edward Lau at MDA who facilitated this award.

RapidEye – Data were provided by RapidEye AG (RapidEye was purchased by Planet in 2015) through a cooperative research agreement between RapidEye and GeoEye. Special thanks to Mr. Clint Graumann.

TerraSAR-X – Data were purchased by GeoEye from Astrium Inc. (now Airbus, Inc.) and provided to the author by GeoEye Inc. (now DigitalGlobe Inc.).

WorldView-2 – Provided by DigitalGlobe Inc.

TABLE OF CONTENTS

Page
List of Tables ix
List of Figures xiii
List of Abbreviations and Symbols xvi
Abstract xviii
1 Introduction 1
1.1 Background 1
1.2 Dissertation Scope 2
1.3 Organization 3
2 Literature Review 5
2.1 Remote Sensing Basics 5
2.2 Atmospheric Compensation 9
2.3 SAR Basics 10
2.4 Speckle Reduction 12
2.5 Texture Measures 14
2.6 EO-SAR Fusion 17
3 Methodology 19
3.1 Sensor Specifications 19
3.1.1 GeoEye-1 19
3.1.2 WorldView-2 20
3.1.3 RapidEye 21
3.1.4 PALSAR 23
3.1.5 RADARSAT-2 23
3.1.6 TerraSAR-X 25
3.2 Study Sites 25
3.2.1 Wad Medani, Sudan 26
3.2.2 Campinas, Brazil 28

3.2.3 Fresno and Kings Counties, California, USA 29
3.3 Climate 30
3.4 Data Sources 33
3.5 Image Pre-Processing 38
3.5.1 Overview 38
3.5.2 Radiometric Calibrations 41
3.5.3 Geometric Calibration and Orthorectification 41
3.5.4 Resampling 41
3.5.5 Image-to-Image Registration 42
3.5.6 SAR Speckle Reduction (Despeckling) 43
3.5.7 Texture Derivation 43
3.5.8 Image Fusion in Layer Stacks 44
3.6 Classification 44
3.6.1 Feature Class Definition 44
3.6.2 Signature Extraction from Training Areas 47
3.6.3 Supervised Classification 48
3.6.4 Ground Truth 48
3.6.5 Accuracy Assessments 49
4 Results 51
4.1 Wad Medani, Sudan 51
4.1.1 Test Series 51
4.1.2 Spectral Signatures 55
4.1.3 Training and Ground Truth 55
4.1.4 Decision Rule Evaluation 59
4.1.5 Classification Accuracy 59
4.1.6 Best Band Combination per Class 75
4.1.7 Summary 77
4.2 Campinas, Brazil 80
4.2.1 Test Series 80
4.2.2 Spectral Signatures 83
4.2.3 Training and Ground Truth 84
4.2.4 Classification Accuracy 86

4.2.5 Best Band Combination per Class 100
4.2.6 Summary 102
4.3 Fresno and Kings Counties, California, USA 105
4.3.1 Test Series 105
4.3.2 Spectral Signatures 108
4.3.3 Training and Ground Truth 108
4.3.4 Classification Accuracy 109
4.3.5 Best Band Combination per Class 124
4.3.6 Summary 132
5 Discussion and Future Research 135
5.1 Discussion 135
5.2 Future Research 143
5.3 Conclusions 145
References 147

LIST OF TABLES

Table **Page**
Table 1. Comparison between EO and SAR imaging satellites. 12
Table 2. Spectral bands for RapidEye, GeoEye-1, and WorldView-2. 22
Table 3. Data sources for Wad Medani, Sudan. Blue highlight is for the GT image. 34
Table 4. Data sources for Campinas, Brazil. Blue highlight is for the GT image. 34
Table 5. Data sources for Fresno-Kings Counties, USA. Blue highlight is for the GT image. 34
Table 6. Original spatial resolution of data sources (in meters) from different satellites for the three study areas and resampled pixel size for the fused layer stack. 42
Table 7. Land Cover classes for Wad Medani, Sudan. 45
Table 8. Land Cover classes for Fresno-Kings Counties, CA, USA. 48
Table 9. Classification Tests Band Packages for Wad Medani, Sudan. 52
Table 10. Test Matrix for Wad Medani, Sudan. 53
Table 11. Training ROI mean and standard deviation for each of the nine classes in Wad Medani. 56
Table 12. Number of pixels and area for training and GT for each land cover class in Wad Medani, Sudan. 58
Table 13. User's and producer's accuracy for four different decision rules using all 44 bands for the Wad Medani study site. 59
Table 14. EO baseline error matrix for the for Wad Medani, Sudan. 60
Table 15. Error matrix result summary for Wad Medani, Sudan using EO imagery. 60
Table 16. Classification results for Wad Medani, Sudan using EO imagery and SAR despeckled HH. 63
Table 17. Classification results for Wad Medani, Sudan using EO imagery, SAR despeckled HH, and three texture variance kernels, per SAR band. 64
Table 18. Classification results for Wad Medani, Sudan using EO imagery, SAR despeckled HH, and three texture variance kernels, per combinations of SAR bands. 65
Table 19. Classification results for Wad Medani, Sudan using EO imagery, SAR despeckled HH, and three texture variance kernels, and all SAR bands. 66
Table 20. Classification results for Wad Medani, Sudan using EO imagery, SAR despeckled HH, and three texture GLCM kernels, per SAR band. 67
Table 21. Classification results for Wad Medani, Sudan using EO imagery, SAR despeckled HH and three texture GLCM kernels, for combinations of SAR bands. 68
Table 22. Classification results for Wad Medani, Sudan using EO imagery, SAR despeckled HH, and three texture GLCM kernels, for all SAR bands together. 69

Table 23. Classification results for Wad Medani, Sudan using EO imagery, SAR despeckled HH, and three texture GLCM kernels, and texture variance per SAR band.. 70
Table 24. Classification results for Wad Medani, Sudan using EO imagery, SAR despeckled HH, and three texture GLCM kernels, and variance for combinations of SAR bands. 71
Table 25. Classification results for Wad Medani, Sudan using EO imagery, SAR despeckled HH, and three texture GLCM kernels, and variance for all SAR bands together. 72
Table 26. Classification results for Wad Medani, Sudan using SAR despeckled HH, and three texture GLCM kernels, and texture variance per SAR band, band combinations and all SAR bands. All texture measures were combined. 73
Table 27. Classification results for Wad Medani, Sudan using EO imagery, SAR despeckled HH and three combined kernels for variance and GLCM texture, per GLCM texture measures separately per SAR band. 74
Table 28. Classification results for Wad Medani, Sudan using EO imagery, SAR despeckled HH and three combined kernels for variance and GLCM texture, per GLCM texture measures separately per SAR band combinations. 75
Table 29. Classification results for tests 7h & 5h for Wad Medani, Sudan using EO imagery, SAR despeckled HH, and three combined kernels for variance and GLCM texture, per combinations of GLCM texture measures. (C=Contrast, E=Entropy, R=Correlation) 76
Table 30. User's accuracy for Wad Medani , Sudan per land cover class and data type using SAR or EO data alone. 77
Table 31. Summary of the classification results for each test series for Wad Medani, Sudan 78
Table 32. Error matrix for the best classification for Wad Medani, Sudan, using EO, despeckled SAR HH, CE, and XCL bands. 79
Table 33. Classification tests band packages for Campinas, Brazil. 81
Table 34. Campinas test matrix with EO, and EO+SAR images for Campinas, Brazil.. 82
Table 35. Campinas test matrix for SAR only images for Campinas, Brazil. 83
Table 36. Training ROI mean and standard deviation of the for each of the five classes in Campinas, Brazil. 83
Table 37. Number of pixels and area for training and GT polygons for each land cover class at Campinas, Brazil. 85
Table 38. EO baseline error matrix for the land cover classification at Campinas, Brazil. 87
Table 39. Classification results comparison for Campinas, Brazil, using EO + SAR despeckled HH. 88
Table 40. Error matrix for Campinas, Brazil using EO + X, C, and L-band SAR despeckled HH. 89
Table 41. Classification results comparison for Campinas, Brazil, using EO + SAR despeckled HH + 21x21 variance. 90
Table 42. Error matrix for Campinas, Brazil, using EO + X, C, and L-band SAR despeckled HH and variance imagery. 91

Table 43. Classification results comparison for Campinas, Brazil, using EO + SAR despeckled HH + entropy. 91
Table 44. Error matrix for Campinas, Brazil, using EO + X-band SAR despeckled HH + entropy. 92
Table 45. Classification results comparison for Campinas, Brazil, using EO + SAR despeckled HH + 21x21 correlation. 93
Table 46. Error matrix for Campinas, Brazil, using EO + L-band SAR despeckled HH + correlation. 93
Table 47. Classification results comparison for Campinas, Brazil, using EO + SAR despeckled HH + 21x21 entropy and 21x21 correlation. 94
Table 48. Error Matrix for Campinas, Brazil, using EO + X-band SAR despeckled HH + entropy and correlation. 94
Table 49. Classification results comparison for Campinas, Brazil, using EO + SAR despeckled HH + variance and entropy. 95
Table 50. Error matrix for Campinas, Brazil, using EO + X-band SAR despeckled HH + variance and entropy. 95
Table 51. Classification results comparison for Campinas, Brazil, using EO + SAR despeckled HH + variance and correlation. 96
Table 52. Error matrix for Campinas, Brazil, using EO + L-band SAR despeckled HH + variance and correlation. 96
Table 53. Classification results comparison for Campinas, Brazil, using EO + SAR despeckled HH + variance, entropy, and correlation. 97
Table 54. Error matrix for Campinas, Brazil, using EO + X-band SAR despeckled HH + variance, entropy and correlation. 98
Table 55. Classification results comparison for Campinas, Brazil, using SAR despeckled HH + variance, entropy and correlation. 99
Table 56. Error matrix for Campinas, Brazil, using SAR despeckled HH + X-band variance, entropy, and correlation. 100
Table 57. Band combinations with the best producer's or user's classification accuracy for EO+SAR (left) and SAR alone (right) tests for Campinas, Brazil. 102
Table 58. Comparison of the best overall accuracy results from test series 1-6 with EO and fusion with SAR data for Campinas, Brazil. 103
Table 59. Classification tests band combinations for Fresno-Kings Counties, USA. 106
Table 60. Classification test matrix for Fresno-Kings Counties, USA. 107
Table 61. Training ROI mean and standard deviation for Fresno-Kings Counties, USA. 109
Table 62. Number of pixels and area for training and GT polygons for each land cover class for Fresno-Kings Counties, USA 110
Table 63. EO baseline classification error matrix for Fresno-Kings Counties, USA. 111
Table 64. Classification fitness ranking using EO for Fresno-Kings Counties, USA. ... 112
Table 65. Comparison of classification results with EO + SAR for Fresno-Kings Counties, USA. 114
Table 66. Error matrix for Fresno-Kings Counties,, USA, using EO + SAR despeckled HH L-band. 115

Table 67. Comparison of FI for Fresno-Kings Counties,, USA, for classifications with EO and SAR despeckled HH. Classes are sorted by FI for each test. 115
Table 68. Comparison of classification results with EO + SAR + 21x21 Variance, for Fresno-Kings Counties, USA..... 116
Table 69. Comparison of classification results with EO + SAR + 21x21 entropy for Fresno-Kings Counties, USA..... 118
Table 70. Comparison of classification results with EO + SAR + 21x21 variance and entropy for Fresno-Kings Counties, USA..... 119
Table 71. Error matrix for the classification with EO + X, C, and L-band SAR + 21x21 variance and entropy for Fresno-Kings Counties, USA. 120
Table 72. Comparison of classification results with SAR + 21x21 variance and entropy for Fresno-Kings Counties, USA. 120
Table 73. Error matrix with C-band SAR + 21x21 entropy for Fresno-Kings Counties, USA..... 122
Table 74. Error matrix with X, C, and L-band SAR + 21x21 variance and entropy for Fresno-Kings Counties, USA..... 122
Table 75. Best band combinations for each class based on the FI using EO+SAR and SAR alone for Fresno-Kings Counties, USA. The table is sorted on FI. 124
Table 76. Best band combinations for each test based on the overall accuracy using EO+SAR and SAR alone for Fresno-Kings Counties, USA. 134
Table 77. Study site comparison of the best band combinations for each test based on the overall accuracy using EO, EO+SAR, and SAR alone..... 136
Table 78. Study site comparison of overall accuracy for different texture measures..... 140

LIST OF FIGURES

Figure **Page**

Figure 1. The Electromagnetic Spectrum with details on visible and RADAR bands. By Phillip Ronan; used under CC Attribution-Share Alike 3.0 Unported license. Modified by Hammann, added RADAR bands and some annotations were deleted. 6
Figure 2. The Sun's radiation from the Top of the Atmosphere, and the Earth's surface at sea level. By Robert A. Rohde used under the CC Attribution-Share Alike 3.0 Unported license. 8
Figure 3. Energy flow profile of light from the Sun to the Earth and back to the satellite. By UCAR/COMET used under the UCAR/COMET license. Modified by Hammann, added the satellite and the energy path to the satellite. 8
Figure 4. Forest penetration is stronger with longer wavelengths. By USGS (Palma, 2011); used under the 'Fair Use' doctrine. The graphics were reordered to show increasing forest penetration by Hammann. 13
Figure 5. SAR geometry terminology. By USGS (Palma, 2011); used under the 'Fair Use' doctrine. 14
Figure 6. SAR geometric distortions with slant range. By Halounová (2009); used under the 'Fair Use' doctrine. 15
Figure 7. Spectral response of the GeoEye-1 camera and detector array. Hammann, Unpublished. 20
Figure 8. Spectral response of the WorldView-2 camera and detector array. Hammann, Unpublished. 21
Figure 9. Spectral response of the RapidEye camera and detector array. Hammann, Unpublished. 22
Figure 10. PALSAR scanning modes. Source: Japan Space Systems (2012); used under the 'Fair Use' doctrine. 24
Figure 11. RADARSAT-2 scanning modes. Source: MDA (2011); used under the 'Fair Use' doctrine. 24
Figure 12. TerraSAR-X scanning modes. Source: InfoTerra (2009); used under the 'Fair Use' doctrine. 25
Figure 13. Left - Location of Sudan, the state of Al Jazirah, Wad Medani City, rivers. Right: settlements in Sudan. Hammann, unpublished. 27
Figure 14. Natural color image of the terrain around Wad Medani, Sudan. Source: Google Earth. 27
Figure 15. Map of South America highlighting Brazil and the state of São Paolo. The insert shows the location of Campinas, the study area. Hammann, unpublished. 28

Figure 16. Natural color image of the terrain around Campinas, Brazil. Source: Google Earth. 29
Figure 17. Location of the study AOI in California, crossing Fresno-Kings Counties, USA. Hammann, unpublished. 30
Figure 18. Natural color image of the terrain around Fresno-Kings Counties, USA. The green line is the county border. Source: Google Earth. 31
Figure 19. Average climate indicators for Fresno, CA, Campinas, Brazil, and Wad Medani, Sudan. a) Mean monthly high and low temperatures; b) monthly mean precipitation. Data are consolidated from Weather.com (2016) and Weather-and-Climate.com (2016). 33
Figure 20. Overlap AOI in Wad Medani, Sudan. Hammann, unpublished. 35
Figure 21. RapidEye EO natural color image of the common AOI in Wad Medani, Sudan. RGB: Red, Green, Blue bands. Hammann, unpublished. 36
Figure 22. Overlap AOI in Campinas, Brazil. Hammann, unpublished. 37
Figure 23. Landsat 5 TM EO natural color image of the common AOI in Campinas Brazil; RGB: Red, Green, Blue bands. The Campinas municipality is shown with a color infrared composite using Landsat 5 TM; RGB: NIR, Red, Green. Hammann, unpublished. 38
Figure 24. Overlap AOI in Fresno-Kings Counties, USA. Hammann, unpublished. 39
Figure 25. RapidEye EO natural color image of the common AOI in Fresno-Kings Counties, USA. RGB: Red, Green, Blue bands. The green line is the county boundary. Hammann, unpublished. 40
Figure 26. Major crops in the common AOI of study area in Fresno-Kings Counties. From data in the 2010 CDL; Hammann, unpublished. 47
Figure 27. Cropland Data Layer for the common AOI of study area in Fresno-Kings Counties, USA. Hammann, unpublished. 50
Figure 28. Mean spectral signatures for the 44 bands for nine classes in Wad Medani, Sudan 57
Figure 29. Training ROI's for the nine land cover classes over the RapidEye NIR band from the image stack over Wad Medani, Sudan. Scene width ~ 30 km. 57
Figure 30. GT ROI's for nine land cover classes over the RapidEye NIR band from the image stack over Wad Medani, Sudan. Scene width ~ 30 km. 58
Figure 31. Land cover classification thematic map for Wad Medani, Sudan using EO imagery. Scene width ~ 30 km. 61
Figure 32. Best land cover classification thematic map for Wad Medani, Sudan using EO + SAR despeckled HH + SAR texture. Scene width ~ 30 km. 79
Figure 33. Mean spectral signatures for the 17 bands for five land cover classes for Campinas, Brazil. 84
Figure 34. Training ROI's over the NIR band image in the image stack for Campinas, Brazil for the five land cover classes. Scene width ~ 55 km. 85
Figure 35. GT ROI's over the NIR band image for Campinas, Brazil. Scene width ~ 55 km. 86
Figure 36. Classification image using only EO bands for Campinas, Brazil. Scene width ~ 55 km. 88

Figure 37. Overall accuracy comparison for test fusing EO bands with SAR for Campinas, Brazil. 104
Figure 38. Overall accuracy comparison for SAR only tests for Campinas, Brazil. 104
Figure 39. Classification map from EO+X-band despeckled HH, SAR variance, entropy, and correlation for Campinas, Brazil. Scene width ~ 55 km. 105
Figure 40. Mean spectral signatures for 11 classes in Fresno-Kings Counties, USA. ... 108
Figure 41. a) Training ROI's, and b) GT ROI's for Fresno-Kings Counties, USA. Scene width ~ 25 km. 110
Figure 42. Land cover classification thematic map using EO imagery for Fresno-Kings Counties, USA. Overall accuracy 64.4%. Scene width ~ 25 km. 113
Figure 43. Land cover classification using EO, X, C, and L-band SAR and 21x21 variance and entropy texture measures for Fresno-Kings Counties, USA. Overall accuracy was 71.7%. Test 5g. Scene width ~ 25 km. 121
Figure 44. Land cover classification using X, C, and L-band SAR and 21x21 variance and entropy texture measures for Fresno-Kings Counties, USA. Overall accuracy was 45.7%.Test 6p. Scene width ~ 25 km. 123
Figure 45. FI for alfalfa using different band combinations for Fresno-Kings Counties, USA..... 126
Figure 46. FI for water using different band combinations for Fresno-Kings Counties, USA..... 126
Figure 47. FI for pistachios using different band combinations for Fresno-Kings Counties, USA. 127
Figure 48. FI for almonds using different band combinations for Fresno-Kings Counties, USA..... 127
Figure 49. FI for developed areas using different band combinations for Fresno-Kings Counties, USA. 128
Figure 50. FI for winter wheat using different band combinations for Fresno-Kings Counties, USA. 128
Figure 51. FI for fallow using different band combinations for Fresno-Kings Counties, USA..... 130
Figure 52. FI for barren ground using different band combinations for Fresno-Kings Counties, USA. 130
Figure 53. FI for cotton using different band combinations for Fresno-Kings Counties, USA..... 131
Figure 54. FI for corn using different band combinations for Fresno-Kings Counties, USA..... 131
Figure 55. FI for tomatoes using different band combinations for Fresno-Kings Counties, USA..... 132
Figure 56. Overall accuracy comparison between different band combinations for Fresno-Kings Counties, USA..... 133

LIST OF ABBREVIATIONS AND SYMBOLS

ACM ..... Atmospheric Compensation Module
ALOS ..... Advanced Land Observing Satellite
ANN ..... Artificial Neural Network
AOI ..... Area of Interest
BGR ..... Blue, Green, Red
CDL ..... Cropland Data Layer
cm ..... Centimeter
COS ..... COmponent Substitution
COTS ..... Commercial-Off-The-Shelf
CVS ..... Canonical Variate Substitution
DEM ..... Digital Elevation Model
EMS ..... Electromagnetic Spectrum
ENVI ..... ENvironment for Visualizing Images
EO ..... Electro-Optical
ESA ..... European Space Agency
ESRI ..... Environmental Systems Research Institute
FI ..... Fitness Index
FLAASH ..... Fast Line-of-sight Atmospheric Analysis of Spectral Hypercubes
FOV ..... Field of View
GCP ..... Ground Control Point
GLCM ..... Gray-Level-Co-occurrence-Matrix
GT ..... Ground Truth
ICC ..... Infrared Color Composite
IDL ..... Interactive Data Language
ha ..... Hectare
HPF ..... High Pass Filter
HSI ..... Hyperspectral Imagery
IHS ..... Intensity-Hue-Saturation
JAXA ..... Japan Aerospace Exploration Agency
LC ..... Land Cover
LIDAR ..... LIght Detection And Ranging
LULC ..... Land Use-Land Cover
m ..... Meter
MCA ..... Minimum Classification Area
MD ..... Mahalanobis Distance
ML ..... Maximum Likelihood

MMU..... Minimum Mapping Unit
MSI ..... Multispectral Imagery
NDVI.....Normalized Difference Vegetation Index
NEST .....Next ESA SAR Toolbox
NIR..... Near-Infrared
nm ..... Nanometer
PALSAR ..... Phased Array Type L-Band Synthetic Aperture Radar
PAN..... Panchromatic
PS ..... Pan-Sharpened
QUAC .....Quick Atmospheric Correction
RADAR..... Radio Detection and Ranging
RGB ..... Red, Green, Blue
RMSE..... Root Mean Squared Error
ROI.....Region of Interest
RST .....Rotation, Scaling, and Translation
RVS..... Regression Variable Substititution
SAR..... Synthetic Aperture Radar
SONAR..... SOund Navigation and Ranging
SRTM..... Shuttle Radar Topography Mission
SVM.....Support Vector Machine
SWIR..... Short Wave Infrared
TD ..... Transformed Divergence
TM..... Thematic Mapper
TOA ..... Top of the Atmosphere
USDA..... United States Department of Agriculture
USGS ..... United States Geological Survey
VNIR..... Visible and Near Infrared
β^0 ..... Beta Naught
σ^0 .....Sigma Naught
µm ..... Micrometer
λ ..... Wavelength

ABSTRACT

LAND COVER CLASSIFICATION ACCURACY FROM ELECTRO-OPTICAL, X, C, AND L-BAND SYNTHETIC APERTURE RADAR DATA FUSION

Mark Gregory Hammann, Ph.D.

George Mason University, 2016

Dissertation Director: Dr. Barry Haack

The fusion of electro-optical (EO) multi-spectral satellite imagery with Synthetic Aperture Radar (SAR) data was explored with the working hypothesis that the addition of multi-band SAR will increase the land-cover (LC) classification accuracy compared to EO alone. Three satellite sources for SAR imagery were used: X-band from TerraSAR-X, C-band from RADARSAT-2, and L-band from PALSAR. Images from the RapidEye satellites were the source of the EO imagery. Imagery from the GeoEye-1 and WorldView-2 satellites aided the selection of ground truth.

Three study areas were chosen: Wad Medani, Sudan; Campinas, Brazil; and Fresno- Kings Counties, USA. EO imagery were radiometrically calibrated, atmospherically compensated, orthorectifed, co-registered, and clipped to a common area of interest (AOI). SAR imagery were radiometrically calibrated, and geometrically corrected for terrain and incidence angle by converting to ground range and Sigma

Naught (σ^0). The original SAR HH data were included in the fused image stack after despeckling with a 3x3 Enhanced Lee filter. The variance and Gray-Level-Co-occurrence Matrix (GLCM) texture measures of contrast, entropy, and correlation were derived from the non-despeckled SAR HH bands. Data fusion was done with layer stacking and all data were resampled to a common spatial resolution. The Support Vector Machine (SVM) decision rule was used for the supervised classifications.

Similar LC classes were identified and tested for each study area. For Wad Medani, nine classes were tested: low and medium intensity urban, sparse forest, water, barren ground, and four agriculture classes (fallow, bare agricultural ground, green crops, and orchards). For Campinas, Brazil, five generic classes were tested: urban, agriculture, forest, water, and barren ground. For the Fresno-Kings Counties location 11 classes were studied: three generic classes (urban, water, barren land), and eight specific crops.

In all cases the addition of SAR to EO resulted in higher overall classification accuracies. In many cases using more than a single SAR band also improved the classification accuracy. There was no single best SAR band for all cases; for specific study areas or LC classes, different SAR bands were better. For Wad Medani, the overall accuracy increased nearly 25% over EO by using all three SAR bands and GLCM texture. For Campinas, the improvement over EO was 4.3%; the large areas of vegetation were classified by EO with good accuracy. At Fresno-Kings Counties, EO+SAR fusion improved the overall classification accuracy by 7%.

For times or regions where EO is not available due to extended cloud cover, classification with SAR is often the only option; note that SAR alone typically results in

lower classification accuracies than when using EO or EO-SAR fusion. Fusion of EO and SAR was especially important to improve the separability of orchards from other crops, and separating urban areas with buildings from bare soil; those classes are difficult to accurately separate with EO.

The outcome of this dissertation contributes to the understanding of the benefits of combining data from EO imagery with different SAR bands and SAR derived texture data to identify different LC classes. In times of increased public and private budget constraints and industry consolidation, this dissertation provides insight as to which band packages could be most useful for increased accuracy in LC classification.

1 INTRODUCTION

As the human population grows, and land and water resources become more limited, an accurate understanding of what covers the Earth becomes critical to understand and manage the human impact on not only those limited resources, but also the health of our planet. Why land cover is distributed the way it is? How and when did it develop? What cover is natural and what is the result of human activities? What has changed and how fast? What caused the changes? Can we predict future changes in land cover? Ryerson and Aronoff (2010) provide an excellent discussion of these questions and how remote sensing technologies can be used.

1.1 Background

Land cover maps are valuable tools to help answers these questions, and over the years, science and technology has made the creation and upkeep of land cover (LC) maps much more manageable. Remote sensing has provided a way to observe large expanses of the Earth much faster with higher accuracy than previously possible with manual boots-on-the-ground methodologies. Ryerson and Haack (2016) present an enlightening summary of the successes and limitations of using remote sensing around the world. The analysis of national programs is critical to better establish the application of geospatial science for the betterment of the human condition.

The Landsat program has provided over 40 years of medium spatial resolution satellite imagery that has been essential to our understanding of LC and how it changes with time (USGS, 2013). Nevertheless, available technology was limited to passive data collection in the visible and near-infrared (VNIR) wavelengths which while valuable, represent a small portion of the electromagnetic spectrum (EMS). Adding more regions of the EMS contributes to and enhances the analysis of the spectra reflected and scattered from materials on the Earth. The development of active RADAR imaging during the 2nd World War, and later synthetic aperture RADAR (SAR) was followed by the commercial availability of data in the RADAR bands important to describe other characteristics of the Earth's surface (Lewis and Henderson, 1998; Woodhouse, 2006). Combining SAR data with electro-optical (EO) data from the VNIR wavelengths, allows for better characterization of the LC by including more of the electromagnetic spectrum. EO and SAR information are complimentary because they respond to different phenomenology; optical wavelengths are differentially absorbed and reflected due to the materials chemistry, while microwave energy from SAR is scattered due to the material's texture, dielectric properties, and physical structure or shape.

1.2 Dissertation Scope

Data fusion of EO multi-spectral satellite imagery with SAR imagery was explored with the working hypothesis that the addition of multi-band SAR imagery will increase the classification accuracy for individual LC classes. Three satellite sources for SAR imagery were used, each of a different band: L-band from PALSAR; C-band from

RADARSAT-2; and X-band from TerraSAR-X. RapidEye imagery was used as the source of the EO imagery.

The outcome of this dissertation adds to the understanding of the benefits of combining data from the VNIR with SAR to identify different classes of LC. Particularly the understanding of which SAR bands can be best fused with the VNIR bands to identify specific LC classes is clarified. This dissertation further contributes to the methodology for identification, quantification, and mapping of LC features and thus may provide some assistance in our search to better understand the Earth, and better support sustainable resource management in the future.

1.3 Organization

The proposed research is organized in sections that address several questions using the classification accuracy assessment as the evaluation metric. Each study area is presented in a separate section. First EO imagery was classified to provide the baseline accuracy. Then the impact of using three different SAR despeckled HH bands was evaluated and the individual and combined impact of each SAR satellite was assessed. Third adding the variance texture measure of each SAR band was tested. Fourth a set of Gray-Level-Co-occurrence-Matrix (GLCM) texture measures was assessed and compared to the more traditional variance texture measure. The impact of three texture window sizes (7x7, 11x11, and 21x21) was investigated for Wad Medani only. Neither texture nor other derived bands from the EO imagery were included in this research given the primary focus was on contribution of information from SAR.

Fifth, the effect of combining EO, SAR despeckled HH with both SAR-derived variance and GLCM texture was evaluated. Sixth the classification accuracy from using SAR and SAR texture only was tested as the SAR baseline. Often there is a need to assess and map a specific material so overall regional classification accuracy for all classes is not sufficient. The band combination that best classified each individual LC class in user's and producer's accuracy for each study site, was determined and compared. In the global discussion, the transportability of the general methodology and procedures performed in this research to other regions and climates are evaluated. Lastly thoughts for future lines of research are discussed.

2 LITERATURE REVIEW

2.1 Remote Sensing Basics

A general definition of remote sensing is the observation of something without physically touching it. Most people have had the experience of medical imaging, which may simply be before and after pictures of a patient undergoing surgery using X-Rays or Magnetic Resonance Imagery, for example. Microscopes of varying degrees of magnification have permitted researchers and physicians to observe very tiny structures … these are examples of remote sensing in the medical and biological domains. Likewise, remote sensing technology has made human observation of the Earth, the moon, other planets, and even the Cosmos possible.

Campbell and Wynne (2011) explain that in the practical sense, application of remote sensing needs to be documented as its development follows closely the development of photography. The first aerial photograph was taken from a balloon by Gaspard-Félix Tournachon in 1858. Campbell and Wynne (2011) provide a clear definition of remote sensing with the focus on understanding the Earth as follows: *"Remote Sensing is the practice of deriving information about the Earth's land and water surfaces using images acquired from an overhead perspective, using electromagnetic radiation in one or more regions of the electromagnetic spectrum, reflected or emitted from the Earth's surface."*

To understand remote sensing and its application one must have a basic understanding of the electromagnetic spectrum (EMS). Figure 1 shows portions of the EMS from gamma rays to beyond AM radio. Visible light is typically described as between 380-720 nm (Campbell and Wynne, 2011), and microwaves (RADAR) between 1-30 cm although P-band RADAR can extend into the FM radio region.

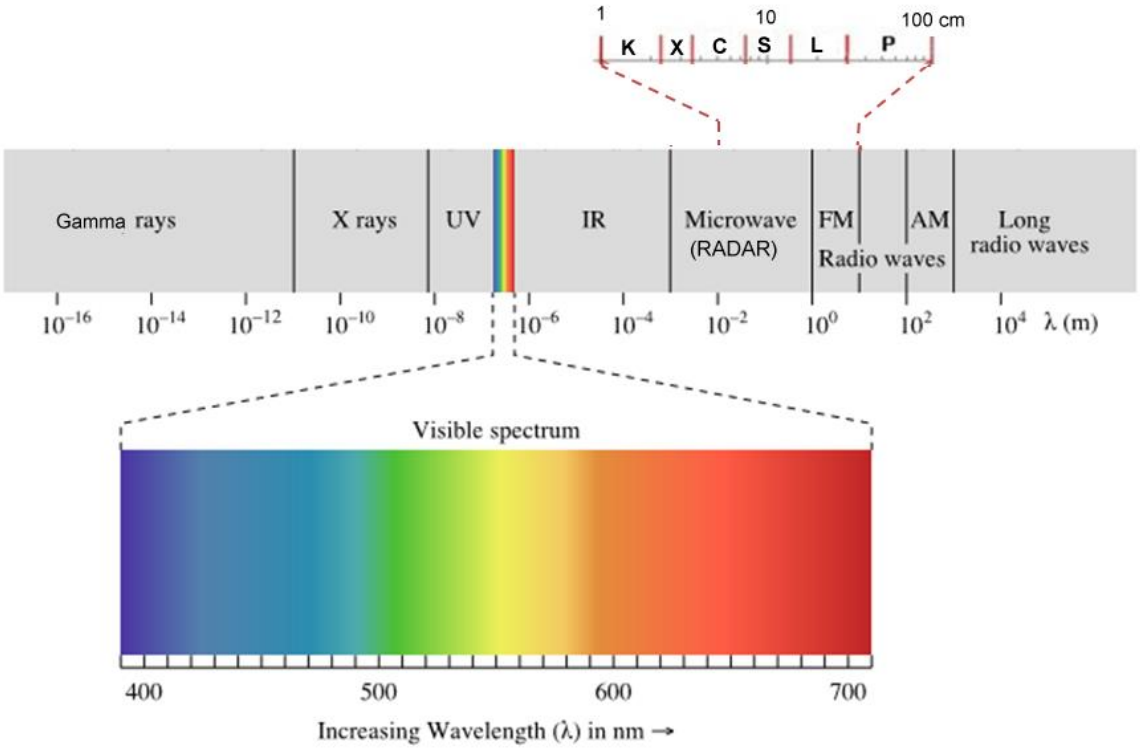

Figure 1. The Electromagnetic Spectrum with details on visible and RADAR bands. By Phillip Ronan; used under CC Attribution-Share Alike 3.0 Unported license. Modified by Hammann, added RADAR bands and some annotations were deleted.

EO imaging satellites operate in the VNIR region of the EMS and passively (only looking) detect the energy reflected from the Earth's surface as well as everything between the satellite and the ground. The Sun's energy or transmitted irradiance is shown

in Figure 2 as well as regions where the Earth's atmosphere absorbs that energy. Regions where much of the Sun's energy is able to reach the ground are called atmospheric windows and EO satellite bands are selected to be mostly within those regions of the EMS. Ozone, water vapor, O_2, and CO_2 are the gases most responsible for atmospheric absorption. EO sensors require sunlight so they can only be used during daylight in good weather; they cannot view the Earth's surface through clouds.

Absorption is not the only process in the atmosphere that alters the energy ultimately detected by the satellite by passive sensors. Scattering from molecules and particles (aerosols) in the atmosphere is also an important consideration. The pathway of energy from the Sun, to the Earth and back to space where it can be detected by a satellite sensor is called the Energy Flow Profile (Haack, 2016) and needs to be understood in order to interpret the data obtained from the satellite (Figure 3). This process has also been called the solar energy profile (Schott, 2007) and the path radiance (Jenson, 2005). What the sensor actually detects is called the Top-of-the-Atmosphere (TOA) radiance although typically the data are delivered as sensor counts and have to be converted to radiance units.

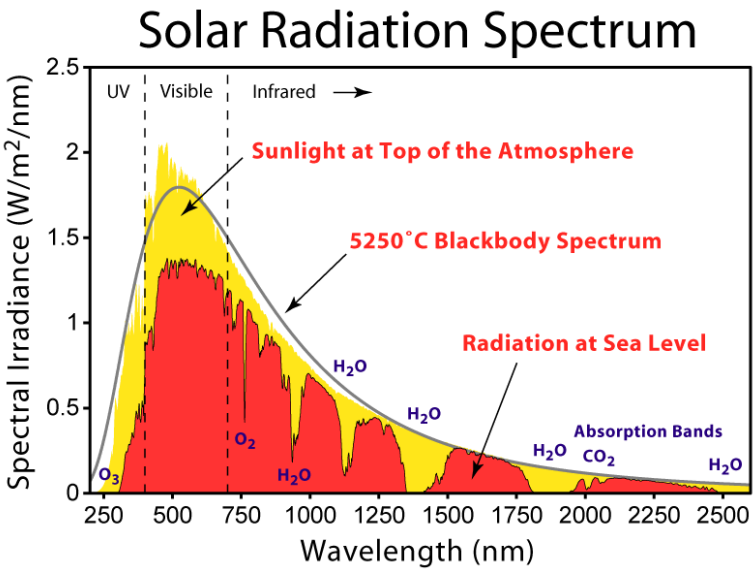

Figure 2. The Sun's radiation from the Top of the Atmosphere, and the Earth's surface at sea level. By Robert A. Rohde used under the CC Attribution-Share Alike 3.0 Unported license.

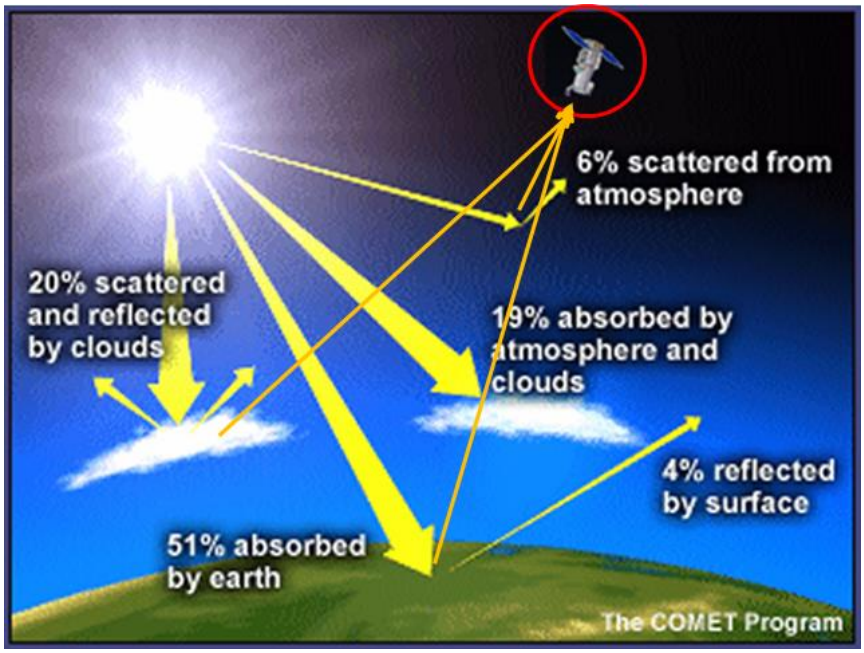

Figure 3. Energy flow profile of light from the Sun to the Earth and back to the satellite. By UCAR/COMET used under the UCAR/COMET license. Modified by Hammann, added the satellite and the energy path to the satellite.

2.2 Atmospheric Compensation

Although imaging satellites directly measure the TOA radiances, scientists really need to understand the materials on the Earth's surface which are best described, when using EO sensors, by the reflectance of VNIR light. Spectral libraries are produced in terms of ground reflectance. There are multiple ways to compensate for the effect of the atmosphere and convert the TOA radiances to ground reflectance. These methods are amply described in the literature, remote sensing text books, and image processing software manuals (Liang, 2004; Jensen, 2005; Schott, 2007; ITT, 2009; ITT, 2010; ERDAS, 2010; Campbell and Wynne, 2011; Richards, 2013). In some cases, with rather clear skies and no desire to compare the imagery to other dates or locations, no atmospheric compensation may be necessary. The dark-body subtraction method is very simple and works well by subtracting the amount of detected radiance from a very dark pixel like water in the NIR band. Because water should absorb the entire NIR signal, any signal detected by the sensor is likely to be from the atmosphere, and that amount is subtracted from the other bands. Band ratios are another good way to compensate for the atmosphere in the sense that light from all wavelengths must travel through the same atmosphere so dividing one band by another lets the atmospheric component cancel itself out … x divided by x is 1.

Lastly there are more comprehensive procedures that often are additional modules to image processing software that typically must be purchased for an additional price. The ENVI software has a module called the Atmospheric Correction Module (ACM) which includes two more advanced algorithms (ITT, 2009): the Quick Atmospheric Correction (QUAC) tool and the Fast Line-of-sight Atmospheric Analysis of Spectral

Hypercubes (FLAASH). QUAC determines the compensation parameters from the image data without additional input and works well with multispectral EO imagery. FLAASH is based on radiative transfer models developed by the US Air Force Research Laboratory and the MODTRAN model (ITT, 2009); FLAASH is used most commonly for hyperspectral imagery.

While the dark-subtract method of atmospheric compensation is most often sufficient, the QUAC tool was used for better EO image quality consistency between sites.

2.3 SAR Basics

SAR sensors work in a similar fashion to LiDAR and SONAR. RADAR means RAdio Detection and Ranging; LiDAR is LIght Detection And Ranging, and SONAR is SOund Navigation and Ranging. These devices are *active* detectors because they provide their own energy source and transmit pulses of energy and measure the time for each pulse to return to the receiving antenna. Table 1 contrasts passive EO and active SAR satellites.

SAR uses microwave energy to bathe an area with pulses and measure the time and amount of pulses scattered back to the receiver, or the backscatter. Henderson and Lewis (1998) and Woodhouse (2006) provide excellent references for imaging RADAR. SAR instruments are side-looking and can arrange the transmitting antennas in a different vertical/horizontal orientation from the receiving antennas; this arrangement allows for polarization. When the transmit and receive antennas are in the same orientation it is called a ‘like’ view; for example, both are either in a vertical or horizontal position. The

SAR polarizations are labeled according to the antenna orientation so despeckled HH and VV are 'like' orientations in the horizontal and vertical planes, respectively. When the transmit and receive antennas are oriented orthogonal to each other it is called a 'cross' view. For example, an HV view is when the transmit antenna is set to horizontal and the receive antenna to vertical. Dual and quad-pole SAR research has been reported by several authors (Sheoran, 2005; Haack and Khatiwada, 2010; Sawaya, et al., 2010; Sheoran and Haack, 2013a; Sheoran and Haack, 2013b; Idol, et al., 2015a; Idol, et al., 2015b).

SAR satellites typically have several data collection modes which basically represent a trade-off between spatial resolution and swath coverage. SAR backscattering is partly determined by the wavelength where longer wavelengths penetrate more than shorter wavelengths (Figure 4). Figure 5 shows the basic SAR geometry terminology; it is important to distinguish between slant and ground range because only ground range data can be projected on a map. The side-looking nature of SAR causes geometric distortions over variable terrain where the data can appear to be in another location. Figure 6 shows geometric distortions in slant range: layover, foreshortening and shadow (Halounová, 2009). These concepts are amply described in Henderson and Lewis (1998) and Woodhouse (2006). Layover is where an elevated surface appears closer to the instrument's nadir position because those returns are received before returns from features on the ground. Elevated surfaces can prevent the pulses from ever reaching the ground behind them causing shadow or areas of no data. Foreshortening is when the RADAR pulse hits a slope directly facing the RADAR.

A characteristic of SAR is a salt-and-pepper appearance with black and white pixels called speckle. Speckle is an artifact of coherence in the SAR design and often can hide the true textural features. Given that each SAR instrument has a number of transponders and receivers, the data can be averaged across them to virtually create a greater number of looks; the spatial resolution of a multi-look SAR scene is lower but the speckle is reduced. Speckle, texture, and EO-SAR fusion will be discussed in the following sections.

Table 1. Comparison between EO and SAR imaging satellites.

	Electro-Optical	SAR
Sensor Type	Passive	Active
Day/Night Acquisition	Day only	Day & Night
Impacted by Clouds	Yes	No
Viewing Angles	Nadir to 30 deg off Nadir	Side looking Geometry
Detected Physical Parameter	Reflectance	Backscatter
Physical Phenomenology	Chemical composition and thermal properties	Target physical properties (roughness, shape & dielectric constant)
DEM Creation	w/Stereo views	w/Stereo views & coherent phase measurements

2.4 Speckle Reduction

Interpretation of SAR imagery is more complicated than EO imagery because SAR texture measures include both a component of surface roughness and speckle due to the coherence of the RADAR and processing system. When RADAR pulse returns coincide, a bright spot speckle is created; when RADAR pulse returns are of opposite signs, they can cancel each other out resulting in a dark spot speckle.

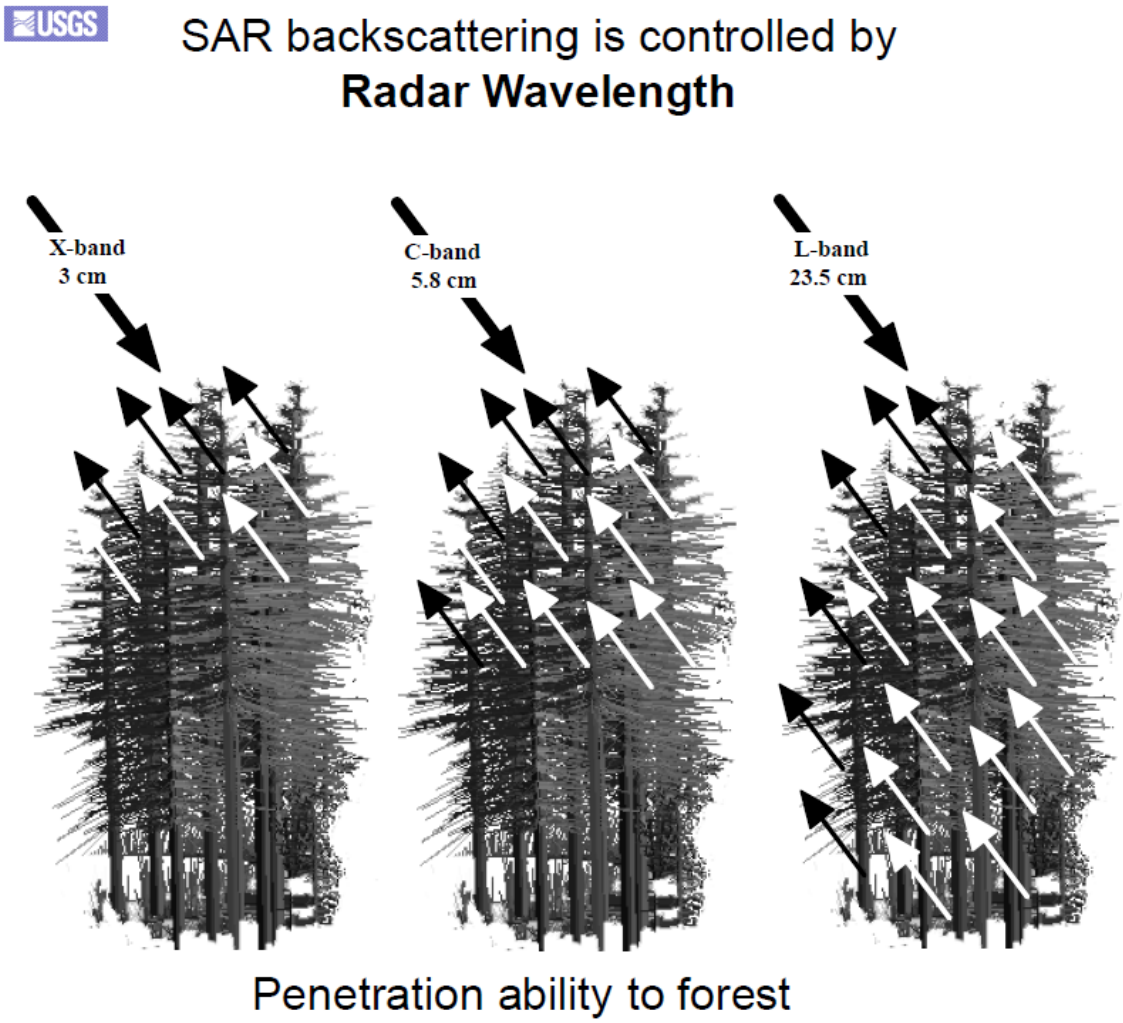

Figure 4. Forest penetration is stronger with longer wavelengths. By USGS (Palma, 2011); used under the 'Fair Use' doctrine. The graphics were reordered to show increasing forest penetration by Hammann.

The issue of speckle is difficult because the analyst does not really know how much of the measured texture is from the material in the scene or how much is from the speckle. Much work has been done on despeckling to find balance and prevent removing the textural information from the image while attempting to reduce the speckle. Nyoungui et al. (2002) reviewed methods of despeckling and texture measures for SAR

imagery. Idol (2012) determined it was best to use the original SAR data for texture derivation but use despeckled SAR as image bands for LULC classification.

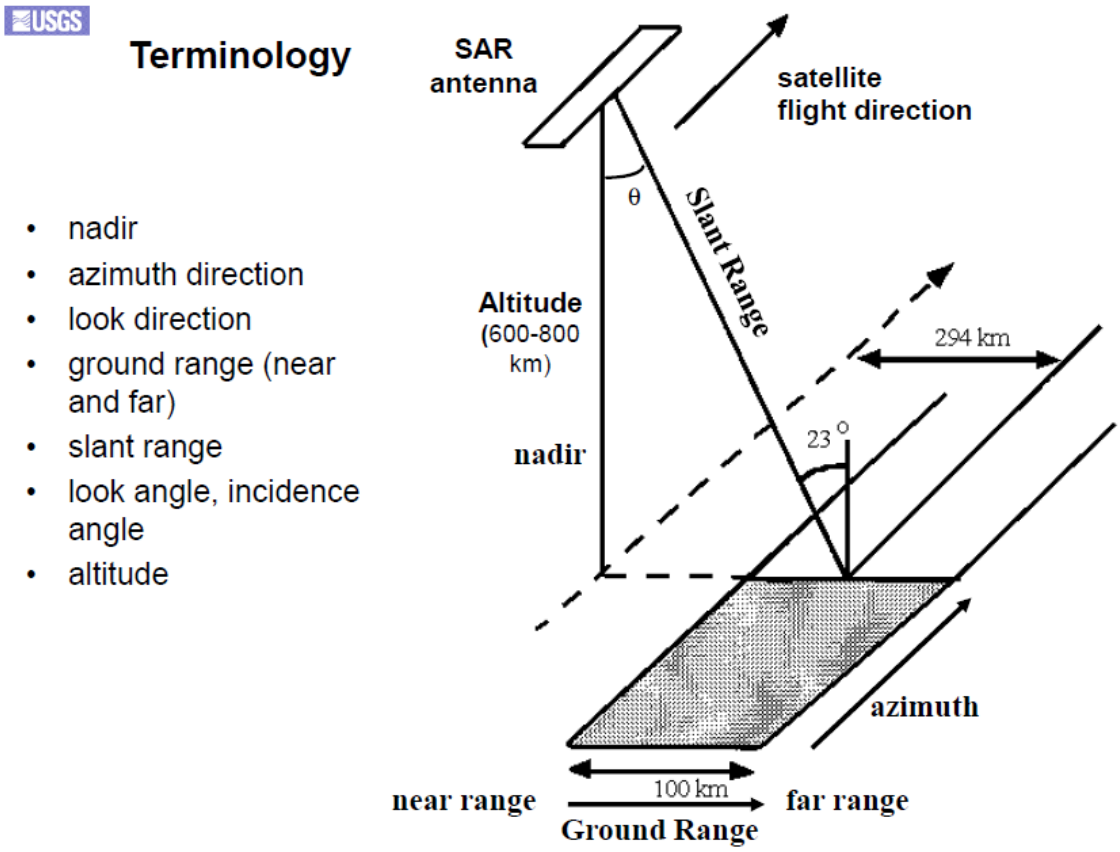

Figure 5. SAR geometry terminology. By USGS (Palma, 2011); used under the 'Fair Use' doctrine.

2.5 Texture Measures

Photo interpretation is an old practice and analysts employ their experience and several cues for their interpretations. Several elements of image interpretation are used: geographic location, tone and color, texture, size, shape, pattern, and association with the surrounding pixels (Campbell and Wynne, 2011). Jensen (2005, 2007) also considers

height/depth/volume as another cue which is measureable with other sensors such as LiDAR and stereo image collections. A qualitative definition of texture is the apparent smoothness or roughness of a region of interest. These interpretations are affected however by the illumination angle and contrast of the scene. Low collection angles also make texture analysis more difficult or impossible to view.

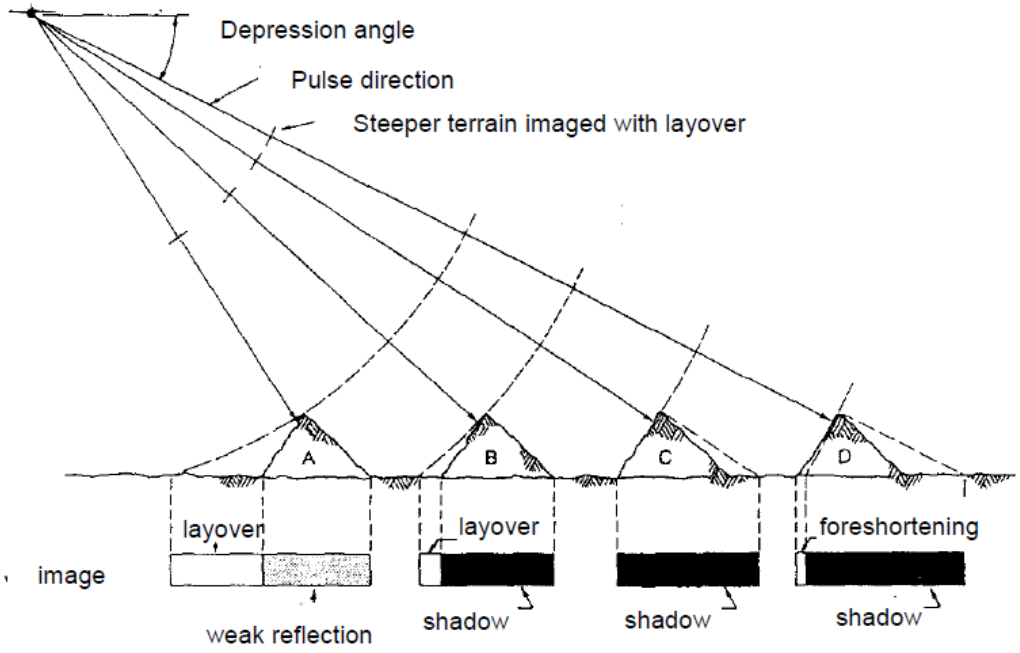

Figure 6. SAR geometric distortions with slant range. By Halounová (2009); used under the 'Fair Use' doctrine.

With digital image processing, different algorithms have been determined to derive quantitative measures of texture allowing their inclusion in digital classification efforts as additional derived bands. Jensen (2005) discussed a wide variety of texture measures including mean and variance, and measures in the spatial domain such as gray-

level co-occurrence-matrices (GLCM), fractals, and variograms. Schott (2007) discussed GLCM texture measures. Texture is an important factor for machine vision and different GLCM algorithms have been tested (Jain et al., 1995).

Much research supporting many applications of texture extraction from EO and SAR imagery has been done. Texture from EO imagery has been used for studying forest canopies (Franklin et al., 2001), defoliation (Moskal and Franklin, 2004), LC with Landsat Thematic Mapper (TM) (Berberoglu et al., 2007), and a variety of environmental applications using Ikonos imagery (Wulder et al., 2004). Ojala et al. (1996) compared several methods of texture derivation and contrasted one-dimensional measures such as means and variances, with two-dimensional measures such as GLCM. Ojala et al. (2002) reported further work on exploiting two-dimensional measures of texture in industrial, medical, and remote sensing applications. Puissant et al. (2005) reported on using texture analysis with high to very high spatial resolution (1-10m) EO imagery to improve classifications.

SAR texture describes the variation in tone and is similar to texture in EO images. Raney (1998) describes tone and texture as being critical first and second order averages of the spatial brightness in the scene. Much work has been done using SAR texture as a derived band(s) in fused images for LC classification (Solberg et al., 1994; Haack et al., 2000; Haack and Bechdol, 2000; Haack et al., 2002; Herold et al., 2005; Haack, 2007; Haack and Khatiwada, 2010; Idol, 2012). Haack and Bechdol (2000) as well as Sheoran (2005) explored three texture measures available in ERDAS Imagine from SAR imagery, and found that the variance measure was more valuable for increasing classification

accuracy. Villiger (2008) used the variance texture measure and found that classification accuracy increased until a window size of 15x15 and then further increases in window size did not help. Clausi (2002) explored seven GLCM measures of texture and found that no single texture measure improved classification accuracy but a set of three (contrast, correlation, and entropy) showed favorable results.

2.6 EO-SAR Fusion

Image or data fusion is typically defined as combining two or more images with complementary spectra or other features in a way that their best characteristics are retained with minimal information loss from each, resulting in greater information content than each image alone (Pohl and Van Genderen, 1998; Pajares and de la Cruz, 2004; Amolins et al., 2007; Haack and Khatiwada, 2010). The Pohl and Van Genderen 1998 review is very complete and widely cited in the literature. For newer methodologies, Amolins et al. (2007) and Pajares and de la Cruz (2004) include a discussion and comparison with standard methodologies. A recent review on data fusion can be found in Klein (2013). The methods from those references are summarized in the following text.

Image fusion can occur at different levels in the processing chain: pixel, feature, or decision level; this study involves pixel level image fusion. There are many methods for image fusion and they fall into two main categories: color or visualization techniques, and statistic-based techniques. Among the color techniques are Red-Green-Blue (RGB) composites, where different bands are selected for different display color channel assignments resulting in more (or less) intuitive visual interpretations. Another color

technique is Intensity-Hue-Saturation (IHS) which attempts to separate the spatial and spectral information from the traditional RGB image; an example is explained in ENVI (2013). In addition to the direct conversion from RGB space to IHS color coordinates, another method substitutes one of the original IHS bands with a fourth band from another sensor. There are variations on this theme when the bands are contrast stretched and the substitution occurs for the different IHS bands. A difficulty for these color techniques is that they are limited to producing a fused image with only three bands.

Among the statistical methods, the Principal Component Analysis (PCA) has been used as a way to decorrelate the image bands and generate a new set of orthogonal axes. Pal et al. (2007) used PCA image fusion to improve geological image interpretations. Several techniques have been used to sharpen the images by replacing one band with a band from another sensor of higher spatial resolution. In general, techniques that involve a forward transformation, a band replacement, and a backward transformation are called a COmponent Substitution (COS) technique originally coined by Shettigara (1992). The High Pass Filtering (HPF), Regression Variable Substitution (RVS), and Canonical Variate Substitution are among COS methods. Lastly wavelets have been increasingly used to determine structure and other image details in a combined band image (Pajares and de la Cruz, 2004). The statistically based techniques are not limited by the number of bands and thus were used in this research.

3 METHODOLOGY

The following software programs were used for data processing and map production in this dissertation:

ArcGIS v10.3.1 from ESRI, Inc.

ENVI+IDL v5.3 from the Harris, Corp.

NEST - Next ESA SAR Toolbox v5.1 from Array Systems Computing (2016)

3.1 Sensor Specifications

For this study data from six satellites were used. RapidEye was the source for the EO data for the classifications; data sources for SAR were TerraSAR-X X-band, RADARSAT-2 C-band, and PALSAR L-band. For ground truth (GT) data were obtained from the very high spatial resolution satellites GeoEye-1 and WorldView-2. Google Earth was not utilized for GT due to the lack of a band in the Near-Infrared (NIR).

3.1.1 GeoEye-1

GeoEye-1 is an EO satellite, and detects light in the VNIR wavelengths. GeoEye-1 has a panchromatic (PAN) band, three visible color bands (blue, green, and red) and a single NIR band (LandInfo, 2016a). Figure 7 shows the spectral response of the GeoEye-1 bands (Hammann, unpublished. using ENVI software). The commercial spatial resolution of GeoEye-1 is 0.5 m PAN and 2 m for the VNIR bands. The native radiometric resolution is 11 bits. GeoEye-1 is owned and operated by DigitalGlobe, Inc.

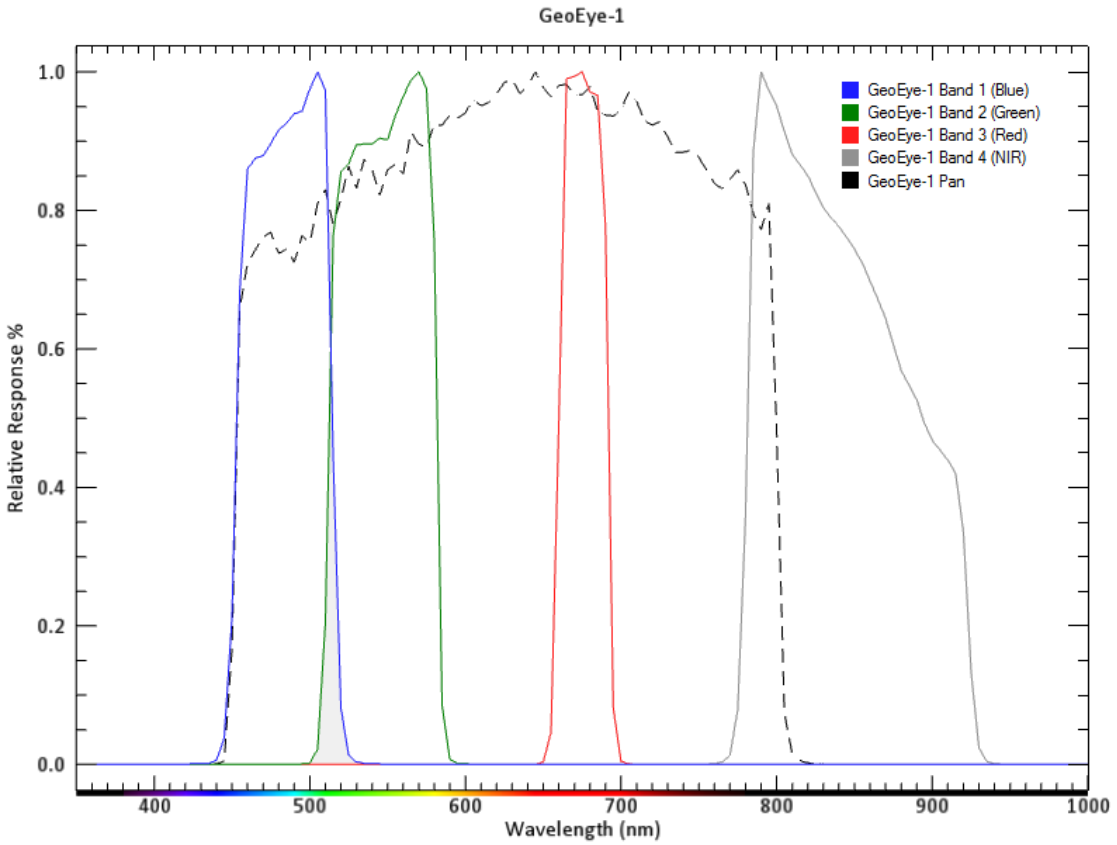

Figure 7. Spectral response of the GeoEye-1 camera and detector array. Hammann, Unpublished.

3.1.2 WorldView-2

WorldView-2 is an EO satellite, detecting light in the VNIR wavelengths. It carries a camera with a 0.50 m PAN band, six visible color bands (coastal blue, blue, green, yellow, red, and red-edge) and a two NIR bands (LandInfo, 2016b). Figure 8 shows the spectral response of the WorldView-2 bands (Hammann, unpublished, using ENVI software). The commercial spatial resolution of WorldView-2 is 0.5 m PAN and 2 m for the VNIR bands. The native radiometric resolution is 11 bits. WorldView-2 is owned and operated by DigitalGlobe, Inc.

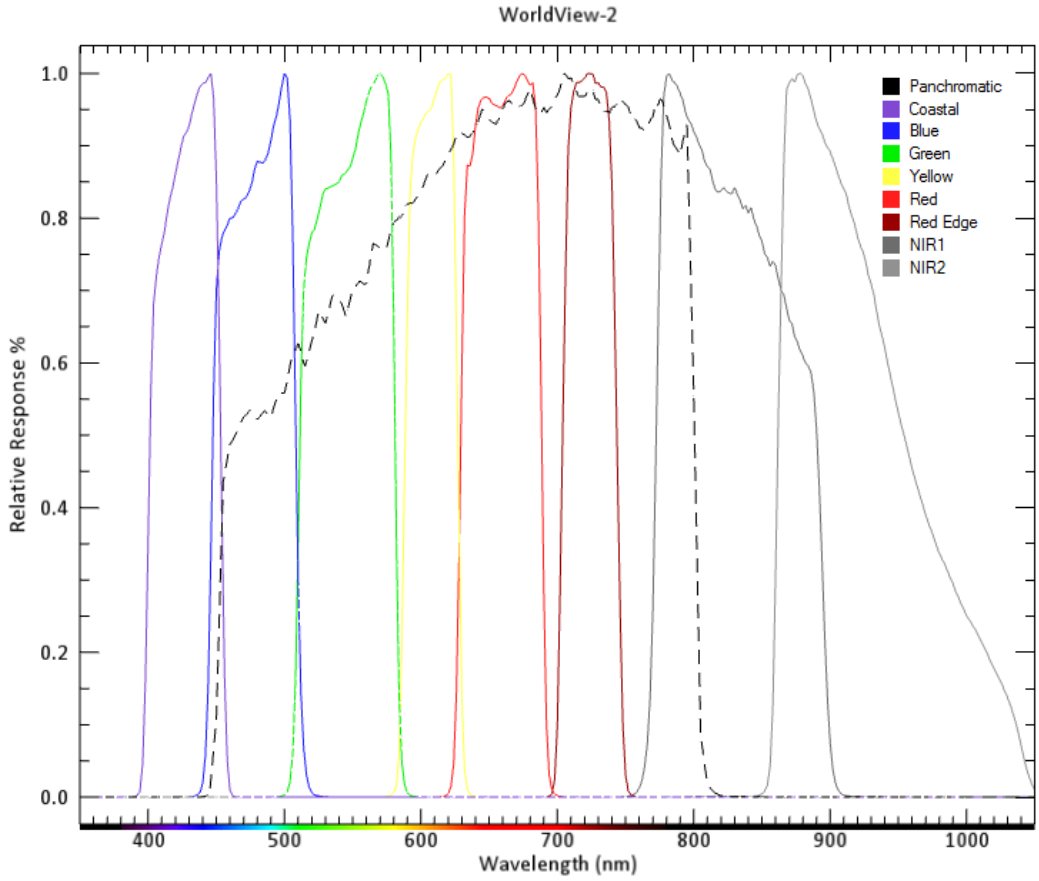

Figure 8. Spectral response of the WorldView-2 camera and detector array. Hammann, Unpublished.

3.1.3 RapidEye

The RapidEye constellation consists of five identical EO satellites each with five bands: four visible color bands (blue, green, red, and red-edge) and a single NIR band. The native spatial resolution is 6.5 m but the level 3A orthorectified products are delivered at 5 m spatial resolution. The radiometric resolution is 12 bits (Planet, 2016). Figure 9 shows the spectral response of the RapidEye bands (Hammann, unpublished, using ENVI software). The RapidEye constellation is owned and operated by Planet

Labs Inc. Table 2 compares the bands of the three EO satellites to be used for this research.

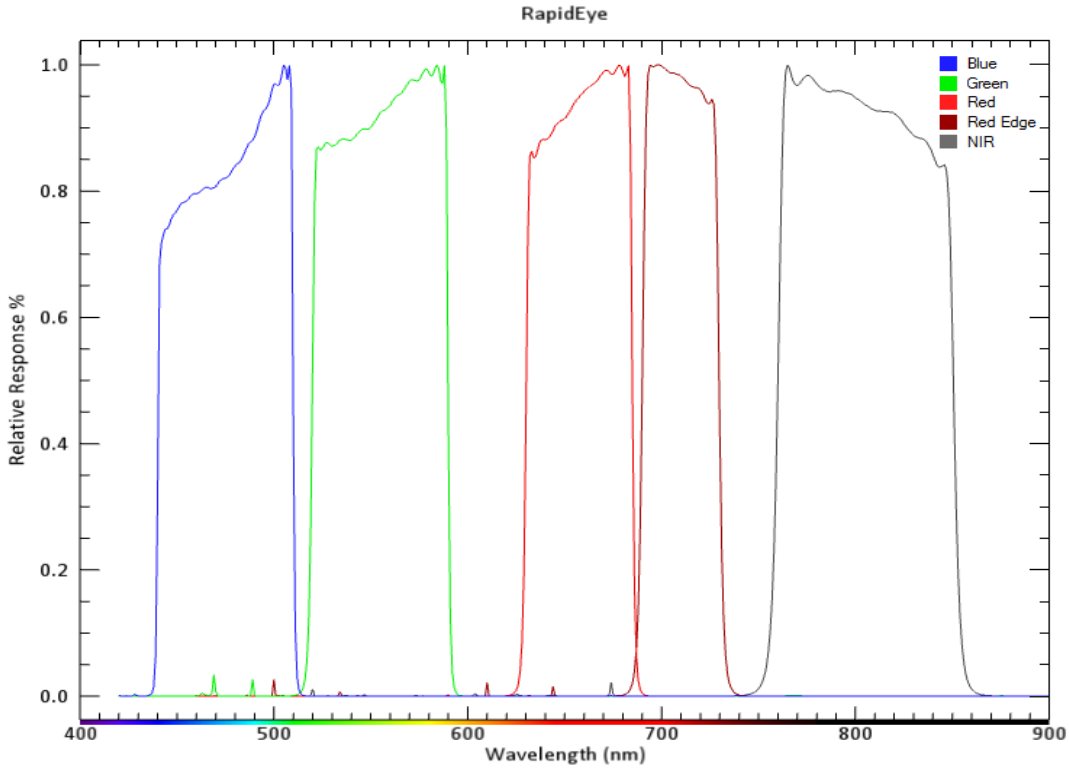

Figure 9. Spectral response of the RapidEye camera and detector array. Hammann, Unpublished.

Table 2. Spectral bands for RapidEye, GeoEye-1, and WorldView-2.

Spectral Range (nm)	RapidEye	GeoEye-1	WorldView-2
Panchromatic	---	450-800	450-800
Coastal Blue	---	---	400-625
Blue	440-510	450-510	450-510
Green	420-590	510-580	510-580
Yellow	---	---	585-625
Red	630-685	655-690	630-690
Red-Edge	---	690-730	705-745
NIR-1	760-850	780-920	770-895
NIR-2	---	---	860-1040

3.1.4 PALSAR

PALSAR is the acronym for the Phased Array Type L-Band Synthetic Aperture Radar. PALSAR is one of three instruments carried aboard the Japan Aerospace Exploration Agency (JAXA) satellite Advanced Land Observing Satellite (ALOS). PALSAR is a SAR sensor detecting scattered microwave energy in the L-band operating in the frequency range between 1-2 GHz and wavelengths 15.0 to 30.0 cm (JAXA, 2008). PALSAR has three scanning modes: fine resolution mode, ScanSAR mode, and the Polarimetric mode (Figure 10). In the fine resolution mode, the spatial resolution is 6.25 m, 12.5 m, or 205 m, for single, dual, or quad polarization data collection, respectively. The ScanSAR mode is a wide area scanning mode and is only available in a single polarization with 100 m spatial resolution. PALSAR collects data by scanning to the right of the satellite's nadir position. Data can be obtained with the processing level 1.5 in 16-bit radiometric resolution.

3.1.5 RADARSAT-2

RADARSAT-2 is owned and operated by MacDonald, Dettwiler and Associates Ltd. (MDA), a commercial Canadian company. It is a SAR satellite using the RADAR C-band with a frequency of 5.405 GHz and wavelengths between 3.75 to 7.3 cm. RADARSAT-2 offers 11 different scanning modes from single polarization to quad-polarization with a spatial resolution between 3–100 m (Figure 11). RADARSAT-2 is able to collect imagery by scanning to the left or right of the satellite and can collect Quad-Pole imagery. Data are delivered with a radiometric resolution of 16 bits (MDA, 2011).

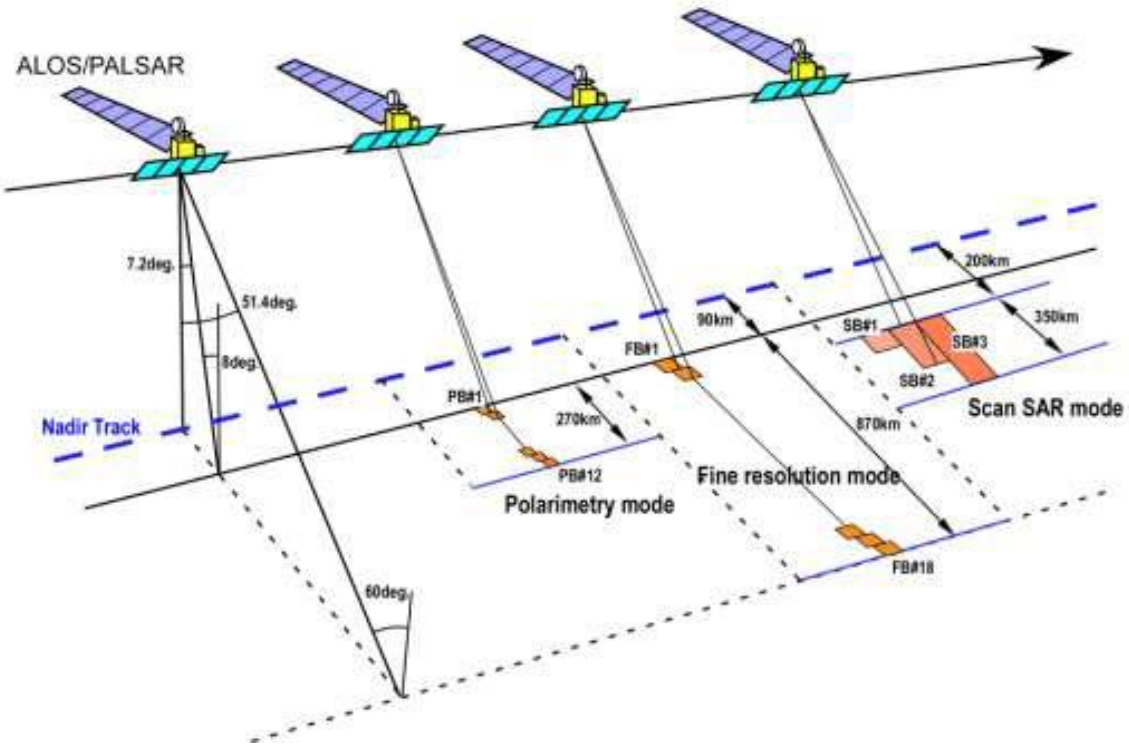

Figure 10. PALSAR scanning modes. Source: Japan Space Systems (2012); used under the 'Fair Use' doctrine.

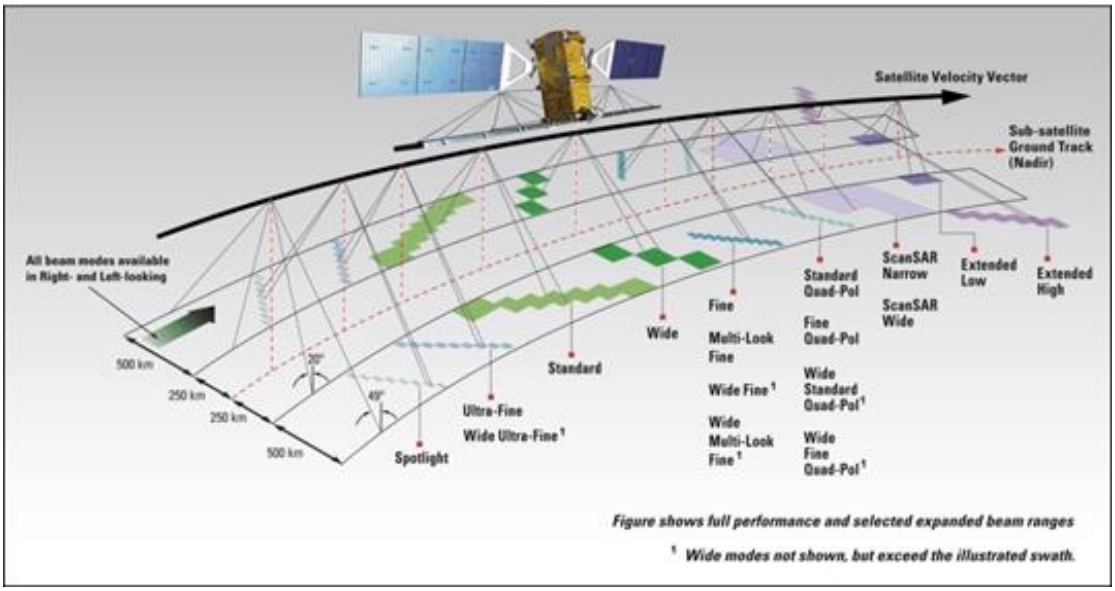

Figure 11. RADARSAT-2 scanning modes. Source: MDA (2011); used under the 'Fair Use' doctrine.

3.1.6 TerraSAR-X

TerraSAR-X is a commercial SAR satellite operated by Airbus A.S, a French company. This sensor operates in the RADAR X-band between the frequencies of 8-12 GHz and wavelengths between 2.50 - 3.75 cm. TerraSAR-X nominally collects imagery in either single or dual polarization; it has five scanning modes (Figure 12) between 1.1 m resolution for the "HighRes Spotlight" mode to the 18.5 m spatial resolution in the "ScanSAR" mode (InfoTerra, 2009).

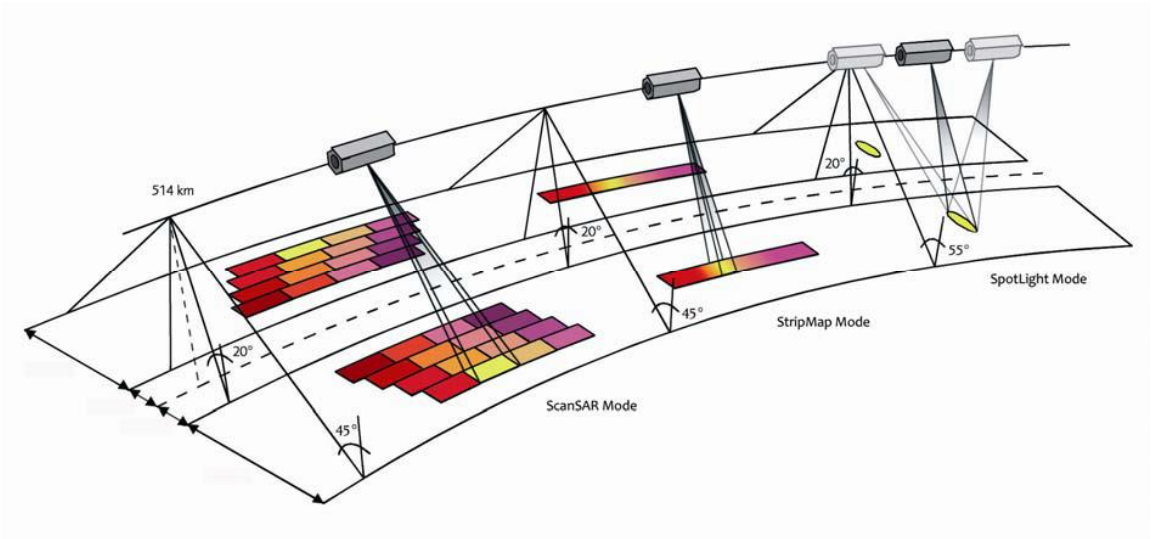

Figure 12. TerraSAR-X scanning modes. Source: InfoTerra (2009); used under the 'Fair Use' doctrine.

3.2 Study Sites

Three test areas were selected from different geographic locations and climate characteristics: dry desert climate at Wad Medani, Sudan; humid tropical climate at Campinas, Brazil; and the Mediterranean climate of Fresno and Kings Counties, CA USA. In this research, the term "Area of Interest" (AOI) is used to define the extents of

the study areas. The term "Region of Interest" (ROI) refers the polygons drawn to gather pixels for classification training and GT for accuracy assessments.

3.2.1 Wad Medani, Sudan

Wad Medani is the capital of the Sudanese state of Al-Jazirah. It is located at $33^{o}30'$N and $14^{o}30'$E (Figure 13) on the west bank of the Blue Nile in the country's major cotton growing area (Metz, 1992). The British established the Gezira irrigation scheme which is based on a network of canals that flow by gravity from the Blue Nile (Metz, 1992). Figure 14 is a natural color satellite view from Google Earth of the area around Wad Medani, including the capital city, Khartoum. The contrast of the agricultural area between the rivers and the surrounding areas is striking. According to the Global Administrative Areas database (GADM, 2013), Wad Medani had a population of 423,863 in 2009.

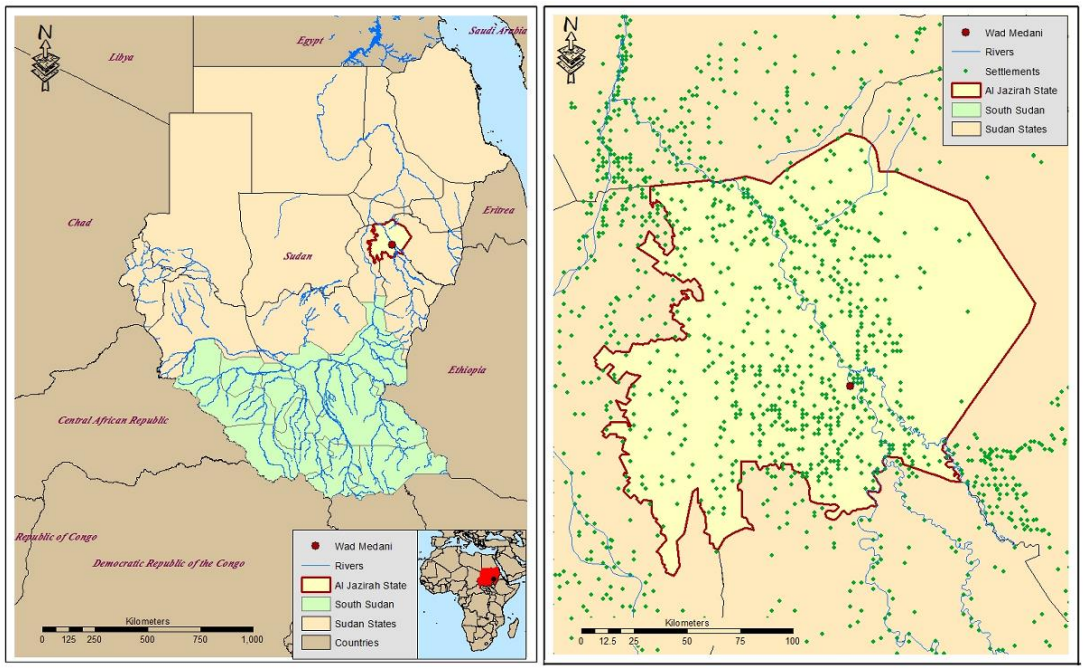

Figure 13. Left - Location of Sudan, the state of Al Jazirah, Wad Medani City, rivers. Right: settlements in Sudan. Hammann, unpublished.

Figure 14. Natural color image of the terrain around Wad Medani, Sudan. Source: Google Earth.

3.2.2 Campinas, Brazil

Campinas City is in Campinas County, State of São Paulo (Figure 15). The city coordinates are 22°54′ S, 47°3′ W. The 2010 population was estimated at 1,080,999 (IBGE, 2010) with over 98.3% in the urban area. The population density was 1,359 inhabitants per sq. km for 2010 (IBGE, 2012). The municipal area of Campinas covers 796 sq. km. A Google Earth natural color image for Campinas (Figure 16) highlights the between vegetation and areas of urban development.

Figure 15. Map of South America highlighting Brazil and the state of São Paolo. The insert shows the location of Campinas, the study area. Hammann, unpublished.

Figure 16. Natural color image of the terrain around Campinas, Brazil. Source: Google Earth.

3.2.3 Fresno and Kings Counties, California, USA

The Fresno-Kings Counties study area AOI is centered on 36°11'N, 119° 52'W (Figure 17). Fresno and Kings Counties are among the top ten producing agricultural counties in California being in 3rd and 10th place respectively (CDFA, 2015). Figure 18 shows a natural color image from Google Earth.

Figure 17. Location of the study AOI in California, crossing Fresno-Kings Counties, USA. Hammann, unpublished.

3.3 Climate

Temperature and precipitation for the three study sites are shown in Figure 19. The climate of Wad Medani is due to the inland location and no proximity to mountain ranges. The Köppen-Geiger climate classification (Kottek et al., 2006) is BWh – Arid, Desert, and Hot Arid. The temperatures are between 15-40^{o}C; the annual total precipitation is 345 mm during the summer mostly in July and August (Figure 19). The

warmest months are during spring. The Nile River water is loaded with suspended material. The soil is of the expansive type and has high clay content (Mohamedzein, et al. 1999) which helps retain water in the canals.

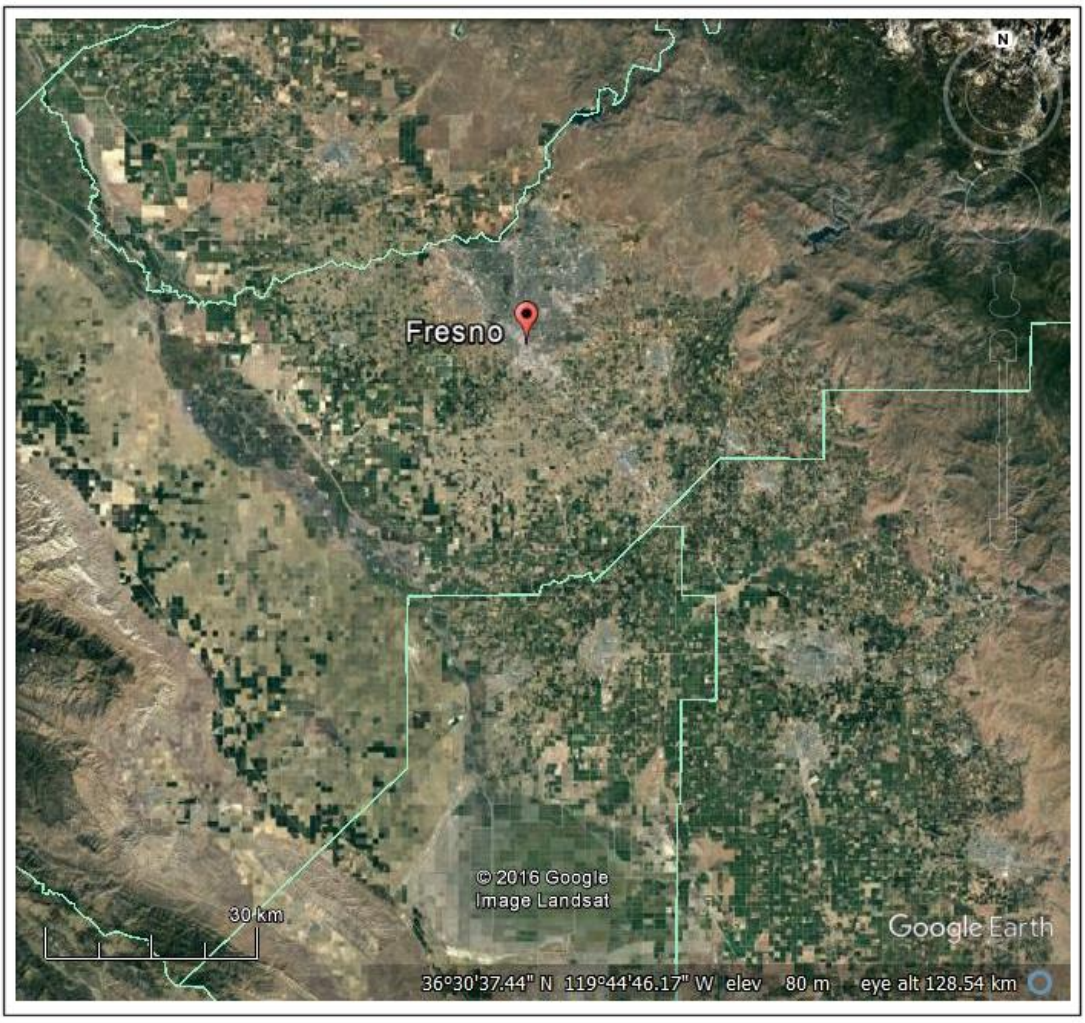

Figure 18. Natural color image of the terrain around Fresno-Kings Counties, USA. The green line is the county border. Source: Google Earth.

The climate of Campinas, Brazil is driven by the inland and leeward side of a coastal mountain range location. The Köppen-Geiger climate classification (Kottek et al., 2006) is Cfb - Warm Temperate, Fully Humid, and Warm Summer. The temperatures are rather mild and stable between 13-30^{o} C; the annual total precipitation is 801 mm (Figure 19). The rainy season is during the austral summer and has the warmest temperatures. No river feeds into the Campinas area, although the great level of rainfall makes irrigation unnecessary. The warm temperatures, high annual rainfall, and dense vegetation create soils with a high fraction of histosols and organic content (Valladares et al., 2007; Instituto Agronômico de Campinas, 2007).

In central California, Fresno-Kings Counties, the climate is dominated by the inland and leeward side of the coastal mountain range location. The Köppen-Geiger climate classification (Kottek et al., 2006) is Bsh – semi-arid, steppe, hot-dry summers; a Mediterranean climate. The temperatures range between about 3-37^{o}C and the annual total precipitation is 294 mm (Figure 19). The rainy season is during the winter as is typical for Mediterranean climates. No river flows directly into the Fresno-Kings Counties area, but there is a network of artificial irrigation canals. The San Joaquin Valley was historically covered by a large water body and many streams carried material from the Coast Range Mountains (Strahorn et al., 1914) creating the soils found today. Strahorn et al. (1914) described the dominant soil being from the San Joaquin series sandy loam and clay loam.

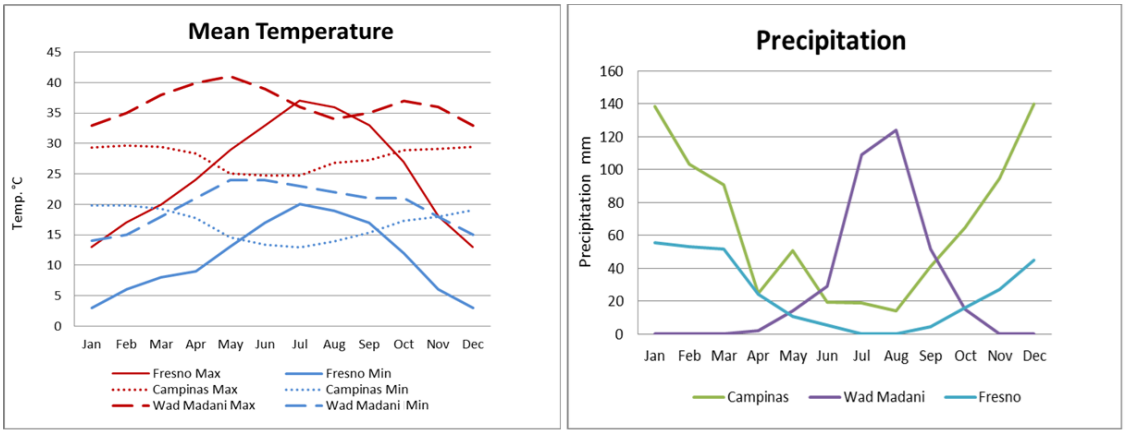

Figure 19. Average climate indicators for Fresno, CA, Campinas, Brazil, and Wad Medani, Sudan. a) Mean monthly high and low temperatures; b) monthly mean precipitation. Data are consolidated from Weather.com (2016) and Weather-and-Climate.com (2016).

3.4 Data Sources

To create the location maps, the administrative, water body, and road shapefiles were obtained from DIVA GIS (2016). For each location, satellite data were obtained for dates as close together as possible. When data were not available for a given sensor during the same month, data from the same climate season in other years were used, as available. RapidEye L3A orthorectified imagery was used for the source of EO imagery. SAR data for all three study sites were from the PALSAR, TerraSAR-X, and RADARSAT-2 satellites. Tables 3, 4, and 5 show the details of the source data for Wad Medani, Campinas, and Fresno-Kings Counties respectively. RADARSAT-2 data at similar spatial resolutions was not available for Campinas, Brazil because RADARSAT-2 is used there primarily for maritime surveillance; the only available SAR images were ScanSAR at 25 m spatial resolution.

Table 3. Data sources for Wad Medani, Sudan. Blue highlight is for the GT image.

Source	Date of Collection	Type or ID /Polarization	Incidence Angle	Pixel Size
Wad Medani	**Sudan**	Fused resolution: 12.5m, 16 bit		
GeoEye-1	10 Aug 2009	2009100808232421603031601661		0.5 m
RapidEye L3A	10 Mar 2010 14 Mar 2011	VNIR Level 3a 16 bit - 2 scenes		5.0 m
PALSAR	24 Jul 2009	ALPSRP186390270 HH Level 1.5	38.74°	12.5 m
RADARSAT-2	6 Jun 2009	Multi-Look Fine HH ID: 40502	30.85°	6.25 m
TerraSAR-X	20 Apr 2010 03 Jun 2010	ScanSAR HH EEC_RE_SC_S_SRA ScanSAR HH EEC_RE_SC_S_SRA	29.16 - 40.40° 40.40°	8.25 m 8.25 m

Table 4. Data sources for Campinas, Brazil. Blue highlight is for the GT image.

Source	Date of Collection	Type or ID/Polarization	Incidence Angle	Pixel Size
Campinas	**Brazil**	Fused resolution: 25m, 16 bit		
GeoEye-1	31 Jul 2010	2010073113110181603031602551		0.5 m
RapidEye L3A	17 Apr 2010 25 Apr 2010	VNIR Level 3a 16 bit - 6 scenes		5.0 m
PALSAR	13 May 2010	ALPSRP229016720 HH Level 1.5	38.91°	12.5 m
RADARSAT-2	30 Apr 2011	ScanSAR Narrow HH ID: 130875	39.57°	25.0 m
TerraSAR-X	12 May 2008	ScanSAR HH EEC_RE_SC_S_SRA	29.16 - 40.40°	8.25 m

Table 5. Data sources for Fresno-Kings Counties, USA. Blue highlight is for the GT image.

Source	Date of Collection	Type or ID/Polarization	Incidence Angle	Pixel Size
Fresno/Kings Counties CA	**USA**	Fused resolution: 12.5m, 16 bit		
WorldView-2	26 Apr 2010	20300100F56BDC00		0.5 m
RapidEye L3A	09 Jun 2010	VNIR Level 3a 16 bit - 4 scenes		5.0 m
PALSAR	14 May 2010 31 May 2010	ALPSRP229190720 HH Level 1.5 ALPSRP231670710 HH Level 1.5	38.68° 38.70°	12.5 m 12.5 m
RADARSAT-2	01 Jul 2010	Multi-Look Fine HH ID: 87853	37.13°	6.25 m
TerraSAR-X	23 Mar 2010	ScanSAR HH EEC_RE_SC_S_SRA	29.16 - 40.40°	8.25 m

The fused AOI for each study region was the maximum area where all data sources overlapped. The coverage area for Wad Medani was 470 sq. km and shown in Figures 20 and 21. The overlap coverage for Campinas, Brazil (2,346 sq. km) is shown in Figures 22 and 23. Lastly, for Fresno-Kings Counties, CA, 1040 sq. km was covered by all image sources (Figs. 24 and 25).

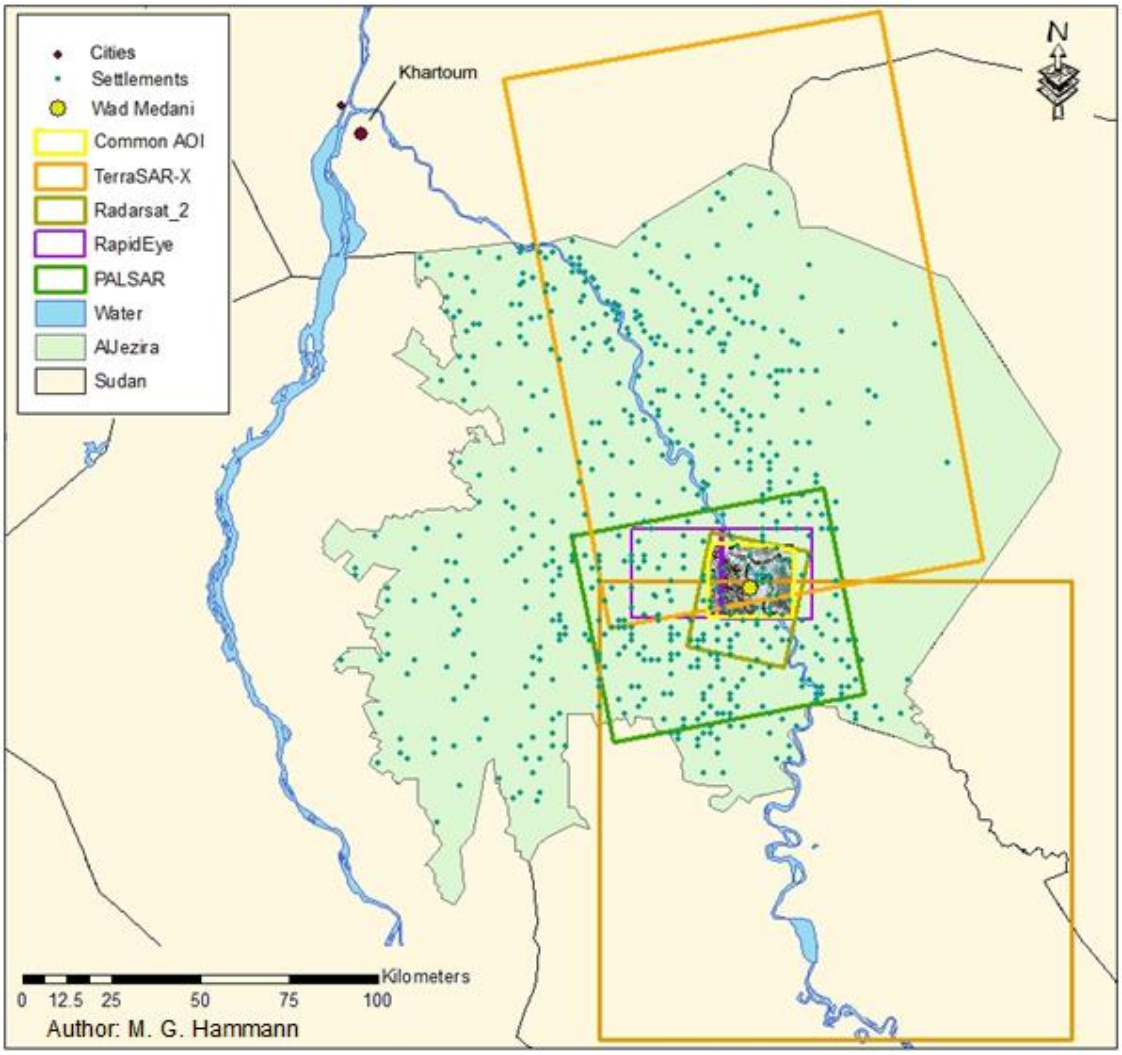

Figure 20. Overlap AOI in Wad Medani, Sudan. Hammann, unpublished.

Figure 21. RapidEye EO natural color image of the common AOI in Wad Medani, Sudan. RGB: Red, Green, Blue bands. Hammann, unpublished.

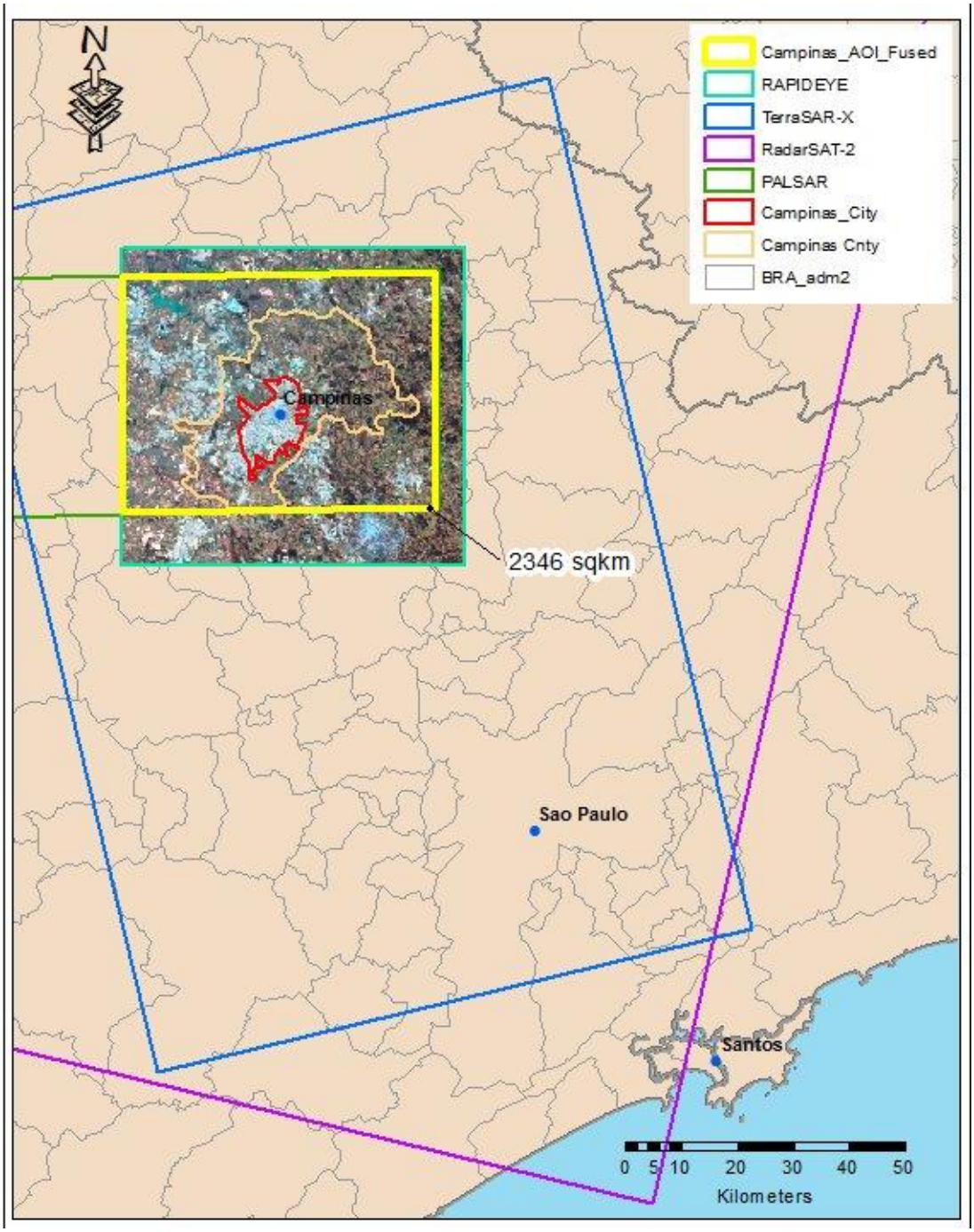

Figure 22. Overlap AOI in Campinas, Brazil. Hammann, unpublished.

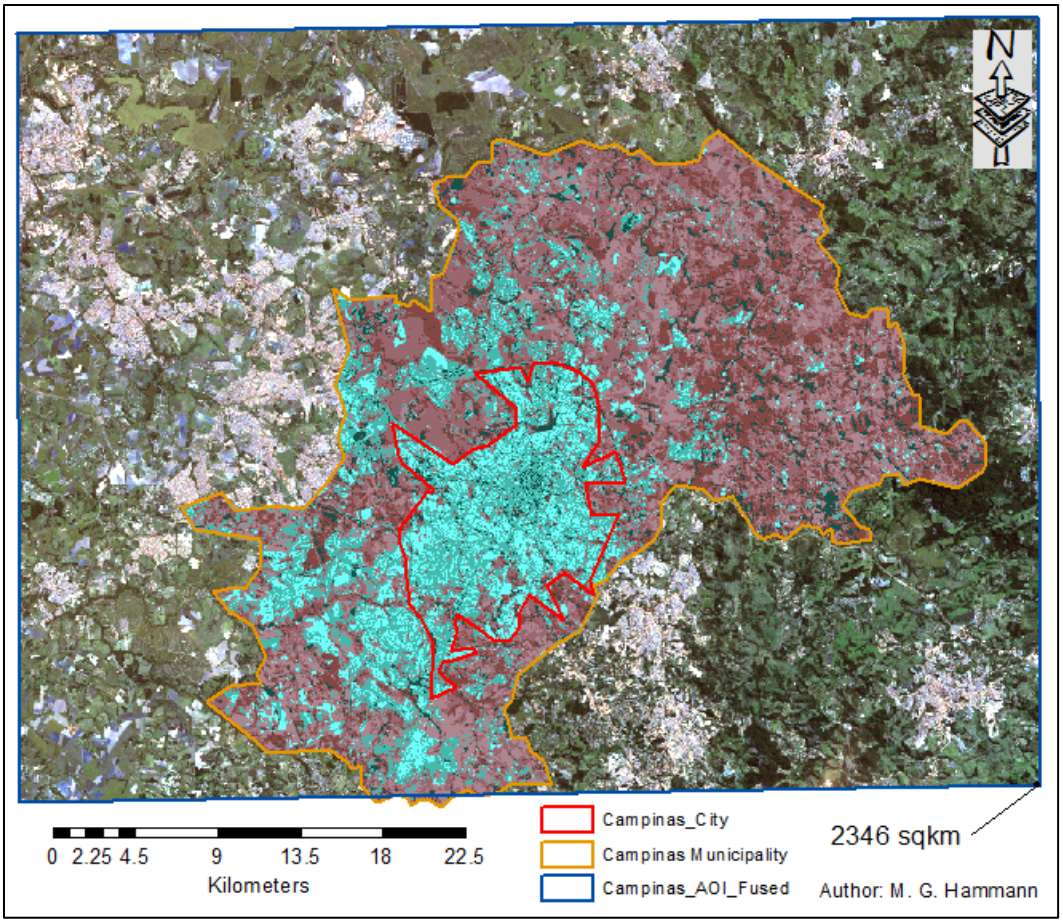

Figure 23. Landsat 5 TM EO natural color image of the common AOI in Campinas Brazil; RGB: Red, Green, Blue bands. The Campinas municipality is shown with a color infrared composite using Landsat 5 TM; RGB: NIR, Red, Green. Hammann, unpublished.

3.5 Image Pre-Processing

3.5.1 Overview

Source imagery was acquired at different processing levels from the different suppliers. RapidEye EO orthorectifed imagery was received as radiometrically TOA calibrated sensor counts. SAR imagery was multi-look and calibrated to represent amplitude and intensity in either digital numbers or Beta Naught (β0, also called radar

brightness) representing the intensity of the radar backscatter in slant range, and accounts for differences in the sensor's incidence angle, flight geometry, and look directions.

All image scenes were orthorectifed to a common UTM map projection for the corresponding area and resampled with the nearest neighbor algorithm to the same spatial resolution. All images were clipped to their common AOI as previously shown, and co-registered to the corresponding UTM WSG84 projection before data fusion. All bands including RADAR texture were combined using layer-stacking into a single multi-band image file for each study area.

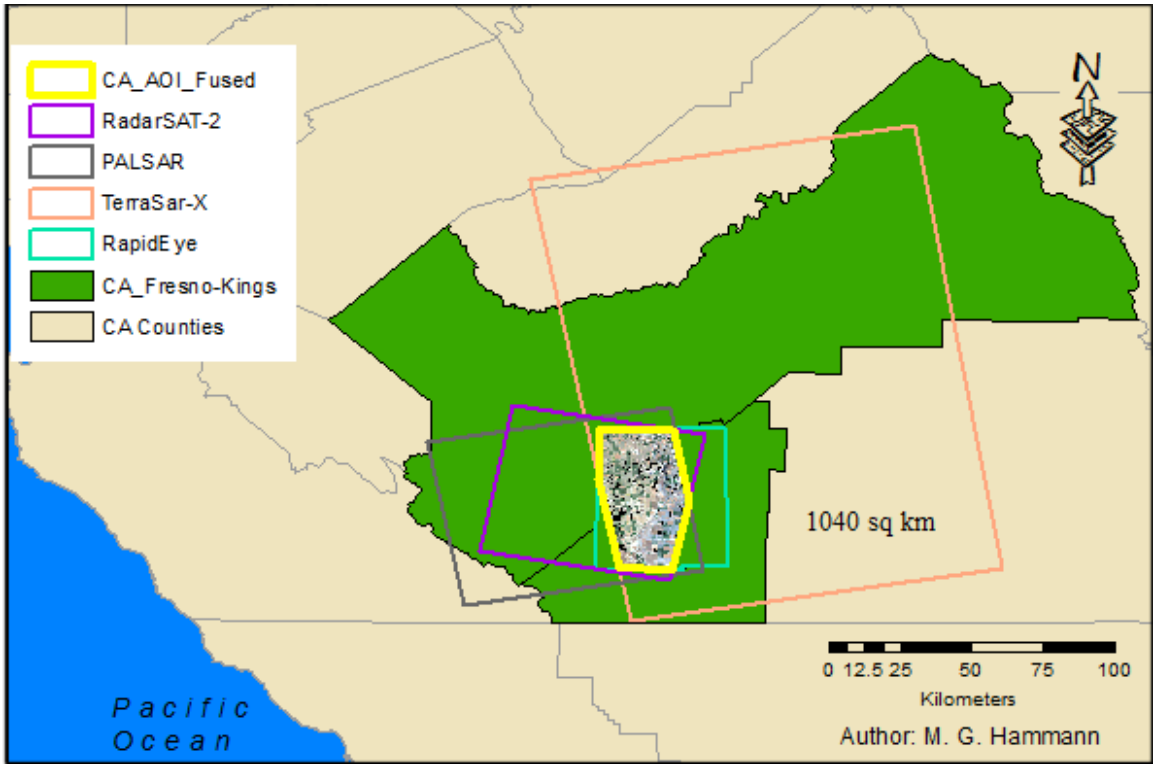

Figure 24. Overlap AOI in Fresno-Kings Counties, USA. Hammann, unpublished.

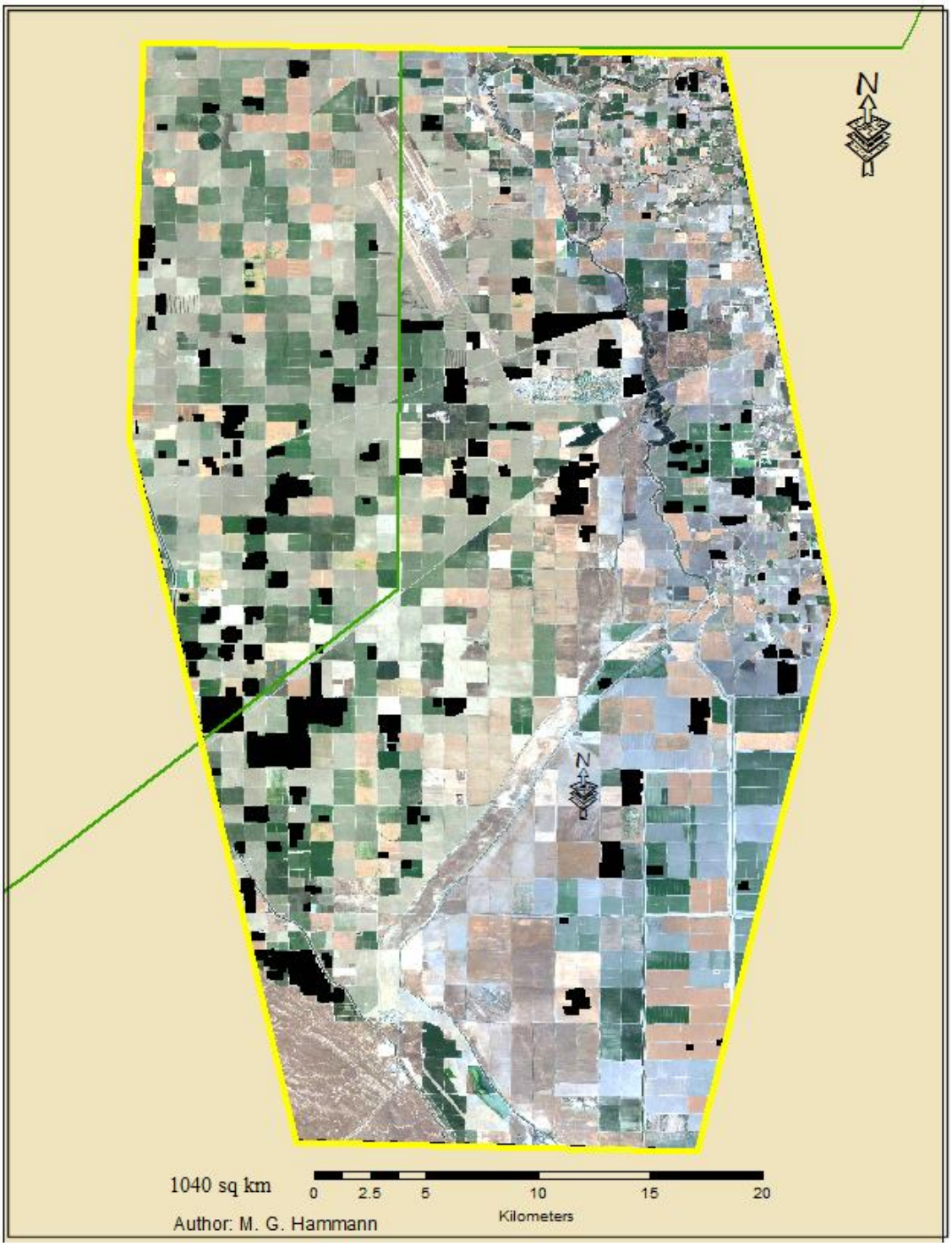

Figure 25. RapidEye EO natural color image of the common AOI in Fresno-Kings Counties, USA. RGB: Red, Green, Blue bands. The green line is the county boundary. Hammann, unpublished.

3.5.2 Radiometric Calibrations

RapidEye L3A TOA sensor counts were converted to TOA radiance using the gains and offsets in the image metadata. EO images were converted to ground reflectance using QUAC in the ENVI software. SAR imagery were converted to ground range and Sigma Naught ($\sigma 0$) identifying the pixels affected by shadow, layover, and foreshortening.

3.5.3 Geometric Calibration and Orthorectification

Basic geometric calibrations were done by the data providers using the sensor model and telemetry. Orthorectification converts the image from a spherical satellite view to a common 2-dimensional map projection, and adjusts for the local terrain with a digital elevation model (DEM). This process minimizes the pixel distortion from off-nadir collections and terrain viewing angle. The output pixel size is adjusted during the orthorectifcation processes and alterations in the spectral information are minimized.

In this research all images were projected using the datum WGS84 and the UTM map projection for the corresponding UTM zone. Some of the SAR images and the RapidEye images were delivered orthorectified using the Shuttle Radar Topography Mission DEM (SRTM) with a 90 m posting. For any images not orthorectified, the SRTM DEM was utilized for consistency.

3.5.4 Resampling

This research involves four different satellite sources for data fusion: one electro-optical and three different bands of SAR. RapidEye has a native resolution of 6.5 m and is delivered as a 5.0 m spatial resolution orthorectified product. EO images from the RapidEye constellation were under-sampled using the pixel aggregation algorithm to

match the largest spatial resolution of the available SAR data over each study site. Resampling error due is minimized by under-sampling to the coarsest resolution for the fused layer stack and the closest match in spatial resolution for the other data sources; this is the most conservative approach but some information from the higher resolution data is lost. For Fresno-Kings Counties and Wad Medani, images were under-sampled to the same 12.5 m native spatial resolution as the PALSAR data. For Campinas, Brazil, images were under-sampled to match the 25.0 m resolution of the ScanSAR data from RADARSAT-2 (Table 6).

Table 6. Original spatial resolution of data sources (in meters) from different satellites for the three study areas and resampled pixel size for the fused layer stack.

Site	RapidEye	PALSAR	TerraSAR-X	RADARSAT-2	Fused (m)
Wad Medani	5.0	12.5	8.25	6.25	12.5
Campinas	5.0	12.5	8.25	25.0	25.0
Fresno-Kings	5.0	12.5	8.25	6.25	12.5

3.5.5 Image-to-Image Registration

With different sensors and orbital geometry, as well as different local view angles during data collection, a small geographic offset between images over the same area is typical. In order to combine all images in a layer stack and perform further analyses, each pixel must represent the same location on the ground. The error should be minimal after orthorectifcation but is still likely to exist. All imagery was evaluated for any errors in the relative position between them and corrected as necessary; the RapidEye EO image was

used as the reference. In some cases no adjustments were necessary. Image-to-Image registration was performed using a polynomial transformation of 1 or 3 degrees. When positional errors were found to be a consistent x/y shift throughout the image, a "rotation, scaling, and translation" (RST) procedure was used with 5 tie points; this uses a 1 degree polynomial. When the positional errors were not consistent throughout the image, image warping was done using a 3rd degree polynomial transformation after editing, deleting or adding at least 25 Ground Control Points (GCP) to derive a Root Mean Squared Error (RMSE) less than 1.0.

3.5.6 SAR Speckle Reduction (Despeckling)

The SAR despeckled HH band was despeckled using the Enhanced Lee filter with a 3x3 kernel. Speckle is not data but noise, and can contaminate the signal in a measure of texture. The PALSAR data at 12.5 m is a multi-look product (4-looks) not likely to require despeckling. However, the data from RADARSAT-2 and TerraSAR-X, while considered multi-look, only use two looks and continue to show a great deal of speckle. Visual examination showed that data from these two satellites benefited from despeckling. For consistency, the same treatment was done to the PALSAR data. Texture measures were calculated on the source SAR data, not the despeckled data.

3.5.7 Texture Derivation

For the Wad Medani study site, three GLCM measures of texture (contrast, correlation, and entropy), as recommended by Clausi (2002), were performed on the SAR HH image band from each SAR satellite; variance texture was also calculated. Idol (2012) described the difficulty of determining a-priori the best kernel size for texture

measures so three different kernels (7x7, 11x11, and 21x21) were applied for data in Wad Medani; all three kernel window sizes were added to the layer stack and the classification accuracy was compared between them. The 21x21 texture kernel size was selected for use for the other two sites. The three GLCM texture measures were used together as a set but their different impacts on accuracy were also determined. The GLCM measures uses an offset parameter of 1 pixel in the x/y direction and 64 levels of gray scale. In a process of elimination and simplification, contrast was eliminated from the data for Campinas and Fresno-Kings Counties, and correlation was eliminated from the Fresno-Kings Counties data leaving only entropy.

3.5.8 Image Fusion in Layer Stacks

For the supervised classification, the multiple bands that have been pre-processed to the same spatial and radiometric resolution were combined in a layer stack (ERDAS, 2010). Any data analysis including classification on the layer stack results is a derived product that represents the information from all the bands through the extraction of the combined signatures. The resulting products are the result of a fusion of all data during the analysis.

3.6 Classification

3.6.1 Feature Class Definition

The LC classification of each study site follows the structural elements of the Anderson et al. (1976) classification scheme but not the exact numbering of classes; it used those classes dominant in each of the three study areas in this research. Different band combinations for each study area were visualized to best determine the relevant land cover classes and aided the signature extraction.

3.6.1.1 Wad Medani, Sudan

Wad Medani is found in the Al Jazirah (or Gezira) state, and is home of the famous gravity-fed irrigation canal network established in 1925 with the damming of the Blue Nile River; it is the largest irrigated agriculture area in The Sudan and even in sub-Saharan Africa (Metz, 1992; FAO, 2005; UNEP, 2007). The major agricultural products of Sudan are cotton, groundnuts (peanuts), sorghum, millet, wheat, gum arabic, sugarcane, cassava (tapioca), mangoes, papaya, bananas, sweet potatoes, and sesame (CIA, 2016). In the area of Wad Medani the main agricultural products are cotton, sorghum, wheat, peanuts, vegetables, and fruits (UNEP, 2007). There are also urban areas, water areas from the Nile River, and the agriculture canals, *Eucalyptus* orchards, and sparse forest on the banks of the river (Herold et al., 2005; Idol, 2012). Table 7 shows nine land cover classes that were identified and used for classification is this study in the general Anderson classification structure.

Table 7. Land Cover classes for Wad Medani, Sudan.

Level I	Level II	Level III	Level IV
1 Urban	11 Residential	111 Low Density	
		112 Medium Density	
2 Agricultural Land	21 Cropland & Pasture	211 Cropland	2111 Green Crops
			2112 Fallow
			2113 Bare Agriculture Soil
	22 Orchards & Trees		
4 Sparse Forest			
5 Water			
6 Barren Ground			

3.6.1.2 Campinas, Brazil

Campinas City in located in the state of São Paolo, Brazil. It is a relatively modern city with over one million residents. The Amazon forest is found to the northeast and evidence of frog-leaping urban sprawl had been described (Hammann, 2011) and can be observed in Figure 23 on page 38. All crops were combined into a single crop category - agriculture. Given the lower spatial resolution of the RADARSAT-2 data the all-band image layer stack was produced at 25.0 m spatial resolution and five general classification levels were used: urban, green agriculture, forest, water, and barren ground.

3.6.1.3 Fresno-Kings Counties, USA

For the case of the Fresno-Kings Counties study site, 11 classes including specific crops were classified. The USDA CropScape – Cropland Data Layer (CDL) (Boryan et al., 2011; Han et al., 2012; USDA, 2013) was used both to identify crops in the image stack layer for training areas as well as for GT. Figure 26 shows the proportions of the most abundant crops in the fused AOI for the study area in Fresno-Kings Counties. Figure 27 is a map of the crops grown during 2010 created using data in the CDL. Cotton, tomatoes, corn, winter wheat, pistachios, almonds, and alfalfa (Table 8) were selected for classification, in addition to classes for developed areas, water, fallow and barren land. All other crops identified in the 2010 CDL were combined into a single class labeled ‘other’, and used as an image mask to remove those areas from the classification process in the fused image.

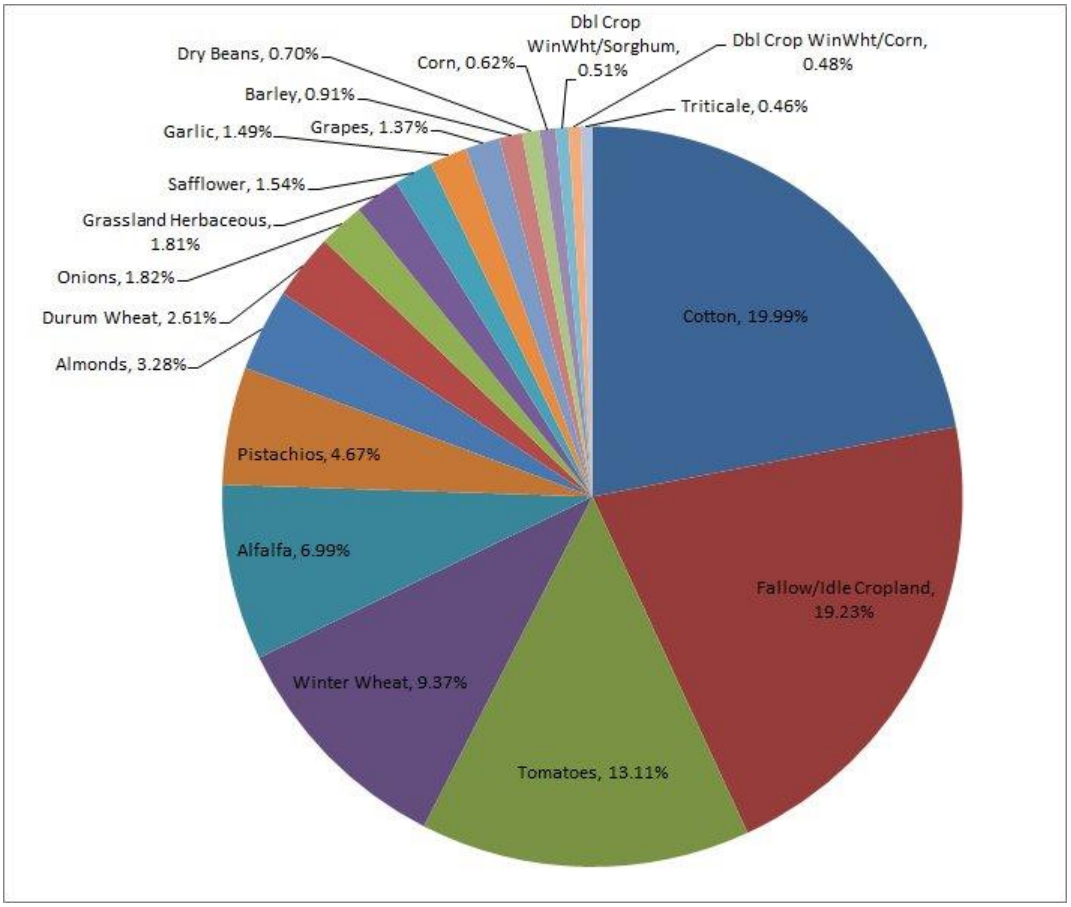

Figure 26. Major crops in the common AOI of study area in Fresno-Kings Counties. From data in the 2010 CDL; Hammann, unpublished.

3.6.2 Signature Extraction from Training Areas

Natural color and infrared color composite (ICC) images were evaluated to determine the training AOIs; other band combinations were also used during this evaluation process. At least five homogeneous training areas were selected for each class, and the total number of pixels was similar when possible.

Table 8. Land Cover classes for Fresno-Kings Counties, CA, USA.

Level I	Level II	Level III	Level IV
1 Urban			
2 Agriculture	21 Cropland and Pasture	211 Cropland	2111 Other Growing
			2112 Fallow
			2113 Cotton
			2114 Tomatoes
			2115 Winter Wheat
			2116 Alfalfa
			2117 Corn
		212 Pasture	
	22 Orchards	224 Pistachios	
		225 Almonds	
5 Water			
6 Barren Ground			

3.6.3 Supervised Classification

A supervised classification for each study area was employed using the extracted spectral signatures. For the Wad Medani test site, several decision rules were compared using the entire band stack and the best performer was used in the rest of the study. From the fused layer stack, different sets of bands were used for each test classification.

3.6.4 Ground Truth

Pixels were collected in polygons for GT over a high spatial resolution image from GeoEye-1 at the Pan-Sharpened (PS) resolution of 0.5 m. Each polygon was coded with the corresponding class code and saved as a thematic map using the same class codes as used for the training polygons and classifications. For the Fresno-Kings Counties study area the Cropland Data Layer (Boryan, et al., 2011), as shown in Figure 27, was used in addition of WorldView-2 imagery to build the GT thematic map. The GT map was resampled to the same fused spatial resolution as the data in each study site. The GT data

were compared statistically to the classification thematic maps to determine the classification errors.

3.6.5 Accuracy Assessments

Congalton and Green (1999) provided a detailed description of the accuracy assessment errors of omission and commission. As indicated and very generally used by other workers, the accuracy assessment was carried out by the statistical comparison of pixels collected in polygons assigned to specific classes and data from ground-truth samples collected from a reference image and from different locations from the training sites. The Confusion (or error) Matrix and the Kappa coefficient were calculated for each tested band combination and summarized in tables showing the user's and producer's accuracies for each trial for each LULC class. The Kappa coefficient is only included as a comparative metric.

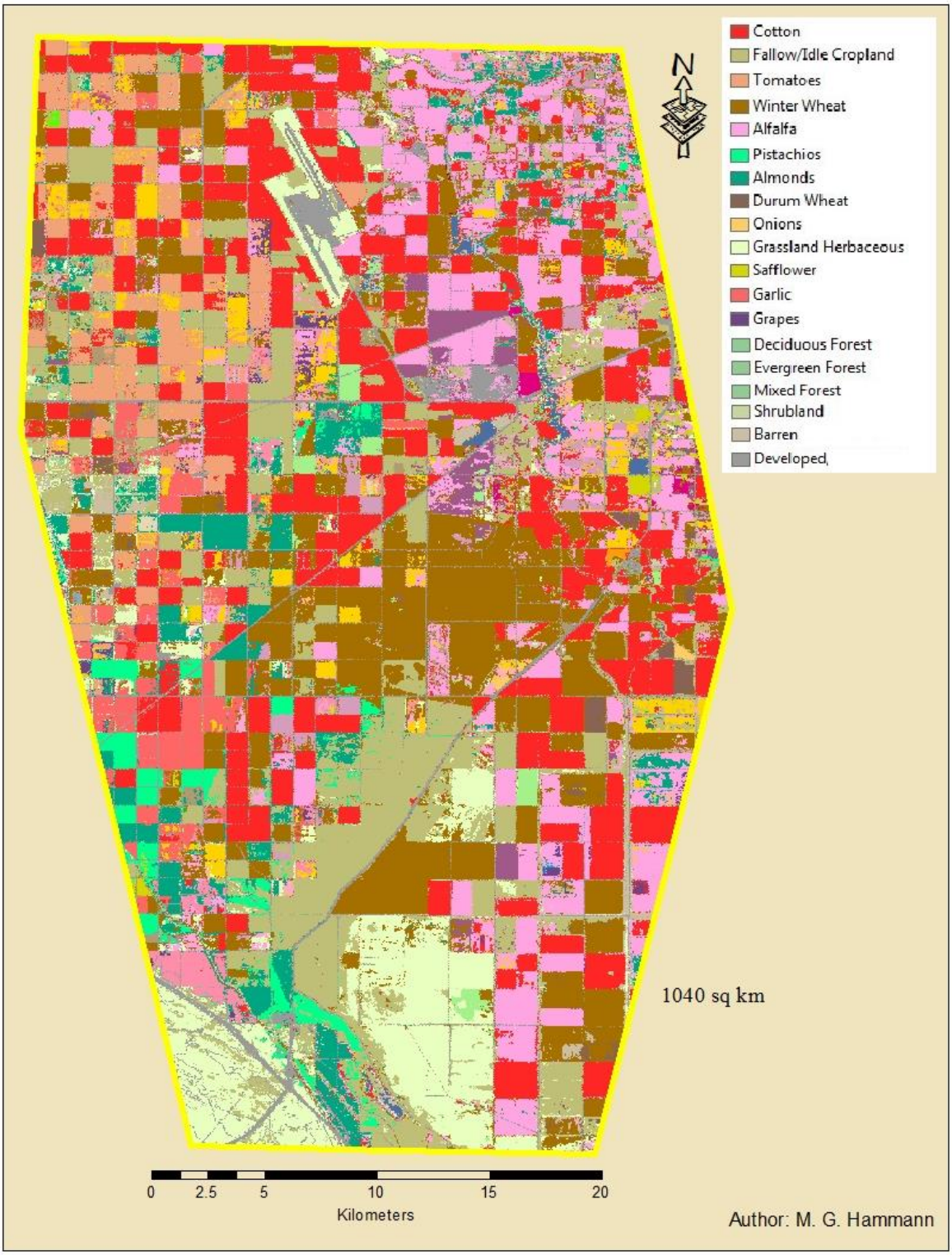

Figure 27. Cropland Data Layer for the common AOI of study area in Fresno-Kings Counties, USA. Hammann, unpublished.

4 RESULTS

4.1 Wad Medani, Sudan

4.1.1 Test Series

Table 9 shows the data used and objectives for seven series of tests. The classification using EO imagery formed the baseline assessment - test series one. Series two added the despeckled HH band from the three SAR sensors separately and combined. The third test series added the variance texture measure for each of three kernel sizes separately and combined. The fourth series tested the impact in classification accuracy from the three GLCM texture measures used together without the variance texture, testing each kernel size separately and combined. In the fifth series, all texture data (variance and GLCM) were used for the classification testing the texture kernels separately and combined. The sixth and seventh series looked at the classification accuracy using only SAR data, including the different texture measures. Series seven tested the different textures measures separately. Table 10 shows the test matrix with the bands selected for each test. There were 119 different classification tests for Wad Medani.

Table 9. Classification Tests Band Packages for Wad Medani, Sudan.

Test	Data	Objective	# Tests
1	EO Bands 1-5	EO baseline	1
2	EO+SAR Despeckled HH	Test effect of adding to EO each SAR band individually and combined	7
3	EO + SAR Despeckled HH + SAR variance 7x7, 11x11, 21x21 kernels	Test effect of adding SAR variance texture: - Each kernel size per SAR band - Each kernel size with SAR band combinations - Combined kernel sizes with all SAR bands - All kernel sizes with all SAR bands w/o SAR despeckled HH	26
4	EO + SAR Despeckled HH + SAR GLCM 7x7, 11x11, 21x21 kernels	Test effect of adding SAR GLCM texture: - Each kernel size per SAR band - Each kernel size with SAR band combinations - Combined kernel sizes with all SAR bands - All kernel sizes with all SAR bands w/o despeckled HH	26
5	EO + SAR Despeckled HH + SAR Variance +All GLCM 7x7, 11x11, 21x21 kernels	Test effect of adding SAR V + GLCM texture: - Each kernel size per SAR band - Each kernel size with SAR band combinations - Combined kernel sizes with all SAR bands - All kernel sizes with all SAR bands w/o despeckled HH	26
6	SAR Despeckled HH + SAR Variance + GLCM 7x7, 11x11, 21x21 kernels	SAR baseline: - Each kernel size per SAR band - Each kernel size with SAR band combinations - Combined kernel sizes with all SAR bands - All kernel sizes with all SAR bands w/o despeckled HH	9
7	EO + SAR Despeckled HH + SAR variance + GLCM individually (using all kernel sizes combined)	Test effect of each GLCM measure: - Each GLCM measure per SAR band - Each GLCM measure with SAR band combinations - Combined kernel sizes with all SAR bands	24
		Total Tests	119

Table 10. Test Matrix for Wad Medani, Sudan.

		TerraSar-X							RADARSAT-2							PALSAR						
Test	**RapidEye**	**HH**	**VAR7**	**VAR11**	**VAR21**	**GLCM7**	**GLCM11**	**GLCM21**	**HH**	**VAR7**	**VAR11**	**VAR21**	**GLCM7**	**GLCM11**	**GLCM21**	**HH**	**VAR7**	**VAR11**	**VAR21**	**GLCM7**	**GLCM11**	**GLCM21**
EO ALONE																						
1	X																					
EO + SAR-HH																						
2a	X	X																				
2b	X								X													
2c	X															X						
2d	X	X							X													
2e	X								X							X						
2f	X	X														X						
2g	X	X							X							X						
EO+SAR-HH+3XVAR																						
3a-7	X	X	X																			
3a-11	X	X		X																		
3a-21	X	X			X																	
3b-7	X								X	X												
3b-11	X								X		X											
3b-21	X								X			X										
3c-7	X															X	X					
3c-11	X															X		X				
3c-21	X															X			X			
3d-7	X	X	X						X	X												
3d-11	X	X		X					X		X											
3d-21	X	X			X				X			X										
3e-7	X								X	X						X	X					
3e-11	X								X		X					X		X				
3e-21	X								X			X				X			X			
3f-7	X	X	X													X	X					
3f-11	X	X		X												X		X				
3f-21	X	X			X											X			X			
3g-7	X	X	X						X	X						X	X					
3g-11	X	X		X					X		X					X		X				
3g-21	X	X			X				X			X				X			X			
3h-7+11	X	X	X	X					X	X	X					X	X	X				
3h-7+21	X	X	X		X				X	X		X				X	X		X			
3h-11+21	X	X		X	X				X		X	X				X		X	X			
3h-7+11+21	X	X	X	X	X				X	X	X	X				X	X	X	X			
3i-7+11+21	X		X	X	X					X	X	X					X	X	X			
EO+SAR-HH+GLCM																						
4a-7	X	X				X																
4a-11	X	X					X															
4a-21	X	X						X														
4b-7	X								X				X									
4b-11	X								X					X								
4b-21	X								X						X							
4c-7	X															X				X		
4c-11	X															X					X	
4c-21	X															X						X
4d-7	X	X				X			X				X									
4d-11	X	X					X		X					X								
4d-21	X	X						X	X						X							
4e-7	X								X				X			X				X		
4e-11	X								X					X		X					X	
4e-21	X								X						X	X						X
4f-7	X	X				X										X				X		
4f-11	X	X					X									X					X	
4f-21	X	X						X								X						X
4g-7	X	X				X			X				X			X				X		
4g-11	X	X					X		X					X		X					X	
4g-21	X	X						X	X						X	X						X
4h-7+11	X	X				X	X		X				X	X		X				X	X	
4h-7+21	X	X				X		X	X				X		X	X				X		X
4h-11+21	X	X					X	X	X					X	X	X					X	X
4h-7+11+21	X	X				X	X	X	X				X	X	X	X				X	X	X
4i-7+11+21	X					X	X	X					X	X	X					X	X	X

Table. 10. Test Matrix for Wad Medani, Sudan. Continued

		TerraSar-X							RADARSAT-2							PALSAR						
Test	RapidEye	HH	VAR7	VAR11	VAR21	GLCM7	GLCM11	GLCM21	HH	VAR7	VAR11	VAR21	GLCM7	GLCM11	GLCM21	HH	VAR7	VAR11	VAR21	GLCM7	GLCM11	GLCM21
EO+SAR-HH+1XVAR+GLCM																						
5a-7	X	X	X			X																
5a-11	X	X		X			X															
5a-21	X	X			X			X														
5b-7	X								X	X			X									
5b-11	X								X		X			X								
5b-21	X								X			X			X							
5c-7	X															X	X			X		
5c-11	X															X		X			X	
5c-21	X															X			X			X
5d-7	X	X	X			X			X	X			X									
5d-11	X	X		X			X		X		X			X								
5d-21	X	X			X			X	X			X			X							
5e-7	X								X	X			X			X				X		
5e-11	X								X		X			X		X	X				X	
5e-21	X								X			X			X	X		X				X
5f-7	X	X	X			X										X	X			X		
5f-11	X	X		X			X									X		X			X	
5f-21	X	X			X			X								X			X			X
5g-7	X	X	X			X			X	X			X			X	X			X		
5g-11	X	X		X			X		X		X			X		X		X			X	
5g-21	X	X			X			X	X			X			X	X			X			X
5h-7+11	X	X	X	X		X	X		X	X	X		X	X		X	X	X		X	X	
5h-7+21	X	X	X		X	X		X	X	X		X	X		X	X	X		X	X		X
5h-11+21	X	X		X	X		X	X	X		X	X		X	X	X		X	X		X	X
5h-7+11+21	X	X	X	X	X	X	X	X	X	X	X	X	X	X	X	X	X	X	X	X	X	X
5i-7+11+21	X		X	X	X	X	X	X		X	X	X	X	X	X		X	X	X	X	X	X
SAR-HH+1VAR+GLCM																						
6a		X							X							X						
6b		X	X	X	X	X	X	X														
6c									X	X	X	X	X	X	X							
6d																X	X	X	X	X	X	X
6e		X	X	X	X	X	X		X	X	X	X	X	X	X							
6f									X	X	X	X	X	X	X	X	X	X	X	X		
6g		X	X	X	X	X	X	X								X	X	X	X	X	X	X
6h		X	X	X	X	X	X	X	X	X	X	X	X	X	X	X	X	X	X	X	X	X
6i			X	X	X	X	X	X		X	X	X	X	X	X		X	X	X	X	X	X	X
SAR-HH+1VAR+GLCM		**HH**	**VAR7**	**VAR11**	**VAR21**	**CONTR**	**ENTROPY**	**CORR**	**HH**	**VAR7**	**VAR11**	**VAR21**	**CONTR**	**ENTROPY**	**CORR**	**HH**	**VAR7**	**VAR11**	**VAR21**	**CONTR**	**ENTROPY**	**CORR**
7a-C	X	X	X	X	X	X																
7a-E	X	X	X	X	X		X															
7a-R	X	X	X	X	X			X														
7b-C	X								X	X	X	X	X									
7b-E	X								X	X	X	X		X								
7b-R	X								X	X	X	X			X							
7c-C	X															X	X	X	X	X		
7c-E	X															X	X	X	X		X	
7c-R	X															X	X	X	X			X
7d-C	X	X	X	X	X	X			X	X	X	X	X									
7d-E	X	X	X	X	X		X		X	X	X	X		X								
7d-R	X	X	X	X	X			X	X	X	X	X			X							
7e-C	X								X	X	X	X	X			X	X	X	X	X		
7e-E	X								X	X	X	X		X		X	X	X	X		X	
7e-R	X								X	X	X	X			X	X	X	X	X			X
7f-C	X	X	X	X	X	X										X	X	X	X	X		
7f-E	X	X	X	X	X		X									X	X	X	X		X	
7f-R	X	X	X	X	X			X								X	X	X	X			X
7g-C	X	X	X	X	X	X			X	X	X	X	X			X	X	X	X	X		
7g-E	X	X	X	X	X		X		X	X	X	X		X		X	X	X	X		X	
7g-R	X	X	X	X	X			X	X	X	X	X			X	X	X	X	X			X
7h-CE	X	X	X	X	X	X	X		X	X	X	X	X	X		X	X	X	X	X	X	
7h-CR	X	X	X	X	X	X		X	X	X	X	X	X		X	X	X	X	X	X		X
7h-ER	X	X	X	X	X		X	X	X	X	X	X		X	X	X	X	X	X		X	X

4.1.2 Spectral Signatures

For the nine classes, pixels were collected from multiple polygons (ROI's) over the 44 band image; SVM uses all the individual pixels assigned to each class, not their statistical attributes. Table 11 reports the means and standard deviations for the data in each band of the 44 band layer stack; Figure 28 shows the mean spectral signatures. Although many of the spectral signatures plotted in Figure 28 appear similar, differences are apparent in several bands. The signatures for water and urban areas seem the most different while, as expected, the vegetation classes appear the most similar. RADARSAT-2 and Palsar despeckled HH despeckled and variance data show low values; RADARSAT-2 entropy and Palsar correlation have high values.

4.1.3 Training and Ground Truth

Multiple polygons for each class were used to collect pixels for classification training covering the extents of the image (Figure 29) and all the pixels were analyzed. The locations of the GT polygons are shown in Figure 30 over a single the NIR band from the RapidEye EO image in the layer stack; classes were selected evaluating natural color and ICC images, as well as visualizations with SAR bands. The GT polygons were displayed alongside the training polygons over the test image to assure they were not located in the same places and were similarly distributed. Table 12 reports the number of pixels and area in square kilometers for the training and GT polygons. The number of pixels collected represented many times the number of classes.

Table 11. Training ROI mean and standard deviation for each of the nine classes in Wad Medani.

		Water		BarrenGnd		UrbanLow		UrbanMed		SparseForest		Orchard&Trees		GreenCrops		Fallow		BareSoil	
Band	Data Type	Mean	Stdev	Mean	Stdev	Mean	Stdev	Mean	Stdev	Mean	Stdev	Mean	Stdev	Mean	Stdev	Mean	Stdev	Mean	Stdev
1	RapidEye_Blue	4,120.08	2,577.24	15,599.82	6,507.67	19,848.60	5,806.60	18,834.10	3,756.78	1,450.47	1,505.62	3,051.26	3,430.23	4,036.79	2,543.92	17,983.56	2,596.51	13,086.50	2,485.34
2	RapidEye_Green	4,004.98	3,013.39	19,844.16	8,532.92	24,903.69	7,929.42	23,976.14	3,936.80	2,091.05	1,622.72	4,973.55	4,235.58	6,867.05	4,418.93	24,138.88	3,198.56	15,846.10	3,125.56
3	RapidEye_Red	5,881.86	5,130.32	31,824.10	11,004.08	38,237.80	9,021.88	38,386.56	6,927.31	6,626.65	4,558.87	8,932.86	7,363.59	14,513.03	5,591.30	42,159.71	5,459.55	26,245.13	3,590.27
4	RapidEye_RedEdge	765.72	3,081.87	21,047.22	7,993.05	26,340.26	6,892.89	26,364.44	3,065.29	2,790.43	3,823.36	11,525.46	7,178.75	14,083.95	7,374.10	29,051.50	3,728.80	16,678.49	4,855.78
5	RapidEye_NIR	5,974.90	6,871.72	29,363.33	7,134.01	34,550.00	5,124.71	37,587.85	3,233.09	30,028.47	5,022.02	43,657.37	6,322.42	37,992.98	4,422.54	41,067.55	3,644.29	24,618.25	3,468.95
6	TerraSar-X_HH_Despeckled	64.87	142.94	38.07	79.96	1,763.10	2,322.47	12,351.72	10,669.13	710.79	639.37	944.09	2,714.72	327.14	277.75	323.62	336.71	366.88	378.45
7	TerraSar-X__Variance_7x7	5,045.34	7,972.27	2,261.66	2,523.60	12,509.92	7,324.13	2,669.76	3,876.77	4,143.27	1,921.65	4,576.58	2,694.52	4,154.94	2,107.44	3,982.21	2,153.56	3,519.02	1,928.02
8	TerraSar-X__Variance_11x11	6,556.34	8,587.78	2,666.34	2,846.67	14,645.69	6,944.47	3,378.53	4,008.74	4,634.64	1,696.26	5,403.85	2,986.30	4,792.64	2,015.71	4,664.21	2,199.21	3,966.57	1,797.82
9	TerraSar-X__Variance_21x21	10,512.43	9,012.30	3,354.81	3,362.54	17,086.49	5,882.76	4,616.92	4,141.37	5,299.57	1,706.82	7,020.19	3,952.94	5,882.36	2,226.51	5,786.90	2,413.96	4,746.61	1,722.43
10	TerraSar-X__Contrast_7x7	4,720.99	5,567.35	3,542.71	3,051.00	18,328.37	9,507.63	4,981.90	6,280.12	7,811.81	3,383.17	7,906.95	4,272.12	7,169.99	3,300.06	6,871.30	3,296.30	6,128.32	3,020.73
11	TerraSar-X__Entropy_7x7	6,860.48	6,457.27	4,913.20	3,551.35	24,977.93	10,117.54	7,343.79	6,788.58	10,765.19	3,443.85	10,945.41	4,517.84	9,844.17	3,319.03	9,399.07	3,465.75	8,453.76	3,231.64
12	TerraSar-X__Correlation_7x7	10,741.27	6,313.64	6,933.45	4,030.15	34,324.67	9,981.27	11,625.92	7,688.20	15,012.78	3,480.42	15,806.48	4,647.82	13,901.18	3,273.67	13,242.48	3,610.60	12,095.40	3,297.20
13	TerraSar-X__Contrast_11x11	60,777.47	3,401.77	62,909.45	2,013.01	51,825.21	14,469.50	20,615.81	14,465.66	57,675.46	8,816.31	51,922.15	12,427.68	61,481.65	8,011.53	62,532.89	6,416.60	61,163.60	11,041.81
14	TerraSar-X__Entropy_11x11	58,753.56	3,782.70	61,452.46	1,807.64	51,581.93	11,955.97	20,742.34	11,294.51	56,280.25	8,014.59	50,893.78	10,503.62	60,567.98	6,843.71	61,823.34	5,212.11	60,336.72	10,441.58
15	TerraSar-X__Correlation_11x11	56,589.75	4,330.30	58,966.01	2,091.37	52,063.08	8,814.75	22,693.89	9,859.46	54,226.38	7,909.50	49,947.51	8,893.42	59,357.76	5,102.10	60,829.29	3,875.37	59,300.55	9,300.42
16	TerraSar-X__Contrast_21x21	43,759.66	10,430.22	39,840.88	8,476.22	41,436.89	10,808.38	31,174.66	15,026.84	35,973.27	8,999.77	37,139.11	10,338.23	38,786.02	8,820.01	38,696.43	8,683.96	38,189.66	8,942.04
17	TerraSar-X__Entropy_21x21	43,631.06	10,316.92	37,047.88	7,588.16	39,340.08	9,736.93	23,658.03	14,297.52	32,141.44	7,608.59	34,025.92	10,036.68	35,658.27	8,050.53	36,177.00	7,763.11	34,421.26	8,325.54
18	TerraSar-X__Correlation_21x21	50,552.49	7,110.16	38,838.54	6,282.31	41,846.64	5,979.63	28,165.13	12,864.46	32,545.07	5,499.28	36,870.53	8,546.68	37,261.05	6,856.02	38,032.07	6,791.02	35,819.05	6,215.29
19	RadarSat-2_HH_Despeckled	661.75	1,853.06	523.92	701.86	2,850.42	5,999.41	3,132.50	3,617.84	2,713.01	2,506.91	3,873.03	4,197.47	2,778.88	3,193.15	3,049.62	3,696.79	2,894.06	2,961.05
20	RadarSat-2__Variance_7x7	259.35	882.99	80.37	486.45	3,324.20	7,185.85	1,652.31	2,140.12	596.12	296.57	2,155.51	2,272.71	1,098.09	1,498.40	1,013.77	1,406.84	857.60	743.66
21	RadarSat-2__Variance_11x11	476.59	1,034.94	137.81	700.01	4,785.15	9,247.42	2,701.02	2,518.21	911.32	358.64	3,464.41	2,937.21	1,767.47	2,096.27	1,544.86	1,791.79	1,422.79	1,054.75
22	RadarSat-2__Variance_21x21	1,431.15	1,062.95	289.02	1,078.06	6,713.21	10,117.66	5,674.02	4,689.79	1,726.86	651.82	6,461.60	5,069.22	3,710.97	3,675.57	2,834.75	2,402.22	2,946.26	1,860.16
23	RadarSat-2__Contrast_7x7	249.45	751.35	52.92	280.36	3,923.43	9,235.38	1,832.87	1,964.25	891.82	601.07	2,380.54	2,605.72	1,113.77	1,511.24	1,477.49	2,613.31	1,087.18	1,072.10
24	RadarSat-2__Entropy_7x7	8,359.22	14,714.28	11,071.75	8,281.67	38,691.04	10,241.19	49,281.00	6,273.56	48,451.40	5,344.99	51,665.24	8,654.97	46,207.05	8,256.45	47,071.43	9,812.24	47,983.45	7,174.53
25	RadarSat-2__Correlation_7x7	47,706.46	20,825.28	24,713.60	13,995.93	23,276.68	7,070.35	20,557.97	6,067.53	20,992.60	6,356.91	22,454.76	7,001.73	22,713.55	6,761.09	22,224.74	6,790.65	23,370.72	6,855.82
26	RadarSat-2__Contrast_11x11	351.74	761.74	79.93	434.36	4,724.33	9,415.34	2,578.89	2,429.39	1,175.27	682.65	3,127.14	2,779.57	1,503.38	1,776.66	1,830.45	2,788.14	1,430.57	1,147.46
27	RadarSat-2__Entropy_11x11	9,286.42	13,195.96	9,961.88	6,767.67	35,288.51	9,529.45	45,661.35	5,768.11	44,402.92	4,871.47	48,555.93	8,157.31	42,808.87	7,871.89	43,408.54	8,672.22	44,349.32	6,530.53
28	RadarSat-2__Correlation_11x11	31,693.01	20,919.40	15,920.41	7,523.70	18,789.90	5,601.82	15,354.08	4,757.55	15,425.67	4,976.91	17,486.21	5,284.66	18,141.94	5,353.78	17,768.75	5,572.65	18,966.85	5,682.85
29	RadarSat-2__Contrast_21x21	837.42	955.84	167.77	830.49	5,411.42	8,414.01	4,368.68	3,028.94	1,723.44	825.51	4,329.44	2,800.92	2,428.52	2,289.53	2,520.50	2,848.88	2,246.66	1,401.65
30	RadarSat-2__Entropy_21x21	13,715.88	11,002.89	9,117.38	5,735.86	30,795.36	8,313.46	40,911.94	5,862.88	39,408.95	4,422.18	43,724.80	6,862.44	39,145.03	7,164.13	39,040.96	7,200.61	40,525.22	5,715.81
31	RadarSat-2__Correlation_21x21	19,457.52	5,982.52	11,728.67	5,023.55	15,294.77	4,507.37	11,993.94	3,475.75	10,825.25	3,816.37	15,279.32	5,282.01	14,742.85	4,301.82	14,762.84	4,929.03	15,849.02	4,446.41
32	Palsar_HH_Despeckled	55.92	91.90	36.56	61.97	1,608.68	1,761.37	11,948.21	8,625.98	725.38	613.93	967.55	2,662.50	321.67	250.14	318.17	302.67	363.90	348.71
33	Palsar__Variance_7x7	7.91	45.41	1.23	24.33	506.45	1,285.95	14,678.74	13,242.91	22.24	27.56	549.86	3,442.41	4.67	7.87	21.85	406.68	8.37	14.48
34	Palsar__Variance_11x11	14.04	48.49	2.45	34.75	685.29	1,606.83	15,350.13	10,803.66	25.73	27.72	657.78	3,947.10	6.02	13.29	54.40	586.60	11.09	24.11
35	Palsar__Variance_21x21	42.40	156.80	10.40	99.37	2,009.06	4,625.36	25,550.60	13,291.47	63.04	63.99	1,603.16	8,233.29	23.71	66.49	167.57	950.73	46.93	199.54
36	Palsar__Contrast_7x7	6.10	39.88	1.54	34.25	623.50	1,398.12	19,974.60	16,314.85	23.33	37.01	635.44	4,017.81	6.22	15.69	16.82	249.00	14.96	29.33
37	Palsar__Entropy_7x7	894.09	3,347.04	127.38	1,391.98	32,856.28	12,972.35	61,710.82	2,802.59	9,254.36	12,048.35	10,955.90	14,429.96	3,102.86	6,406.09	3,060.32	6,927.06	5,951.76	9,166.25
38	Palsar__Correlation_7x7	61,898.78	12,264.36	34,291.53	32,561.44	28,916.92	9,563.70	27,669.06	10,357.68	31,480.49	25,420.97	38,944.33	22,427.24	53,731.01	19,282.36	46,454.69	25,832.57	49,469.14	21,087.86
39	Palsar__Contrast_11x11	12.61	49.24	2.87	42.26	838.20	1,864.30	21,206.27	14,273.13	26.29	39.73	683.92	4,138.35	8.12	28.10	43.56	482.97	18.39	34.66
40	Palsar__Entropy_11x11	1,512.03	4,032.53	175.21	1,643.83	29,433.69	10,800.28	60,127.86	2,823.58	7,924.92	10,151.52	9,896.22	12,900.82	2,885.66	4,988.27	2,797.94	5,723.69	5,300.55	7,435.46
41	Palsar__Correlation_11x11	57,883.40	16,597.59	33,296.94	32,480.69	24,481.09	8,538.02	24,547.53	10,259.88	27,160.42	25,396.26	27,581.29	21,320.47	44,746.07	24,467.92	39,325.78	27,450.03	40,913.93	24,929.24
42	Palsar__Contrast_21x21	42.20	239.29	10.11	103.04	2,083.01	4,457.66	29,346.95	14,670.65	47.62	66.40	1,446.26	7,237.53	23.82	78.97	147.41	936.06	52.14	228.79
43	Palsar__Entropy_21x21	2,375.24	3,896.50	337.91	2,189.23	25,482.62	8,529.54	56,888.12	4,281.67	6,886.18	8,531.34	8,775.20	11,706.51	2,922.67	3,679.09	2,334.20	4,229.09	4,954.57	5,767.11
44	Palsar__Correlation_21x21	39,069.86	25,162.79	28,777.15	31,671.81	22,178.03	8,370.64	24,487.57	7,241.35	27,040.29	25,562.09	16,142.00	12,137.28	26,946.18	25,195.93	29,852.30	26,941.68	30,786.57	25,413.22

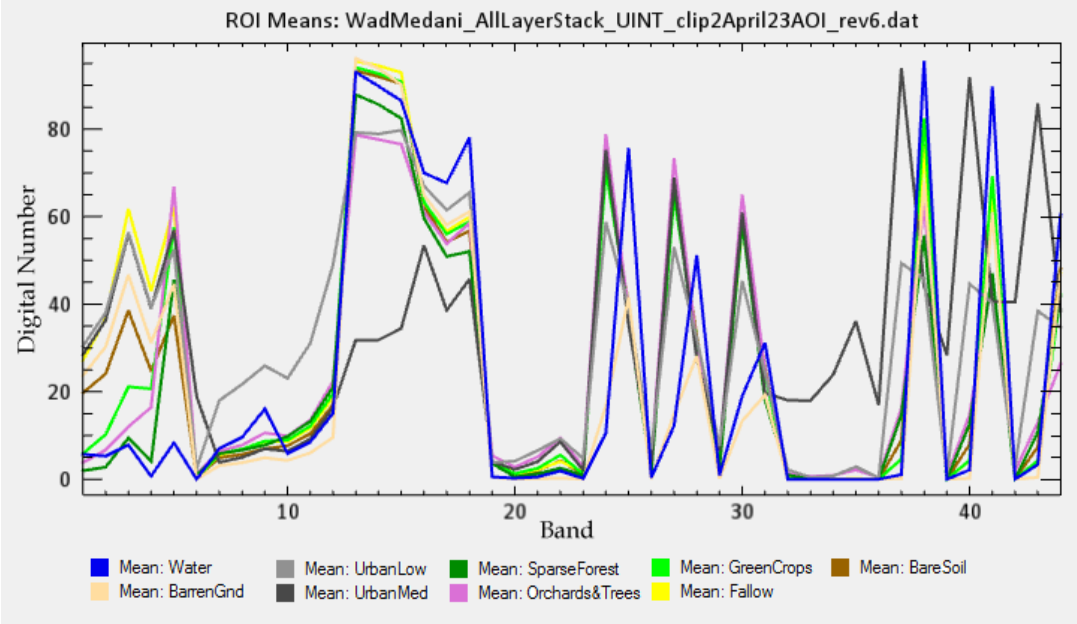

Figure 28. Mean spectral signatures for the 44 bands for nine classes in Wad Medani, Sudan.

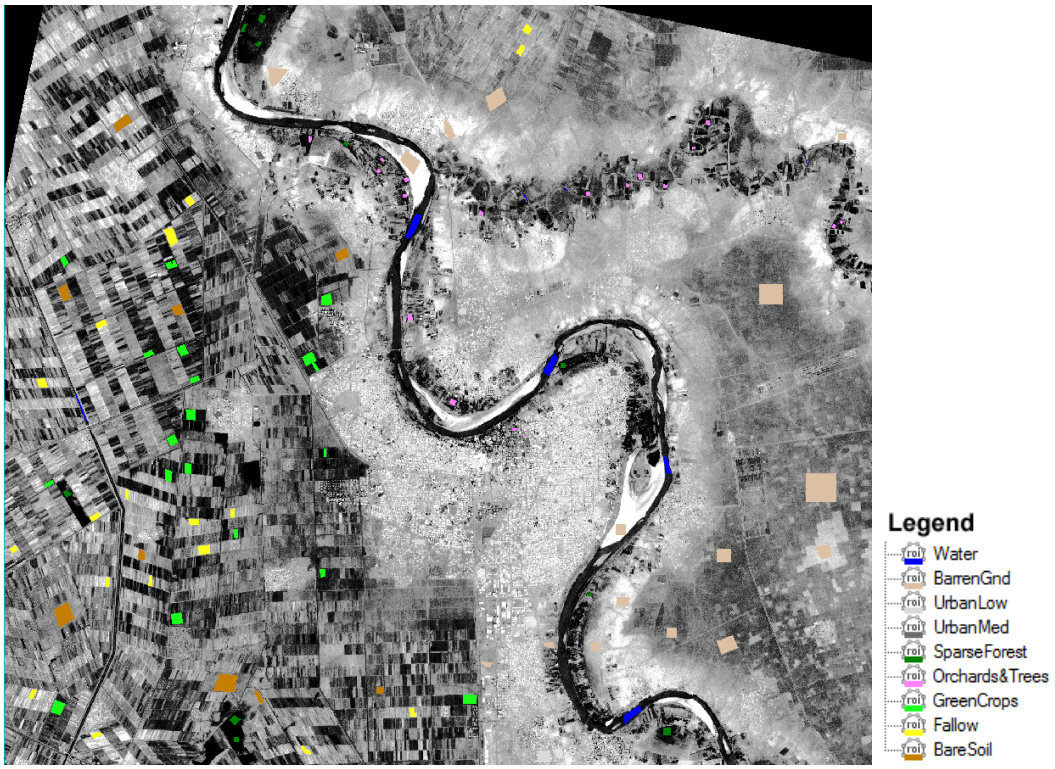

Figure 29. Training ROI's for the nine land cover classes over the RapidEye NIR band from the image stack over Wad Medani, Sudan. Scene width ~ 30 km.

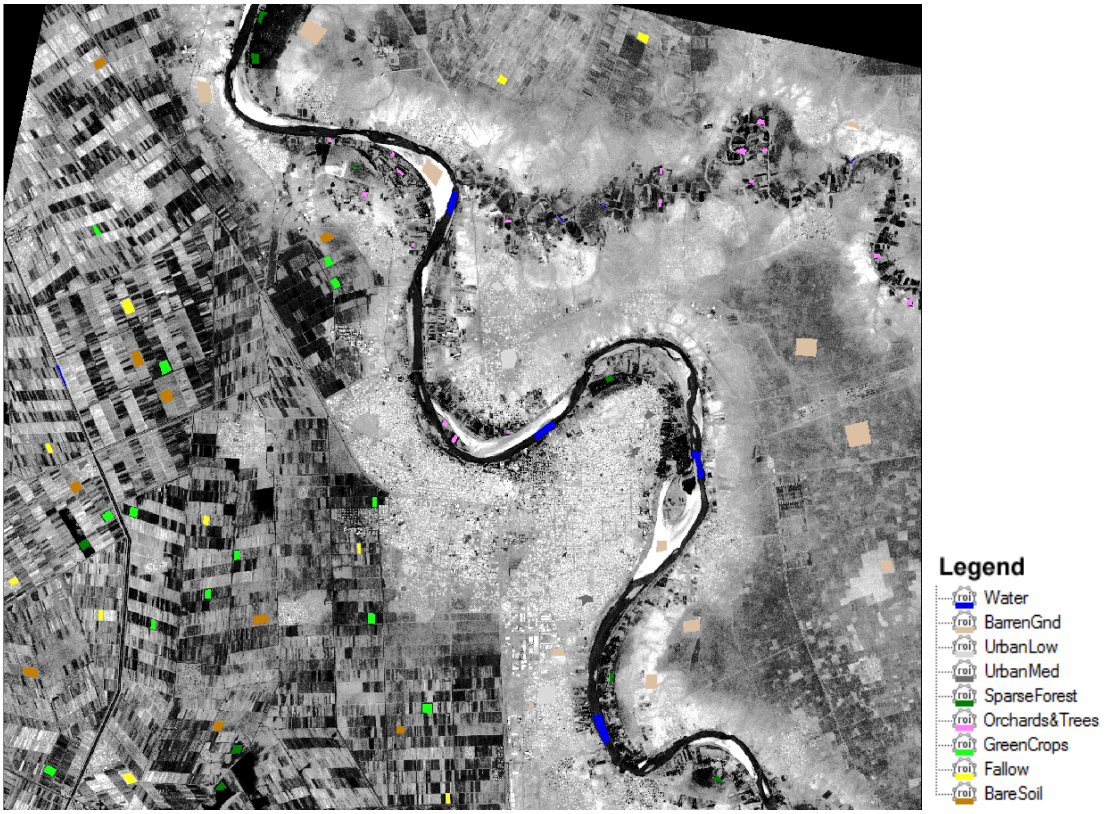

Figure 30. GT ROI's for nine land cover classes over the RapidEye NIR band from the image stack over Wad Medani, Sudan. Scene width ~ 30 km.

Table 12. Number of pixels and area for training and GT for each land cover class in Wad Medani, Sudan.

	Training		Ground Truth	
Class	Pixels	sq km	Pixels	sq km
BareSoil	6,192	0.97	3,801	0.59
Fallow	4,835	0.76	2,587	0.40
GreenCrops	6,672	1.04	3,822	0.60
Orchards&Trees	1,446	0.23	1,594	0.25
SparseForest	1,596	0.25	1,951	0.30
UrbanMed	1,062	0.17	1,623	0.25
UrbanLow	2,528	0.40	4,369	0.68
BarrenGnd	16,043	2.51	10,415	1.63
Water	2,796	0.44	3,375	0.53

4.1.4 Decision Rule Evaluation

The decision rule is the algorithm that assigns one of the classes to each pixel. Although the maximum likelihood algorithm is one of the most common does not always have the best performance. With the advance in the computational capability of personal computers and commercial-off-the-shelf (COTS) software, several other decision rule algorithms are available to the researcher. Four decision rules were compared in this study using the entire 44 band layer stacked image and the results are presented in Table 13. The support vector machine (SVM) decision rule was the best algorithm in overall accuracy and in all but two of the classes (sparse forest and orchards&trees) in user's accuracy. It was more accurate than the maximum likelihood algorithm in all classes but urban-med. For the rest of the tests for Wad Medani, the SVM decision rule was used.

Table 13. User's and producer's accuracy for four different decision rules using all 44 bands for the Wad Medani study site.

User's Accuracy	Maximum	Mahalanobis	Neural	Support Vector	Producer's Accuracy	Maximum	Mahalanobis	Neural	Support Vector
Class/Decision Rule	Liklihood	Distance	Network	Machine	Class/Decision Rule	Liklihood	Distance	Network	Machine
Water	98.23	95.86	97.77	98.25	Water	90.28	85.04	93.48	96.39
BarrenGnd	94.86	97.41	97.07	97.59	BarrenGnd	92.94	86.63	97.88	98.77
UrbanLow	89.37	98.54	94.57	97.08	UrbanLow	99.08	91.42	96.93	95.79
UrbanMed	99.15	99.14	96.28	97.63	UrbanMed	93.59	99.38	98.95	96.55
SparseForest	89.21	76.43	96.80	92.27	SparseForest	53.00	82.27	72.78	73.40
Orchards&Tree	44.56	50.22	63.60	56.18	Orchards&Tree	51.88	63.11	22.15	57.03
GreenCrops	69.99	67.69	69.52	77.46	GreenCrops	80.93	62.77	92.15	85.58
Fallow	80.76	55.48	88.29	93.02	Fallow	89.10	74.80	86.86	93.74
BareSoil	95.35	84.21	92.85	97.51	BareSoil	89.48	98.95	98.42	96.69
Overall Accuracy	87.17	84.10	90.86	92.45					
Kappa Coefficient	0.85	0.81	0.89	0.91					

4.1.5 Classification Accuracy

4.1.5.1 Test 1 - EO Imagery

The first of seven test series was to establish the base-line classification accuracies for nine land-cover classes with EO imagery in five bands (blue, green, red,

red-edge, and near-infrared). The error matrix results are in Table 14. The overall accuracy was 68%; water was classified with the highest accuracy and the urban-med class with the lowest (Table 15). Figure 31 contains the classification thematic map and class color legend using only EO data. The following test series have many possible combinations and comparisons so only the error matrix with the best overall accuracy is presented.

Table 14. EO baseline error matrix for the for Wad Medani, Sudan.

Number of Pixels											
Class	**Water**	**BarrenGnd**	**UrbanLow**	**UrbanMed**	**SparseForest**	**Orchards&Tree**	**GreenCrops**	**Fallow**	**BareSoil**	**Total**	**User's Acc.**
Water	3232	0	0	0	0	1	3	0	0	3236	99.88%
BarrenGnd	74	9766	3083	827	3	0	5	251	2049	16058	60.82%
UrbanLow	7	174	673	195	0	0	1	46	11	1107	60.79%
UrbanMed	1	28	226	211	1	11	3	94	0	575	36.70%
SparseForest	6	0	0	0	1087	4	101	0	0	1198	90.73%
Orchards&Tree	0	0	0	0	184	532	208	0	0	924	57.58%
GreenCrops	27	2	12	35	672	1023	3439	47	1	5258	65.41%
Fallow	0	433	372	311	4	23	61	2133	0	3337	63.92%
BareSoil	28	12	3	44	0	0	1	16	1740	1844	94.36%
Total	3375	10415	4369	1623	1951	1594	3822	2587	3801	33537	overall
Producer's Acc.	95.76%	93.77%	15.40%	13.00%	55.72%	33.38%	89.98%	82.45%	45.78%		68.02%
Overall Accuracy = (22813/33537) 68.02%											
Kappa Coefficient = 0.60											

Table 15. Error matrix result summary for Wad Medani, Sudan using EO imagery.

Class	Prod. Acc. (Percent)	User Acc. (Percent)
Water	95.76	99.88
BarrenGnd	93.77	60.82
UrbanLow	15.40	60.79
UrbanMed	13.00	36.70
SparseForest	55.72	90.73
Orchards&Tree	33.38	57.58
GreenCrops	89.98	65.41
Fallow	82.45	63.92
BareSoil	45.78	94.36

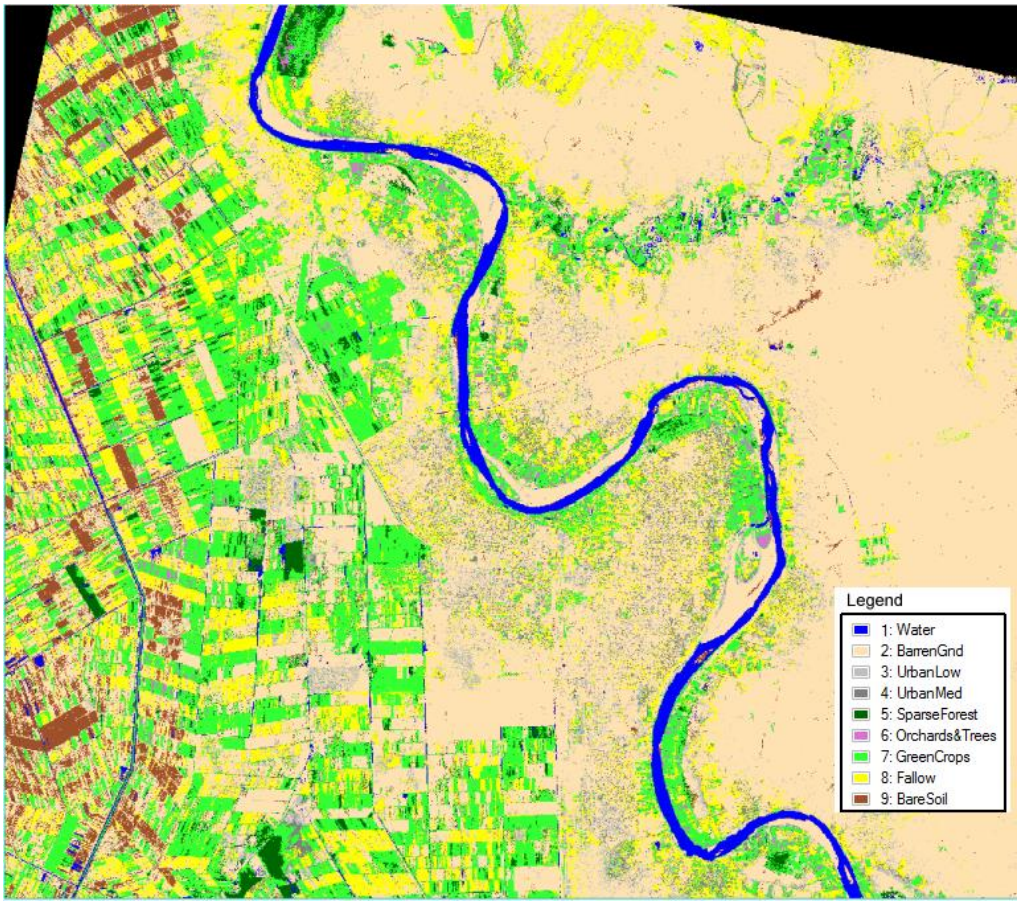

Figure 31. Land cover classification thematic map for Wad Medani, Sudan using EO imagery. Scene width ~ 30 km.

4.1.5.2 Test Series 2 - EO + SAR-HH

Test series 2 added despeckled HH SAR polarization data to EO imagery and compares between X, C, and L-band SAR as well as combinations of the different SAR bands. Table 16 summarizes the results of the seven tests. The best overall accuracy of 84.1% was achieved using all three SAR bands with EO; the worst was with the C-band and EO but it was still 5.1% better than EO alone.

X and L-band SAR individually improved the classification user's accuracy by about same amount compared to EO alone while C-band SAR was less effective. The

combination of C-band with the other bands was slightly better than L-band with the other two. In all cases, the land cover classes that had poor accuracies with EO alone were classified better by adding SAR. The orchards&trees LC class had the worst accuracy even with the addition of the SAR bands; urban areas were classified much better.

4.1.5.1 Test Series 3 – EO + SAR-HH + SAR-Variance

Test series 3 added the variance texture calculated with three different kernel sizes from the original SAR despeckled HH data, not from the despeckled data. The addition of texture to EO and SAR despeckled HH was compared for each SAR band and each kernel size. Different combinations of variance kernel windows were compared using all SAR bands together. The main question was to understand the impact of kernel size on classification accuracy because each SAR band has a different wavelength, so the impact of kernel size could be different. The results for each SAR band and different kernel sizes are in Table 17.

With the exception of the 7x7 kernel window and X-band SAR, there was less than 1% difference between the SAR bands and different kernel sizes. For X-band, the 7x7 kernel window overall accuracy was about 5% higher than with the other kernel sizes, about 7% better than with L-band SAR, and about 14% better than with C-band SAR. Table 18 shows the results for the different variance texture kernels for all the SAR bands combined, and Table 19 reveals the results for combinations of the variance window kernels. The difference in classification accuracy between the different kernel windows was less than 1% when using all the SAR bands and different combinations of

the variance kernels. The best overall classification accuracy of 83.93% was 15.91% higher than using EO alone.

Table 16. Classification results for Wad Medani, Sudan using EO imagery and SAR despeckled HH.

Producers Accuracy							
Class	X	C	L	X+C	C+L	X+L	X+C+L
Water	95.82	95.67	95.79	95.67	95.67	95.82	95.82
BarrenGnd	94.54	91.61	94.29	93.38	93.45	94.34	93.81
UrbanLow	81.09	36.74	78.12	78.35	73.22	82.03	80.45
UrbanMed	92.61	15.83	91.56	92.85	91.62	94.89	94.95
SparseForest	60.48	55.46	59.30	60.84	59.71	59.97	60.58
Orchards&Tree	38.14	33.38	36.83	38.14	37.77	38.27	38.39
GreenCrops	89.04	88.25	89.64	87.49	88.30	88.72	87.81
Fallow	86.01	81.37	85.85	85.35	85.35	86.01	85.16
BareSoil	43.36	73.59	43.30	73.38	73.32	47.28	73.51
Users Accuracy							
Class	X	C	L	X+C	C+L	X+L	X+C+L
Water	99.91	99.88	99.91	99.88	99.88	99.91	99.91
BarrenGnd	78.62	75.05	78.16	85.97	85.17	79.74	86.45
UrbanLow	94.45	68.18	93.87	95.43	94.45	96.03	96.49
UrbanMed	95.92	37.03	95.13	95.87	95.08	97.10	97.16
SparseForest	93.50	90.77	93.08	93.10	93.27	94.58	94.48
Orchards&Tree	55.58	53.63	56.66	53.10	55.03	55.10	53.87
GreenCrops	67.55	64.95	66.91	67.18	66.73	67.16	67.08
Fallow	71.80	57.42	70.24	71.80	69.54	71.29	72.02
BareSoil	83.87	79.91	83.22	83.03	83.22	83.78	84.00
Overall Accuracy	81.07%	73.12%	80.48%	83.55%	82.85%	81.63%	84.09%
Kappa Coefficient	0.77	0.67	0.76	0.80	0.79	0.78	0.81

Table 17. Classification results for Wad Medani, Sudan using EO imagery, SAR despeckled HH, and three texture variance kernels, per SAR band.

Producer's Accuracy		X			C			L	
Class	7	11	21	7	11	21	7	11	21
Water	97.60	95.97	95.73	95.61	95.59	95.67	95.73	95.73	95.73
BarrenGnd	95.30	92.02	91.83	91.51	91.41	91.55	94.53	94.53	93.93
UrbanLow	75.87	78.92	79.81	37.03	37.03	36.58	81.76	81.96	82.19
UrbanMed	88.32	92.73	92.91	14.60	14.73	15.34	93.10	92.67	92.85
SparseForest	84.27	59.10	61.92	55.30	55.51	55.20	60.69	61.51	62.22
Orchards&Tree	46.75	38.64	41.03	33.38	33.75	33.56	37.14	37.01	35.32
GreenCrops	96.45	87.99	86.11	87.18	87.10	87.10	88.33	88.33	88.93
Fallow	93.42	83.65	85.89	81.72	81.37	81.37	85.85	85.78	84.96
BareSoil	64.29	70.22	74.88	73.24	73.22	72.93	42.36	42.36	42.25
User's Accuracy		X			C			L	
Class	7	11	21	7	11	21	7	11	21
Water	97.60	99.72	99.72	99.88	99.88	99.85	99.91	99.91	99.91
BarrenGnd	95.30	84.94	86.58	74.94	74.85	74.63	78.50	78.39	78.08
UrbanLow	75.87	92.61	95.07	67.93	67.84	68.32	94.47	94.54	95.00
UrbanMed	88.32	95.92	95.93	36.52	36.43	37.50	98.24	99.60	99.41
SparseForest	84.27	93.06	92.71	90.60	90.78	90.73	92.79	92.88	92.96
Orchards&Tree	46.75	54.23	52.53	51.85	51.98	51.84	54.51	55.50	56.30
GreenCrops	96.45	67.21	68.00	64.50	64.60	64.52	67.05	67.01	66.78
Fallow	93.42	70.60	72.50	57.26	57.02	57.20	71.25	70.99	70.86
BareSoil	64.29	81.62	80.01	79.95	80.11	80.00	83.51	83.55	81.15
Overall	87.63%	82.72%	83.52%	72.92%	72.88%	72.84%	80.93%	80.97%	80.78%
Kappa	0.84	0.79	0.80	0.67	0.67	0.67	0.77	0.77	0.77

Combining all SAR bands with at least one variance texture shows about a 1% improvement over using two SAR bands. The best classification accuracy for this test series was with X-band SAR and the 7x7 variance texture kernel although only about 2% better. Removing the despeckled SAR despeckled HH data from the test for this series resulted in a drop of about 2% in the classification accuracy using all variance texture kernels and all SAR bands.

Table 18. Classification results for Wad Medani, Sudan using EO imagery, SAR despeckled HH, and three texture variance kernels, per combinations of SAR bands.

Producer's Accuracy		X+C			C+L			X+L	
Class	7	11	21	7	11	21	7	11	21
Water	95.73	95.76	95.56	95.82	95.88	95.82	96.44	96.98	97.19
BarrenGnd	93.35	92.94	94.43	94.84	95.46	95.24	91.14	89.89	88.70
UrbanLow	77.73	76.75	77.20	80.89	81.92	83.66	87.32	88.17	82.79
UrbanMed	93.22	92.73	93.10	92.48	89.46	89.77	95.75	95.19	94.95
SparseForest	58.89	59.05	62.74	61.97	63.81	66.07	60.84	61.25	63.15
Orchards&Tree	38.21	38.64	40.59	37.20	37.33	35.70	36.95	38.21	43.16
GreenCrops	87.07	85.66	84.96	84.85	84.14	85.53	87.83	88.10	88.88
Fallow	83.61	83.88	86.16	84.19	83.76	83.92	85.62	85.70	85.16
BareSoil	79.87	82.24	79.69	73.22	73.03	69.51	58.35	59.25	63.67
User's Accuracy		X+C			C+L			X+L	
Class	7	11	21	7	11	21	7	11	21
Water	99.69	99.75	99.78	99.75	99.75	99.81	99.88	99.60	99.18
BarrenGnd	88.01	88.69	88.33	86.22	86.31	85.59	82.18	82.43	83.49
UrbanLow	92.61	92.65	95.01	95.54	94.09	92.34	92.80	91.91	87.71
UrbanMed	95.76	95.86	95.94	97.98	99.66	98.45	98.54	99.36	99.68
SparseForest	92.59	92.38	92.66	93.22	93.89	94.29	93.24	93.00	95.14
Orchards&Tree	52.59	50.74	51.07	48.33	48.37	51.12	53.06	54.91	60.03
GreenCrops	66.75	66.57	67.65	66.65	66.60	66.84	67.02	67.45	68.85
Fallow	72.12	70.50	72.02	73.91	74.70	76.85	73.49	72.76	68.10
BareSoil	83.89	83.67	85.04	85.11	86.02	85.95	84.21	82.98	83.88
Overall	83.93%	83.81%	84.44%	83.95%	84.11%	84.10%	82.54%	82.51%	82.34%
Kappa	0.81	0.81	0.81	0.81	0.81	0.81	0.79	0.79	0.79

4.1.5.2 Test Series 4 - EO+SAR-HH+SAR-GLCM (w/o Variance)

Test series 4 tested the impact of the Gray Level Co-occurrence Matrix texture measures (combined) using three kernel sizes without variance texture. Table 20 shows the results for the different kernel sizes for each SAR band alone. In this case, the 21x21 kernel seemed to perform better and the accuracy improved with kernel size. For the X-band SAR, there was a 3% increase to 84.2%. For C-band SAR the difference was less than 1% reaching 80.38%. The classification accuracy for the L-band SAR with the 21x21 kernel size reached 88.32%, over a 4% improvement over the 7x7 kernel.

Table 19. Classification results for Wad Medani, Sudan using EO imagery, SAR despeckled HH, and three texture variance kernels, and all SAR bands.

Producer's Accuracy				X+C+L				W/O HH
Class	7	11	21	7+11	7+21	11+21	7+11+21	7+11+21
Water	96.44	96.98	97.3	96.92	97.24	97.16	97.19	97.21
BarrenGnd	94.09	95.01	94.97	94.9	94.93	95.1	95.03	93.9
UrbanLow	89.72	92.06	93.22	92.13	93.59	93.45	93.18	86.54
UrbanMed	94.89	91.99	91.13	91.68	89.28	88.42	88.6	87.55
SparseForest	62.02	63.2	64.74	62.58	65.25	64.38	63.81	56.79
Orchards&Tree	36.76	38.02	43.6	38.83	42.16	43.16	42.47	40.09
GreenCrops	84.77	85.06	86.29	83.99	85.06	84.82	84.46	83.57
Fallow	84.04	83.84	85.16	83.84	84.89	84.69	84.77	84.62
BareSoil	75.95	74.98	71.01	75.66	72.3	72.93	73.72	70.17
User's Accuracy				X+C+L				W/O HH
Class	7	11	21	7+11	7+21	11+21	7+11+21	7+11+21
Water	99.85	99.63	98.83	99.76	99.42	99.06	99.36	99.3
BarrenGnd	87.58	87.75	87.18	87.87	87.4	87.68	87.86	86.2
UrbanLow	93.62	92.93	91.2	92.76	90.77	90.77	91.11	87.48
UrbanMed	98.21	99.53	99.4	99.4	99.66	99.65	99.79	99.79
SparseForest	93.15	94.12	95.39	93.49	95	94.94	94.97	91.87
Orchards&Tree	47.84	49.35	55.82	47.95	52.38	52.08	50.19	49.23
GreenCrops	66.49	66.91	68.82	66.82	68.54	68.7	68.3	65.49
Fallow	78.37	79.92	81.47	80.1	81.36	81.24	80.65	74.91
BareSoil	91.27	93.84	94.7	93.86	94.76	94.54	94.73	93.97
Overall	85.31%	85.85%	86.13%	85.77%	86.02%	86.03%	85.97%	83.67%
Kappa	0.82	0.83	0.83	0.83	0.83	0.83	0.83	0.80

For the case using two SAR bands, as with the variance texture measures, the overall classification accuracy increased to 91.19% for C+X-band and the 21x21 kernel. For X+C and C+L the differences between the kernel for each pair of SAR bands varied less than 1%; however, for the X+L band combination the accuracy increased with kernel size up to 88.55%. The best SAR band combination with GLCM textures measures was the C+L bands (Table 21).

Table 20. Classification results for Wad Medani, Sudan using EO imagery, SAR despeckled HH, and three texture GLCM kernels, per SAR band.

Producer's Accuracy		X			C			L	
Class	7x7	11x11	21x21	7x7	11x11	21x21	7x7	11x11	21x21
Water	95.85	96.00	95.97	95.61	95.32	95.82	96.50	96.86	97.27
BarrenGnd	93.36	91.45	90.38	94.34	94.90	95.63	90.03	89.92	90.85
UrbanLow	94.64	96.15	98.58	51.13	61.50	48.39	86.52	89.36	95.40
UrbanMed	95.93	96.12	91.37	41.28	27.48	37.15	93.96	94.64	94.58
SparseForest	60.74	64.07	65.61	62.99	58.94	63.71	65.15	67.09	66.32
Orchards&Tree	35.82	36.89	37.26	37.95	37.45	44.10	48.93	50.94	49.87
GreenCrops	89.53	88.91	89.93	82.10	81.66	83.52	91.26	90.55	91.08
Fallow	85.93	86.01	81.18	82.14	83.88	86.32	85.78	86.43	88.75
BareSoil	30.26	40.75	62.75	94.98	96.55	96.66	65.80	74.69	87.00
User's Accuracy		X			C			L	
Class	7x7	11x11	21x21	7x7	11x11	21x21	7x7	11x11	21x21
Water	99.81	99.57	99.66	99.75	99.69	99.75	99.75	99.15	98.18
BarrenGnd	76.26	78.75	84.58	95.76	97.66	94.70	83.82	87.05	92.74
UrbanLow	96.84	97.09	91.52	74.24	72.80	72.65	91.55	93.11	95.05
UrbanMed	99.05	100.00	100.00	47.38	46.51	34.72	94.02	93.94	98.59
SparseForest	90.94	91.44	94.60	88.16	89.84	89.81	93.80	94.10	96.57
Orchards&Tree	55.38	56.65	60.00	50.46	48.81	56.88	62.85	60.87	58.89
GreenCrops	67.66	68.04	68.05	65.59	63.85	67.41	72.62	73.75	73.73
Fallow	74.25	72.12	79.13	53.98	58.41	63.64	74.87	75.72	76.38
BareSoil	87.19	85.30	81.65	83.88	82.79	86.10	84.18	86.48	91.08
Overall Accuracy	81.11%	82.11%	84.20%	79.51%	80.34%	80.38%	84.08%	85.67%	88.32%
Kappa Coefficient	0.77	0.78	0.81	0.76	0.77	0.77	0.81	0.83	0.86

Testing with all three SAR bands combined (Table 22) the best classification overall accuracy (92.7%) resulted from the 21x21 kernel, although combining with the 7x7 kernel the accuracy was nearly the same. The best overall classification accuracy using the GLCM texture measures together was 6.57% higher than the best accuracy using the variance measure (86.13%).

Table 21. Classification results for Wad Medani, Sudan using EO imagery, SAR despeckled HH and three texture GLCM kernels, for combinations of SAR bands.

Producer's Accuracy		X+C			C+L			X+L	
Class	7x7	11x11	21x21	7x7	11x11	21x21	7x7	11x11	21x21
Water	95.97	95.76	95.97	96.18	96.62	97.24	96.65	97.07	97.07
BarrenGnd	96.68	97.05	98.31	96.66	97.17	98.84	91.08	89.82	91.03
UrbanLow	92.93	96.45	87.14	83.84	89.63	80.04	96.13	97.18	98.67
UrbanMed	94.64	95.87	94.89	94.02	93.59	92.85	95.93	95.44	97.72
SparseForest	65.81	66.38	65.86	69.66	72.12	72.37	61.56	67.35	67.45
Orchards&Tree	37.83	38.83	42.10	51.38	49.44	57.90	47.11	50.19	53.89
GreenCrops	83.10	82.21	87.36	88.72	88.23	90.71	90.74	89.09	83.70
Fallow	85.81	87.86	89.91	88.02	90.72	95.40	85.00	85.58	88.94
BareSoil	94.55	97.53	94.55	94.58	97.68	98.21	62.17	74.77	88.61
User's Accuracy		X+C			C+L			X+L	
Class	7x7	11x11	21x21	7x7	11x11	21x21	7x7	11x11	21x21
Water	99.78	99.57	99.51	99.39	98.76	97.42	99.69	99.15	98.56
BarrenGnd	95.47	97.30	93.21	95.58	97.80	98.70	84.11	88.06	93.58
UrbanLow	96.07	97.39	95.37	95.54	95.75	95.68	96.82	96.04	96.57
UrbanMed	98.65	99.81	97.59	92.04	92.85	95.62	98.79	99.94	99.81
SparseForest	92.31	92.30	96.62	92.07	91.54	92.05	93.39	93.32	96.13
Orchards&Tree	47.29	48.21	55.96	63.69	61.61	68.12	60.27	60.38	50.09
GreenCrops	67.06	66.62	68.85	73.27	73.26	77.04	71.34	73.02	74.05
Fallow	81.05	84.72	89.63	75.52	83.23	74.90	77.54	76.29	79.92
BareSoil	94.08	94.30	95.76	93.60	94.67	97.65	83.09	85.06	89.91
Overall Accuracy	88.80%	89.89%	89.57%	89.28%	90.77%	91.19%	84.94%	86.47%	88.55%
Kappa Coefficient	0.87	0.88	0.87	0.87	0.89	0.89	0.82	0.84	0.86

4.1.5.1 Test Series 5 – EO+SAR-HH+SAR-Variance+SAR GLCM

In test series 5 the combined contribution of variance texture and GLCM texture was tested, using the three kernel sizes and the three SAR bands. The kernel sizes used for all the texture measures were the same for each test. Table 23 shows the results per individual SAR band.

As previously reported, the differences within each SAR band between the kernel sizes were very small but greater between the SAR bands; the overall accuracy slightly increased with kernel size. The highest overall accuracy using a single SAR band was 86.28% for X-band using the 21x21 kernel window. The SAR band that resulted in the

higher accuracy was the X-band for all kernels sizes, followed by L-band and then the C-band.

Table 22. Classification results for Wad Medani, Sudan using EO imagery, SAR despeckled HH, and three texture GLCM kernels, for all SAR bands together.

Producer's Accuracy				X+C+L				W/O HH
Class	7x7	11x11	21x21	7+11	7+21	11+21	7+11+21	7+11+21
Water	96.41	97.01	96.98	97.30	96.59	97.24	96.86	96.95
BarrenGnd	97.07	97.57	98.60	98.39	98.80	99.13	98.53	98.50
UrbanLow	95.10	97.85	96.38	93.36	96.80	92.90	95.28	94.62
UrbanMed	94.58	95.81	97.84	95.19	97.04	97.91	96.43	94.52
SparseForest	67.56	72.37	73.60	71.76	72.22	71.86	71.40	69.91
Orchards&Tree	48.18	49.50	57.34	51.76	56.84	52.57	55.14	55.52
GreenCrops	88.41	87.91	84.43	89.06	83.75	83.86	83.99	83.62
Fallow	87.55	90.26	95.05	91.38	96.02	94.86	94.74	94.86
BareSoil	94.16	97.82	97.66	95.79	98.13	96.76	96.55	96.37
User's Accuracy				X+C+L				W/O HH
Class	7x7	11x11	21x21	7+11	7+21	11+21	7+11+21	7+11+21
Water	99.33	98.85	97.56	98.41	97.99	97.71	97.90	97.91
BarrenGnd	95.68	97.91	97.98	97.31	98.57	97.93	97.94	97.89
UrbanLow	96.36	96.68	97.66	96.32	97.74	98.16	97.04	96.41
UrbanMed	98.27	99.62	99.69	98.47	98.81	98.03	97.81	97.40
SparseForest	93.14	92.65	95.35	93.71	94.44	94.28	94.19	94.26
Orchards&Tree	59.21	59.82	55.83	60.89	53.77	50.60	51.55	50.00
GreenCrops	72.08	73.57	76.29	75.06	76.47	75.39	76.34	76.30
Fallow	85.05	89.84	93.68	88.27	92.89	90.29	91.66	91.19
BareSoil	95.26	96.47	97.74	95.72	97.82	97.61	97.43	97.55
Overall Accuracy	90.54%	92.08%	92.70%	91.81%	92.69%	91.93%	92.02%	91.72%
Kappa Coefficient	0.89	0.91	0.91	0.90	0.91	0.90	0.90	0.90

Table 23. Classification results for Wad Medani, Sudan using EO imagery, SAR despeckled HH, and three texture GLCM kernels, and texture variance per SAR band.

Producer's Accuracy		X			C			L	
Class	7x7	11x11	21x21	7x7	11x11	21x21	7x7	11x11	21x21
Water	95.73	95.82	96.03	95.44	95.32	95.67	95.59	95.61	96.09
BarrenGnd	91.93	92.38	92.94	94.34	94.97	95.65	90.92	93.92	93.65
UrbanLow	94.76	96.22	98.40	51.02	61.66	50.79	95.10	96.73	98.63
UrbanMed	96.12	95.93	92.11	41.34	26.62	35.98	88.23	83.49	78.43
SparseForest	60.58	64.38	65.91	62.94	59.15	63.61	54.59	57.15	62.89
Orchards&Tree	38.90	39.52	39.40	37.83	37.33	41.97	37.14	36.95	36.20
GreenCrops	87.23	87.81	88.10	81.74	81.32	82.31	86.50	86.21	88.67
Fallow	80.98	80.60	82.53	81.64	84.31	86.39	82.84	79.32	80.25
BareSoil	63.38	70.48	73.77	94.90	96.55	96.79	53.01	45.91	56.59
User's Accuracy		X			C			L	
Class	7x7	11x11	21x21	7x7	11x11	21x21	7x7	11x11	21x21
Water	99.72	99.63	99.69	99.75	99.75	99.78	99.85	99.78	99.69
BarrenGnd	83.83	86.13	88.66	95.76	97.66	95.95	80.90	79.37	82.50
UrbanLow	96.73	97.02	91.70	74.15	72.56	73.53	95.80	94.99	91.80
UrbanMed	99.17	100.00	100.00	47.19	46.15	34.43	99.31	100.00	100.00
SparseForest	90.44	91.61	94.63	87.84	89.46	90.06	87.37	87.93	93.38
Orchards&Tree	53.08	56.60	56.22	50.33	48.41	53.52	51.21	50.82	56.13
GreenCrops	67.92	68.36	68.45	65.34	63.81	66.51	65.88	65.91	66.67
Fallow	76.74	75.71	80.29	53.78	58.64	62.98	72.94	76.00	76.55
BareSoil	82.84	86.87	89.56	83.57	82.92	85.62	80.89	85.21	91.26
Overall Accuracy	83.93%	85.34%	86.28%	79.38%	80.34%	80.40%	81.71%	81.66%	83.49%
Kappa Coefficient	0.81	0.82	0.84	0.75	0.77	0.77	0.78	0.78	0.80

The results for the tests using two and three SAR bands are shown in Table 24. In all cases the overall accuracy was higher than using a single SAR band. The best accuracy was 91.33% combining all three SAR bands using the 11x11 kernel. The difference in accuracy between the three kernel sizes was <1% for each SAR band and did not increase with kernel size. The overall classification accuracy for the two SAR band cases X+C and C+L was about the same while L+X was slightly lower. By adding a second SAR band, the overall accuracy was improved by 3.69%; adding a third SAR satellite source improved the accuracy only by 1.36%.

Table 24. Classification results for Wad Medani, Sudan using EO imagery, SAR despeckled HH, and three texture GLCM kernels, and variance for combinations of SAR bands.

Producer's Accuracy		X+C			X+L			C+L			X+C+L	
Class	7x7	11x11	21x21	7x7	11x11	21x21	7x7	11x11	21x21	7x7	11x11	21x21
Water	95.88	95.94	95.91	95.79	95.91	96.03	96.50	97.10	97.57	96.00	97.30	97.45
BarrenGnd	97.11	97.18	98.43	96.88	97.82	98.19	88.81	93.57	91.45	97.46	98.76	98.88
UrbanLow	92.74	96.34	88.65	94.19	95.17	84.53	97.32	97.21	98.74	96.96	96.13	96.34
UrbanMed	94.45	96.12	95.07	87.99	85.09	81.64	92.36	88.11	81.82	91.81	88.60	83.18
SparseForest	66.43	66.17	66.79	61.10	65.91	64.68	56.23	56.23	64.58	62.94	65.04	66.17
Orchards&Tree	38.90	40.34	43.35	36.32	35.88	37.14	42.10	49.56	46.61	40.03	53.39	47.11
GreenCrops	83.07	82.47	86.29	81.97	79.98	84.72	82.78	87.96	87.96	80.51	87.26	83.96
Fallow	84.65	87.28	89.37	86.05	85.31	89.83	86.43	82.95	85.23	88.71	88.60	94.40
BareSoil	94.98	97.34	94.19	96.19	96.74	95.61	87.11	74.43	78.74	97.03	96.71	95.69
User's Accuracy		X+C			X+L			C+L			X+C+L	
Class	7x7	11x11	21x21	7x7	11x11	21x21	7x7	11x11	21x21	7x7	11x11	21x21
Water	99.81	99.60	99.54	99.39	99.48	99.26	99.66	98.56	95.45	99.75	98.95	97.54
BarrenGnd	95.44	97.08	93.58	96.20	96.14	92.42	91.92	87.70	90.02	96.69	96.99	97.55
UrbanLow	95.81	97.21	95.75	95.76	95.39	93.59	97.19	96.63	93.56	97.49	97.27	96.54
UrbanMed	98.71	99.68	98.28	98.89	99.07	100.00	99.14	99.58	100.00	98.48	96.70	100.00
SparseForest	92.11	92.74	96.52	89.36	88.51	89.69	86.86	91.34	92.44	88.03	92.83	90.72
Orchards&Tree	48.02	49.61	54.84	43.27	44.20	52.07	46.86	50.48	57.02	44.27	53.12	53.60
GreenCrops	67.44	67.02	69.24	66.25	65.50	66.71	67.35	72.18	70.42	67.21	74.38	70.16
Fallow	81.99	85.43	89.09	81.15	82.85	84.72	69.44	77.00	77.72	85.32	89.36	88.25
BareSoil	94.03	94.10	95.54	93.50	95.38	95.76	89.34	92.51	90.95	96.29	96.99	97.43
Overall Accuracy	88.93%	89.97%	89.72%	88.42%	88.75%	88.07%	85.69%	86.24%	86.54%	89.58%	91.33%	90.87%
Kappa Coefficient	0.87	0.88	0.88	0.86	0.87	0.86	0.83	0.83	0.84	0.88	0.90	0.89

Using all three SAR bands Table 25 presents the results combining texture kernel sizes along with the test removing the despeckled HH SAR data. The results are within 0.22%, but compared to the previous tests accuracy increased to 92.26%, an increase of only 0.93% over the three SAR band example and nearly 6% compared to the case with a single SAR band. A practical implication for the researcher is that adding the third SAR band is less important that using multiple kernel sizes.

Table 25. Classification results for Wad Medani, Sudan using EO imagery, SAR despeckled HH, and three texture GLCM kernels, and variance for all SAR bands together.

Producer's Accuracy	X+C+L				w/o hh
Class	7+11	7+21	11+21	7+11+21	7+11+21
Water	96.80	96.53	97.33	96.53	96.50
BarrenGnd	98.95	98.98	98.81	98.88	98.91
UrbanLow	96.20	97.85	96.68	96.68	96.66
UrbanMed	89.22	84.78	86.57	87.00	86.14
SparseForest	67.86	69.66	74.27	75.24	74.68
Orchards&Tree	55.14	44.98	60.35	57.59	57.78
GreenCrops	85.53	83.12	82.81	83.94	83.70
Fallow	90.10	95.17	94.74	95.05	95.13
BareSoil	97.74	98.53	95.69	97.26	97.24
User's Accuracy	**X+C+L**				**w/o hh**
Class	**7+11**	**7+21**	**11+21**	**7+11+21**	**7+11+21**
Water	99.27	98.46	98.41	98.43	98.52
BarrenGnd	97.34	98.65	97.60	98.07	98.04
UrbanLow	97.54	97.00	96.59	96.35	96.15
UrbanMed	96.73	99.64	97.23	97.58	97.08
SparseForest	89.82	92.26	93.42	93.38	93.10
Orchards&Tree	51.22	50.14	54.32	54.45	53.83
GreenCrops	76.56	70.69	77.55	77.53	77.51
Fallow	90.98	89.85	90.81	91.34	91.69
BareSoil	97.00	97.20	97.38	97.11	97.14
Overall Accuracy	92.26%	92.18%	92.04%	92.26%	92.18%
Kappa Coefficient	0.91	0.91	0.90	0.91	0.91

4.1.5.2 Test Series 6 - SAR-HH+SAR-Variance+SAR-GLCM (w/o EO)

Using all the texture measures and the SAR despeckled HH this test series eliminated EO and showed a baseline for the classification accuracies possible using SAR alone (Table 26). The accuracy using the despeckled HH bands alone and all the texture without the despeckled HH bands were also tested. The lowest user's accuracy was derived from the despeckled HH band alone (49.3%), and the highest accuracy achieved was 60.63%. The removal of the despeckled HH bands increased the accuracy by 2%.

However, a greater accuracy was achieved using the X-band despeckled HH and texture bands (69.61%). The C-band data alone were almost as accurate as the X-band data at 69.02%, and the L-band SAR data were more than 12% less accurate.

Table 26. Classification results for Wad Medani, Sudan using SAR despeckled HH, and three texture GLCM kernels, and texture variance per SAR band, band combinations and all SAR bands. All texture measures were combined.

Producer's Error								L+C+X
Class	L	C	X	L+C	C+X	L+X	L+C+X	w/o HH
Water	41.96	79.32	79.38	67.41	68.50	65.87	80.33	78.61
BarrenGnd	86.36	95.50	95.83	91.90	83.20	82.3	96.00	95.58
UrbanLow	67.54	73.29	71.41	66.74	80.09	82.01	75.94	75.3
UrbanMed	97.41	96.98	96.92	97.23	94.70	94.52	85.52	95.13
SparseForest	24.96	43.67	45.77	36.80	47.72	37.01	44.08	42.49
Orchards&Trees	3.70	39.77	45.04	7.28	38.83	34.38	41.84	44.1
GreenCrops	57.14	44.92	47.44	56.23	46.42	54.63	38.12	43.85
Fallow	3.56	29.65	30.65	23.66	23.70	18.9	36.10	32.93
BareSoil	38.17	46.80	46.70	36.70	34.18	36.67	34.04	48.67
User's Error								L+C+X
Class	L	C	X	L+C	C+X	L+X	L+C+X	w/o HH
Water	73.56	81.89	84.43	70.87	78.48	78.36	82.96	81.43
BarrenGnd	70.30	92.73	92.21	88.83	84.47	80.38	93.19	91.59
UrbanLow	71.42	94.82	95.44	90.81	91.96	91.43	95.67	95.03
UrbanMed	96.52	98.99	98.99	99.81	99.29	98.71	98.51	97.66
SparseForest	44.97	60.94	61.59	64.11	51.35	59.18	62.55	60.47
Orchards&Trees	9.59	27.39	27.62	7.79	31.96	35.79	25.65	28.88
GreenCrops	30.48	32.89	34.57	36.34	33.89	34.07	31.54	34.27
Fallow	13.79	32.69	35.18	25.04	24.63	21.03	29.88	35.96
BareSoil	41.26	53.99	56.64	36.78	37.05	41.51	43.97	56.01
Overall Accuracy	57.29%	69.02%	69.61%	63.60%	63.36%	63.07%	67.47%	69.63%
Kappa Coefficient	0.48	0.63	0.64	0.56	0.56	0.56	0.61	0.64

4.1.5.3 Test Series 7 - EO+SAR-HH+SAR-Variance+SAR-GLCM

The last test series attempted to determine the impact of each individual GLCM texture measure on the classification accuracy. The highest overall accuracy for EO plus a single SAR band was for 88.23% for X-band (Table 27); entropy resulted in higher accuracy for the two SAR cases with X+C and X+L bands as well as for the three band

SAR combination with 92.86% (Table 28). The correlation texture measure performed better for the combination with C+L band SAR.

Table 27. Classification results for Wad Medani, Sudan using EO imagery, SAR despeckled HH and three combined kernels for variance and GLCM texture, per GLCM texture measures separately per SAR band.

Producer's Accuracy		X			C			L	
Class	Contrast	Entropy	Corr.	Contrast	Entropy	Corr.	Contrast	Entropy	Corr.
Water	97.39	97.30	97.51	95.59	95.50	95.11	95.59	95.67	95.91
BarrenGnd	87.83	87.81	90.83	94.79	95.26	89.34	94.04	93.13	93.42
UrbanLow	82.93	86.63	95.01	52.53	41.75	46.21	81.55	97.99	91.74
UrbanMed	94.52	94.02	93.47	29.14	40.17	14.05	81.15	84.04	87.12
SparseForest	65.20	66.07	65.81	57.25	67.15	55.87	62.38	59.25	59.46
Orchards&Tree	50.94	52.07	52.51	35.19	39.40	34.19	34.88	33.31	39.02
GreenCrops	91.50	90.42	90.82	81.45	82.65	84.12	86.16	86.60	86.92
Fallow	85.70	86.20	89.06	82.37	84.34	80.83	84.62	84.00	80.79
BareSoil	73.48	78.85	86.14	76.98	95.74	76.87	44.15	31.78	68.93
User's Accuracy		X			C			L	
Class	Contrast	Entropy	Corr.	Contrast	Entropy	Corr.	Contrast	Entropy	Corr.
Water	99.46	98.06	98.44	99.85	99.78	99.78	99.94	99.91	99.75
BarrenGnd	85.68	87.96	92.38	85.14	98.74	76.99	77.92	76.46	85.93
UrbanLow	88.09	90.03	95.38	73.63	66.16	67.75	91.10	95.22	92.61
UrbanMed	92.63	95.14	98.44	37.96	39.71	43.68	99.92	100.00	99.93
SparseForest	94.22	94.92	94.76	90.96	88.27	90.91	92.83	92.33	88.69
Orchards&Tree	62.13	59.67	59.15	45.87	55.67	50.09	49.69	47.75	52.89
GreenCrops	73.67	74.05	74.90	62.95	66.67	63.27	66.10	65.87	66.71
Fallow	70.58	71.70	74.73	62.26	53.93	57.87	70.16	73.24	75.26
BareSoil	86.15	86.69	91.61	82.91	81.52	77.90	84.83	86.16	87.77
Overall Accuracy	84.03%	85.11%	88.23%	76.67%	79.13%	73.43%	80.01%	80.37%	84.10%
Kappa Coefficient	0.81	0.82	0.86	0.72	0.75	0.68	0.76	0.76	0.81

Combining texture from two or three GLCM measures did better than using a single measure alone for all three SAR satellite cases (Table 29).

Table 28. Classification results for Wad Medani, Sudan using EO imagery, SAR despeckled HH and three combined kernels for variance and GLCM texture, per GLCM texture measures separately per SAR band combinations.

Producer's Accuracy		X+C			X+L			C+L			X+C+L	
Class	Contrast	Entropy	Corr.	Contrast	Entropy	Corr.	Contrast	Entropy	Corr.	Contrast	Entropy	Corr.
Water	97.19	97.04	96.95	95.76	95.70	95.88	97.13	97.10	97.57	97.16	97.07	96.50
BarrenGnd	94.50	98.02	95.14	95.72	98.04	95.45	88.31	89.76	92.54	95.09	98.70	96.23
UrbanLow	88.01	86.70	96.89	82.88	96.91	92.72	84.28	98.24	97.02	92.63	97.76	97.62
UrbanMed	92.79	88.60	87.92	75.91	83.12	86.81	85.71	87.55	91.93	79.79	86.26	94.64
SparseForest	69.50	78.88	75.04	64.58	69.81	61.51	66.99	66.79	59.05	70.68	78.63	76.93
Orchards&Tree	48.56	55.14	49.94	34.63	36.26	34.82	51.76	49.50	53.83	49.87	51.13	50.25
GreenCrops	88.78	87.47	87.15	82.94	82.60	82.52	90.69	90.32	84.30	88.70	88.30	82.91
Fallow	86.32	93.82	89.10	84.19	91.15	82.57	84.23	83.61	86.78	85.74	94.12	86.59
BareSoil	81.35	98.63	83.82	74.80	98.92	74.95	71.74	64.59	88.32	78.95	98.82	85.21
User's Accuracy		X+C			X+L			C+L			X+C+L	
Class	Contrast	Entropy	Corr.	Contrast	Entropy	Corr.	Contrast	Entropy	Corr.	Contrast	Entropy	Corr.
Water	99.06	97.07	98.97	99.69	99.81	99.63	99.54	97.44	98.65	99.30	98.76	99.00
BarrenGnd	90.08	97.55	91.80	87.39	97.69	88.18	85.29	84.83	92.88	89.23	98.08	91.71
UrbanLow	90.15	93.25	94.21	89.25	94.89	90.79	85.63	95.95	94.35	88.34	96.19	96.43
UrbanMed	87.71	88.17	97.54	99.92	99.63	99.86	99.93	99.65	99.27	99.69	100.00	98.52
SparseForest	93.78	91.50	91.56	93.54	90.86	89.69	95.19	95.46	92.68	94.65	93.65	92.65
Orchards&Tree	58.20	61.95	59.45	44.27	44.91	45.09	61.29	56.48	47.22	57.48	59.19	51.64
GreenCrops	73.28	77.31	74.25	65.75	68.82	65.15	73.70	73.92	73.41	73.63	76.37	74.63
Fallow	83.85	88.87	84.00	75.86	86.09	80.97	68.72	74.33	79.78	83.92	93.01	86.69
BareSoil	95.17	97.40	96.17	85.87	95.89	92.08	85.92	84.28	94.22	94.73	97.63	97.09
Overall Accuracy	87.43%	91.38%	89.22%	83.66%	90.17%	85.07%	83.65%	84.98%	87.95%	87.39%	92.86%	89.54%
Kappa Coefficient	0.85	0.90	0.87	0.80	0.88	0.82	0.80	0.82	0.86	0.85	0.91	0.87

4.1.6 Best Band Combination per Class

Although comparisons with overall accuracy are useful and provide guidance as to which combinations of different satellite sources make an optimal use of a budget, often the researcher or field practitioner needs to find the best classification for specific land cover classes. Table 30 documents which band combinations achieved the best classification accuracy for EO or SAR alone, without data fusion. Bare soil and water are best classified with EO (94.36% and 99.88% user's accuracy respectively) although SAR classified water with >80% user's accuracy. Both SAR and EO were good at classifying sparse forest (93.1% and 90.73% user's accuracy). SAR was better than EO at classifying barren ground, fallow, and urban areas. Green crops and orchards & trees were poorly classified by both EO and SAR (<80%).

Table 29. Classification results for tests 7h & 5h for Wad Medani, Sudan using EO imagery, SAR despeckled HH, and three combined kernels for variance and GLCM texture, per combinations of GLCM texture measures. (C=Contrast, E=Entropy, R=Correlation)

Producer's Accuracy	All Satellites			All
Class	CE	CR	ER	Texture
Water	96.98	96.36	96.59	96.53
BarrenGnd	98.71	96.33	98.89	98.88
UrbanLow	97.00	97.28	96.84	96.68
UrbanMed	85.52	90.39	86.69	87.00
SparseForest	79.19	76.78	74.53	75.24
Orchards&Tree	51.63	53.14	57.84	57.59
GreenCrops	88.38	83.10	83.59	83.94
Fallow	94.12	86.70	95.17	95.05
BareSoil	98.90	86.53	96.63	97.26
User's Accuracy		All Satellites		All
Class	CE	CR	ER	Texture
Water	99.06	98.84	98.43	98.43
BarrenGnd	97.94	92.15	98.03	98.07
UrbanLow	95.88	96.18	96.44	96.35
UrbanMed	99.28	98.32	97.44	97.58
SparseForest	93.75	92.30	93.44	93.38
Orchards&Tree	60.96	50.90	53.51	54.45
GreenCrops	76.67	75.53	77.23	77.53
Fallow	91.54	87.31	91.52	91.34
BareSoil	97.54	97.11	97.12	97.11
Overall Accuracy	92.79%	89.62%	92.15%	92.26%
Kappa Coefficient	0.91	0.88	0.91	0.91

Table 30. User's accuracy for Wad Medani , Sudan per land cover class and data type using SAR or EO data alone.

Data Source	BaseSoil	BarrenGnd	Fallow	GreenCrops	Orchards & Trees	Sparse Forest	UrbanLow	UrbanMed	Water
SAR LCX HH	16.81	98.04	91.69	77.51	53.83	93.10	96.15	97.08	0.00
SAR L HHVG	41.26	58.24	10.53	28.23	2.47	22.09	66.74	97.86	73.56
SAR C HHVG	53.99	70.30	13.79	30.48	9.59	44.97	71.42	96.52	73.56
SAR X HHVG	56.64	92.73	32.69	32.89	27.39	60.94	94.82	98.99	81.89
SAR LC HHVG	36.78	92.21	35.18	34.57	27.62	61.59	95.44	98.99	84.43
SAR CX HHVG	37.05	88.83	25.04	36.34	7.79	64.11	90.81	99.81	70.87
SAR LX HHVG	56.64	84.47	24.63	33.89	31.96	51.35	91.96	99.29	78.48
SAR LCX HHVG	56.64	92.21	35.18	34.57	27.62	61.59	95.44	98.99	84.43
SAR LCX VG	56.46	92.21	35.18	34.57	27.62	61.59	95.44	98.99	84.43
EO	94.36	60.82	63.92	65.41	57.58	90.73	60.79	36.70	99.88

Key:	EO	Electro-optical	HH	Despeckled SAR HH polarization
	L	L-band SAR	V	Variance Texture
	C	C-band SAR	G	GLCM, Gray Level Co-ocurrence Matrix
	X	X-band SAR		

4.1.7 Summary

Table 31 summarizes the main results of the different test series. The accuracy from using only the SAR despeckled HH band was the lowest within that group, but the accuracy was improved by using all three SAR bands (49.33%). The EO information did better than SAR alone although, as mentioned earlier, not for all the land cover classes. Using variance and three measures of GLCM texture improved the accuracy compared to using the despeckled data alone and the X-band resulted in the highest accuracy of the group (69.61%).

Fusing EO and SAR greatly improved the classification accuracy by more than 14% when adding the despeckled HH bands from all three SAR satellites. Using three SAR bands was better than using one or two bands. Adding variance with the largest kernel size of 21x21 pixels increased the overall accuracy by another 2%. Using together all three GLCM texture measures with two kernel windows (11x11 and 21x21) increased accuracy more than the variance texture measure; 8.6% higher compared to 2.04%. Combining variance and GLCM texture for all three SAR bands and the three kernels

slightly decreased the accuracy from using GLCM texture alone by 0.43%. Finally using contrast and entropy GLCM texture measures slightly improved (0.53%) classification accuracy using all three kernel sizes and all three SAR bands. The best land cover classification for Wad Medani (92.79 overall accuracy) was achieved using all three SAR bands, and all three variance kernels (Table 31); this represented an improvement over EO alone of 24.77%. The resulting thematic map is Figure 32and the corresponding error matrix is Table 32.

Table 31. Summary of the classification results for each test series for Wad Medani, Sudan.

Test #	1	2g	3d	4d	5h	6a	7h
Band Combo				EO+HH	EO+HH	SAR-X HH	EO+HH
Producer's Acc	EO	EO+SAR HH	EO+HH+V21	+GLCM721	+V+GLCM	+V+GLCM	+CE71121
Class		X, C, L	X, C, L	X, C, L	X, C, L	X, C, L	X, C, L
Water	95.76	95.82	97.30	96.59	96.53	79.38	96.98
BarrenGnd	93.77	93.81	94.97	98.80	98.88	95.83	98.71
UrbanLow	15.40	80.45	93.22	96.80	96.68	71.41	97.00
UrbanMed	13.00	94.95	91.13	97.04	87.00	96.92	85.52
SparseForest	55.72	60.58	64.74	72.22	75.24	45.77	79.19
Orchards&Tree	33.38	38.39	43.60	56.84	57.59	45.04	51.63
GreenCrops	89.98	87.81	86.29	83.75	83.94	47.44	88.38
Fallow	82.45	85.16	85.16	96.02	95.05	30.65	94.12
BareSoil	45.78	73.51	71.01	98.13	97.26	46.70	98.90
User's Acc							
Class							
Water	99.88	95.82	98.83	97.99	98.43	84.43	99.06
BarrenGnd	60.82	93.81	87.18	98.57	98.07	92.21	97.94
UrbanLow	60.79	80.45	91.20	97.74	96.35	95.44	95.88
UrbanMed	36.70	94.95	99.40	98.81	97.58	98.99	99.28
SparseForest	90.73	60.58	95.39	94.44	93.38	61.59	93.75
Orchards&Tree	57.58	38.39	55.82	53.77	54.45	27.62	60.96
GreenCrops	65.41	87.81	68.82	76.47	77.53	34.57	76.67
Fallow	63.92	85.16	81.47	92.89	91.34	35.18	91.54
BareSoil	94.36	73.51	94.70	97.82	97.11	56.64	97.54
Overall Accuracy	68.02%	84.09%	86.13%	92.69%	92.26%	69.61%	92.79%
Kappa Coefficient	0.60	0.81	0.83	0.91	0.91	0.64	0.91

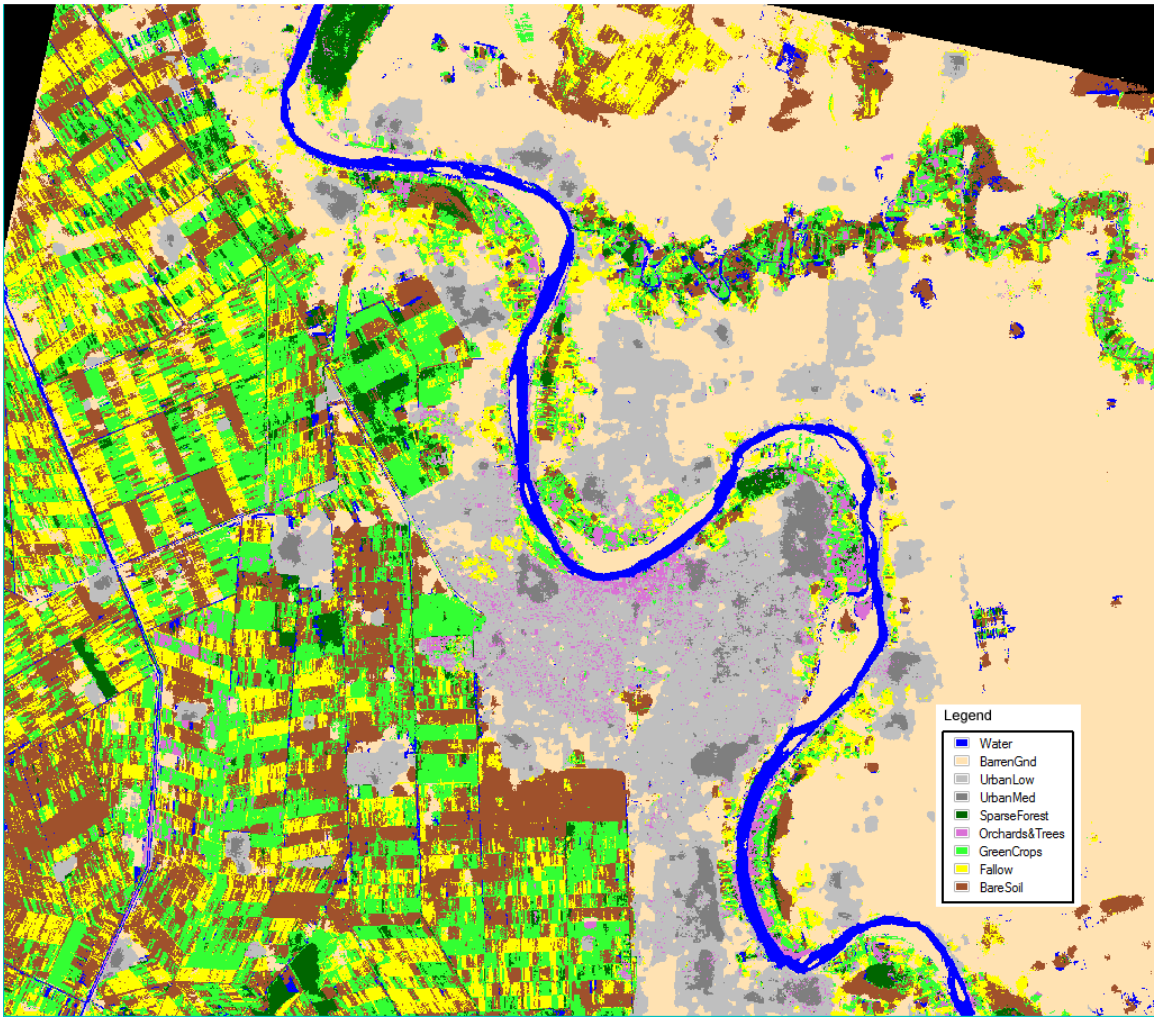

Figure 32. Best land cover classification thematic map for Wad Medani, Sudan using EO + SAR despeckled HH + SAR texture. Scene width ~ 30 km.

Table 32. Error matrix for the best classification for Wad Medani, Sudan, using EO, despeckled SAR HH, CE, and XCL bands.

Ground Truth (Pixels)											
Class	Water	BarrenGnd	UrbanLow	UrbanMed	SparseForest	Orchards&Trees	GreenCrops	Fallow	BareSoil	Total	User's Acc
Water	3273	1	0	0	0	4	4	0	22	3304	99.06%
BarrenGnd	23	10281	70	47	0	6	1	54	15	10497	97.94%
UrbanLow	1	68	4238	107	0	6	0	0	0	4420	95.88%
UrbanMed	0	0	10	1388	0	0	0	0	0	1398	99.28%
SparseForest	8	0	0	0	1545	15	80	0	0	1648	93.75%
Orchards&Trees	3	0	26	21	157	823	320	0	0	1350	60.96%
GreenCrops	20	0	1	0	241	706	3378	58	2	4406	76.67%
Fallow	3	65	20	60	5	33	36	2435	3	2660	91.54%
BareSoil	44	0	4	0	3	1	3	40	3759	3854	97.54%
Total	3375	10415	4369	1623	1951	1594	3822	2587	3801	33537	
Producer's Acc	96.98%	98.71%	97.00%	85.52%	79.19%	51.63%	88.38%	94.12%	98.90%	Overall	92.79%
Overall Accuracy = (31120/33537) 92.79%											
Kappa Coefficient = 0.91											

4.2 Campinas, Brazil

4.2.1 Test Series

Six test series with specific bands were carried out, each with specific objectives (Table 33). As before, test 1 was to establish the EO baseline. Then in test series 2 the effect of adding despeckled HH SAR band from each SAR satellite was evaluated. SAR variance was added in test series 3; only the 21x21 kernel was used because after extensive testing from 3x3 to 51x51 kernels (not reported in this dissertation) no clear trend with kernel size was found. The 21x21 kernel gave good results for Wad Medani. Tests were made for each SAR satellite as well as combinations. Test series 4 evaluated adding the GLCM texture measures of entropy and correlation, separately and combined. For simplification the contrast GLCM measure was eliminated, and for consistency the same 21x21 kernel used for variance was used for the GLCM texture measures. Test series 5 included both variance and GLCM with EO and SAR despeckled HH. The accuracy of using SAR alone, without EO was evaluated in test series 6, with and without variance and with GLCM entropy, correlation, and combined, as in earlier tests.

Table 33. Classification tests band packages for Campinas, Brazil.

Test	Data	Objective	# Tests
1	EO Bands 1-5	EO baseline	1
2	EO+SAR Despeckled HH	Test effect of adding each SAR band individually and combined to EO	7
3	EO + SAR Despeckled HH + SAR variance 21x21 kernel	Test effect of adding SAR variance texture to EO + SAR despeckled HH	7
4	EO + SAR Despeckled HH + SAR GLCM entropy and correlation 21x21 kernel	Test effect of adding SAR GLCM entropy and correlation texture to EO + SAR despeckled HH i. entropy ii. correlation iii. entropy and correlation	21
5	EO + SAR Despeckled HH + SAR variance + GLCM entropy and correlation 21x21 kernel	Test effect of adding SAR variance + GLCM entropy and correlation texture to EO + SAR despeckled HH i. entropy ii. correlation iii. entropy and correlation	21
6	SAR Despeckled HH + SAR variance + GLCM entropy and correlation 21x21 kernel	SAR baseline for each SAR satellite, variance and GLCM texture and combinations	16
		Total	73

The test matrix shows the bands used for each test with EO (Table 34), and for the tests with only SAR (Table 35).

Table 34. Campinas test matrix with EO, and EO+SAR images for Campinas, Brazil.

		TerraSar-X				RADARSAT-2				PALSAR			
Test	RapidEye	HH	V21	E21	R21	HH	V21	E21	R21	HH	V21	E21	R21
Test 1 - EO ALONE													
1	X												
Test 2 - EO + SAR-HH													
2a	X	X											
2b	X					X							
2c	X									X			
2d	X	X				X							
2e	X	X								X			
2f	X					X				X			
2g	X	X				X				X			
Test 3 - EO+SAR-HH+VAR													
3a	X	X	X										
3b	X					X	X						
3c	X									X	X		
3d	X	X	X			X	X						
3e	X	X	X							X	X		
3f	X					X	X			X	X		
3g	X	X	X			X	X			X	X		
Test 4i - EO+SAR-HH+GLCM Entropy													
4i-a	X	X		X									
4i-b	X					X		X					
4i-c	X									X		X	
4i-d		X		X		X		X					
4i-e		X		X						X		X	
4i-f						X		X		X		X	
4i-g		X		X		X		X		X		X	
Test 4ii - EO+SAR-HH+GLCM Correlation													
4ii-a	X	X			X								
4ii-b	X					X			X				
4ii-c	X									X			X
4ii-d	X	X			X	X			X				
4ii-e	X	X			X					X			X
4ii-f	X					X			X	X			X
4ii-g	X	X			X	X			X	X			X
Test 4iii - EO+SAR-HH+GLCM Entropy & Correlation													
4iii-a	X	X		X	X								
4iii-b	X					X		X	X				
4iii-c	X									X		X	X
4iii-d		X		X	X	X		X	X				
4iii-e		X		X	X					X		X	X
4iii-f						X		X	X	X		X	X
4iii-g		X		X	X	X		X	X	X		X	X
Test 5i - EO+SAR-HH+V+GLCM Entropy													
5i-a	X	X	X	X									
5i-b	X					X	X	X					
5i-c	X									X	X	X	
5i-d	X	X	X	X		X	X	X					
5i-e	X	X	X	X						X	X	X	
5i-f	X					X	X	X		X	X	X	
5i-g	X	X	X	X		X	X	X		X	X	X	
Test 5ii - EO+SAR-HH+V+GLCM Correlation													
5ii-a	X	X	X		X								
5ii-b	X					X	X		X				
5ii-c	X									X	X		X
5ii-d	X	X	X		X	X	X		X				
5ii-e	X	X	X		X					X	X		X
5ii-f	X					X	X		X	X	X		X
5ii-g	X	X	X		X	X	X		X	X	X		X
Test 5iii - EO+SAR-HH+V+GLCM Entropy & Correlation													
5iii-a	X	X	X	X	X								
5iii-b	X					X	X	X	X				
5iii-c	X									X	X	X	X
5iii-d	X	X	X	X	X	X	X	X	X				
5iii-e	X	X	X	X	X					X	X	X	X
5iii-f	X					X	X	X	X	X	X	X	X
5iii-g	X	X	X	X	X	X	X	X	X	X	X	X	X

Table 35. Campinas test matrix for SAR only images for Campinas, Brazil.

Test 6 - SAR w/o EO		TerraSar-X				RADARSAT-2				PALSAR			
	RapideEye	HH	V21	E21	R21	HH	V21	E21	R21	HH	V21	E21	R21
6a		X											
6b						X							
6c										X			
6d		X	X										
6e						X	X						
6f										X	X		
6g		X		X									
6h						X		X					
6i										X		X	
6j		X			X								
6k						X			X				
6l										X			X
6m		X	X	X	X								
6n						X	X	X	X				
6o										X	X	X	X
All Sar Bands & Kernels		X	X	X	X	X	X	X	X	X	X	X	X

4.2.2 Spectral Signatures

The mean spectral signatures for the training pixels of the five land cover classes were extracted from the image stack and the means and standard deviations were calculated (Figure 33, Table 36). Although some classes show similar intensities in certain bands, the 17 band signatures are noticeably different.

Table 36. Training ROI mean and standard deviation of the for each of the five classes in Campinas, Brazil.

		BareGround		Water		Forest		Agriculture		Urban	
Band	DataType	Mean	StdDev	Mean	StdDev	Mean	StdDev	Mean	StdDev	Mean	StdDev
1	RapidEye_Blue	30763.73	12898.40	19244.15	10939.69	3681.94	3546.74	17441.31	6683.31	44432.61	11911.66
2	RapidEye_Green	34434.68	16249.98	21411.13	15347.23	3133.61	3850.89	24564.82	9071.13	41898.88	11581.98
3	RapidEye_Red	42119.33	16883.72	13608.32	10133.60	2022.35	2756.27	21090.63	8920.47	42805.66	12682.79
4	RapidEye_RedEdge	40177.63	19572.40	3226.23	6206.51	5701.68	5533.44	31802.47	10786.50	38540.94	13474.77
5	RapidEye_NIR	28481.44	18724.45	891.29	4371.11	35289.39	16325.14	42147.35	19918.74	22841.62	10758.18
6	TerraSar-X_HH_Despeckled	16974.03	8260.74	2490.62	5256.14	23702.83	9693.61	17006.03	8499.66	29599.22	20909.24
7	RadarSat-2_HH_Despeckled	2023.40	10119.50	41.83	1156.32	1125.96	7191.20	1.00	0.00	12408.12	20153.08
8	Palsar_HH_Despeckled	6608.05	5446.77	2689.71	6606.91	14839.72	8865.28	8054.40	14003.73	28923.50	22986.55
9	TerraSar-X_Variance_21x21	3038.01	13053.70	3970.11	15057.37	2809.85	10263.75	398.50	1876.67	22356.18	19104.31
10	TerraSar-X_Entropy_21x21	9425.35	9037.50	11068.91	10616.29	18589.77	11585.92	7839.62	8179.86	41006.01	21403.03
11	TerraSar-X_Correlation_21x21	23887.45	19808.92	15044.91	13508.95	23197.21	15947.38	16430.61	16972.29	29873.35	16229.15
12	RadarSat-2_Variance_21x21	63.65	206.38	52.61	194.36	34.91	83.91	10.05	5.46	776.37	1197.05
13	RadarSat-2_Entropy_21x21	1111.52	3467.03	611.23	3219.05	489.81	2399.69	4.84	76.88	18257.71	15088.97
14	RadarSat-2_Correlation_21x21	55687.14	21119.59	56252.40	21818.93	62327.84	12605.60	65331.77	3637.73	29935.12	20583.81
15	Palsar_Variance_21x21	2029.41	10728.52	392.50	2266.48	2400.11	9143.21	3143.04	13687.43	5308.46	11638.14
16	Palsar_Entropy_21x21	1619.26	5430.16	3347.44	6647.61	5134.22	8991.73	4250.57	13712.26	30362.65	23213.08
17	Palsar_Correlation_21x21	32655.69	31008.74	20169.73	26112.51	17857.15	24489.58	38740.23	29311.17	18096.84	14786.65

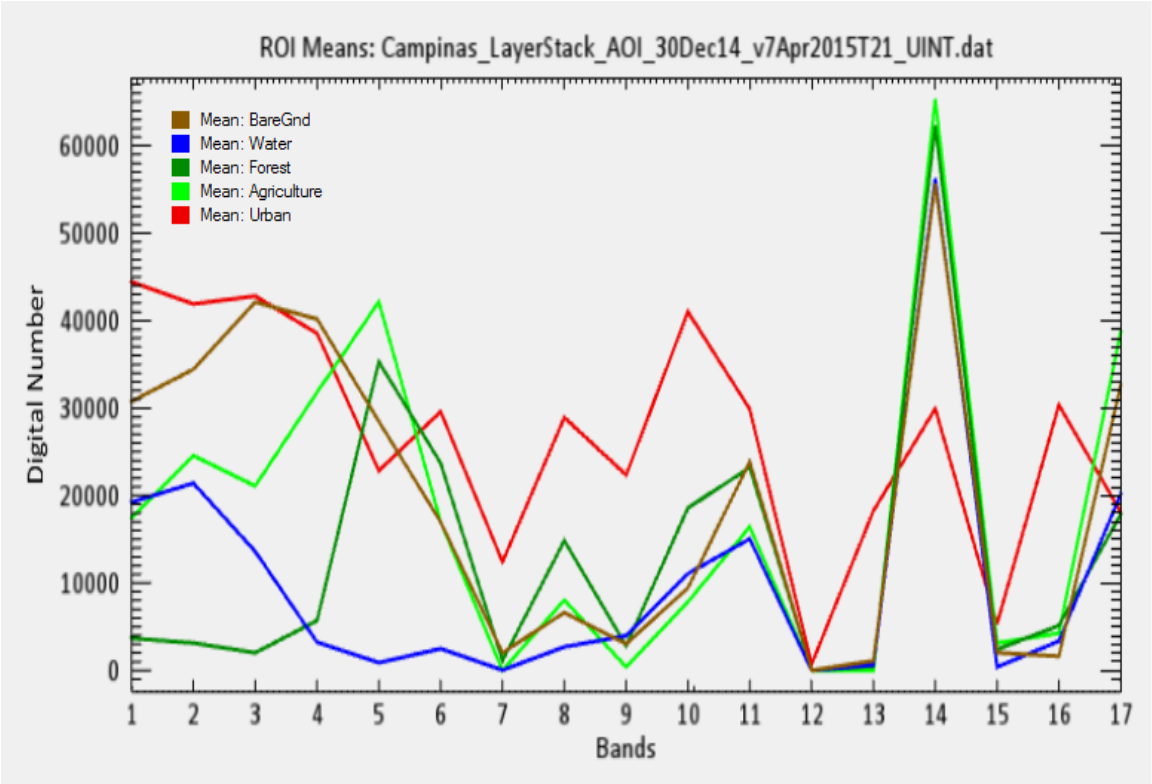

Figure 33. Mean spectral signatures for the 17 bands for five land cover classes for Campinas, Brazil.

4.2.3 Training and Ground Truth

Training pixels were collected from multiple polygons per class distributed over the AOI for the five land cover classes to be separated (Figure 34). The locations of the ROI's for the GT polygons were selected separately from training ROI's and distributed over the AOI (Figure 35). About 1,600 pixels representing 1 sq. km were used for the training and GT (Table 37).

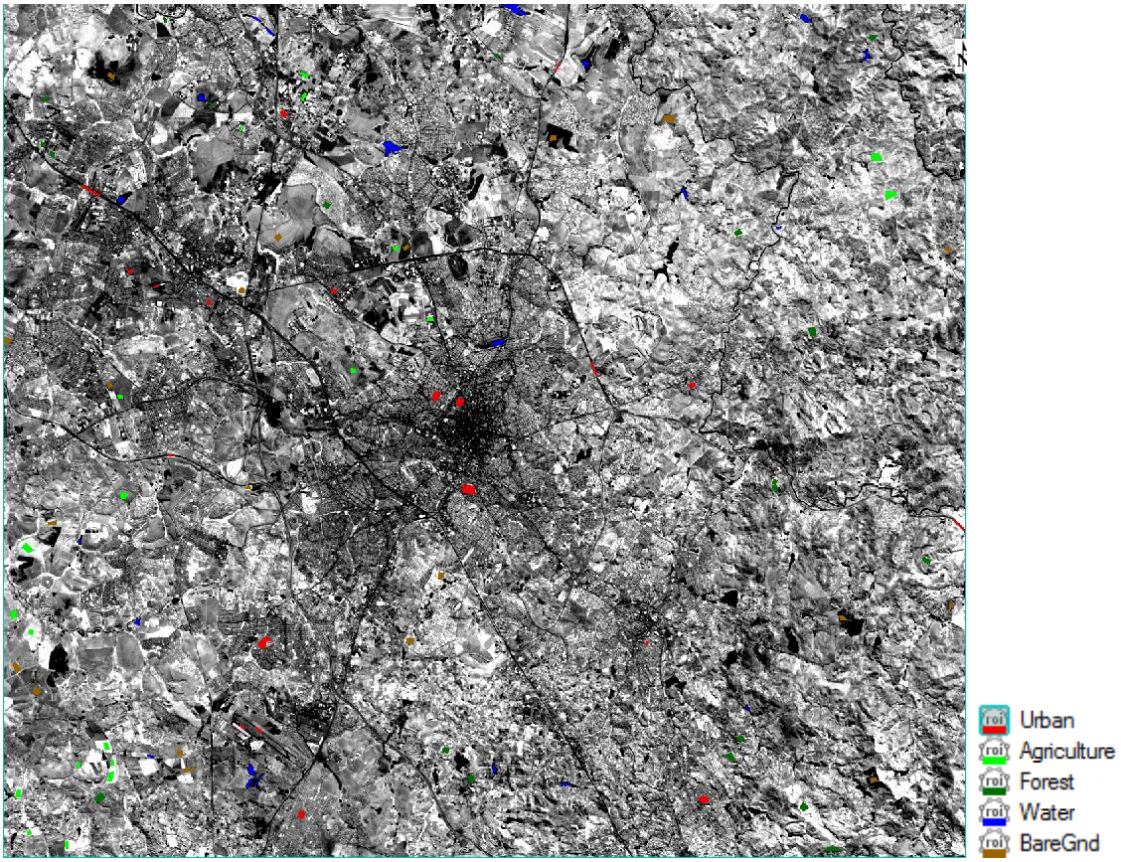

Figure 34. Training ROI's over the NIR band image in the image stack for Campinas, Brazil for the five land cover classes. Scene width ~ 55 km.

Table 37. Number of pixels and area for training and GT polygons for each land cover class at Campinas, Brazil.

	Training Areas		Ground Truth	
Class	Pixels	sq km	Pixels	sq km
Urban	1,611	1.007	1,622	1.014
Agriculture	1,606	1.004	1,651	1.032
Forest	1,602	1.001	1,651	1.032
Water	1,605	1.003	1,602	1.001
BareGnd	1,604	1.003	1,654	1.034

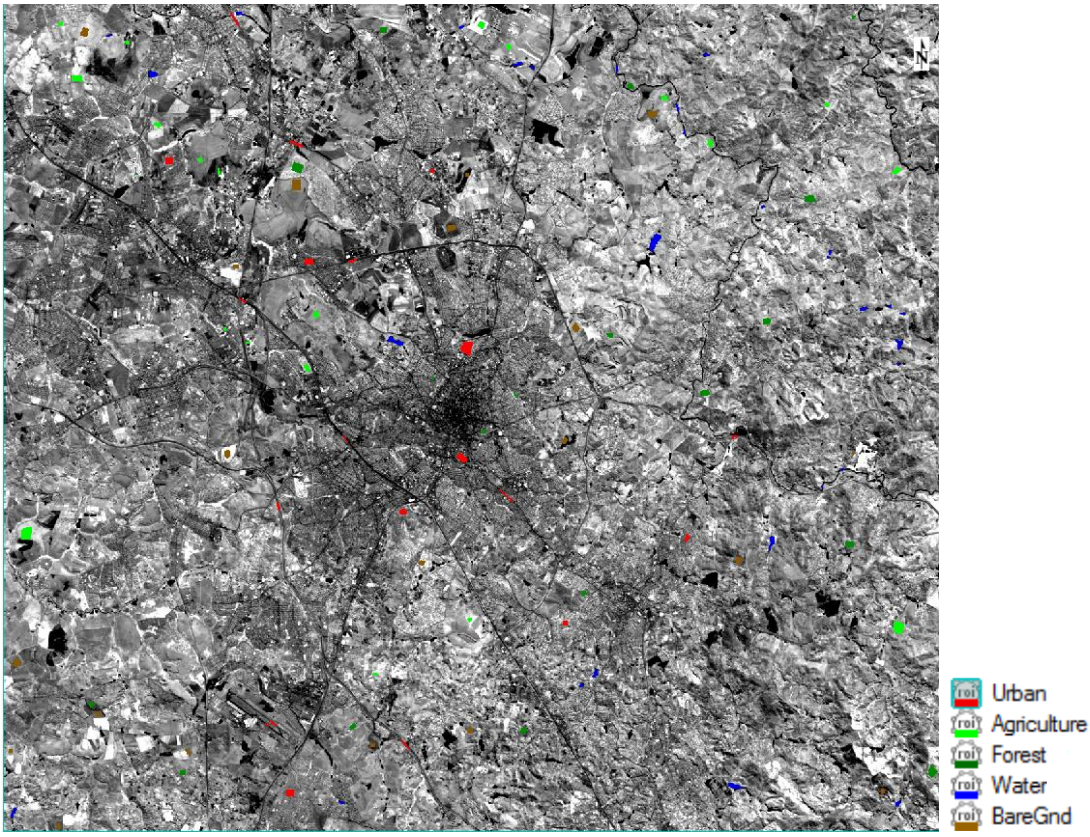

Figure 35. GT ROI's over the NIR band image for Campinas, Brazil. Scene width ~ 55 km.

4.2.4 Classification Accuracy

4.2.4.1 Test 1 - EO Imagery

Using EO alone an overall accuracy of 83.8% was achieved. User's accuracy ranged between 78.5% for urban areas and as high as 95.2% for water; the producer's accuracy was between 67.5% for bare ground and 99.0% for forest areas (Table 38). Bare ground was confused mostly with urban areas because many roads were made of dirt and other areas clearly under development were also dirt surfaces. This suggests confusion between land cover and land use in the selection of the training areas and class definition. The resulting land cover thematic map is Figure 36.

Table 38. EO baseline error matrix for the land cover classification at Campinas, Brazil.

Class	BareGnd	Water	Forest	Agriculture	Urban	Total	User's Acc
BareGnd	1117	73	0	15	191	1396	80.01%
Water	54	1315	0	0	12	1381	95.22%
Forest	6	74	1635	242	2	1959	83.46%
Agriculture	143	100	11	1393	26	1673	83.26%
Urban	334	40	5	1	1391	1771	78.54%
Total	1654	1602	1651	1651	1622	8180	
Producer's Acc	67.5%	82.1%	99.0%	84.4%	85.8%	Overall	83.75%
Overall Accuracy = (6851/8180)	83.75%						
Kappa Coefficient = 0.80							

4.2.4.2 Test Series 2 - EO + SAR-HH

This test series added the despeckled HH SAR bands individually. The addition of SAR resulted in a slightly higher overall accuracy compared to EO alone (+0.46% to 4.06%). The user's and producer's accuracy for each class were very similar (Table 39). The addition of the C-band had no effect in the classification accuracy compared to EO alone. The addition of L-band despeckled HH data, however improved the EO classification by 3.2%; bare ground was better separated from urban areas, and agriculture and forest areas were better separated. Using two SAR bands improved the classification accuracy more than with a single SAR band. Using all three bands an overall accuracy of 87.86% was achieved although this was only 0.22% better than the combination of X and L-band so the additional expense and processing of the third band was not warranted. Compared to the EO-only classification, bare ground was better separated from urban areas (Table 40) with the addition of SAR.

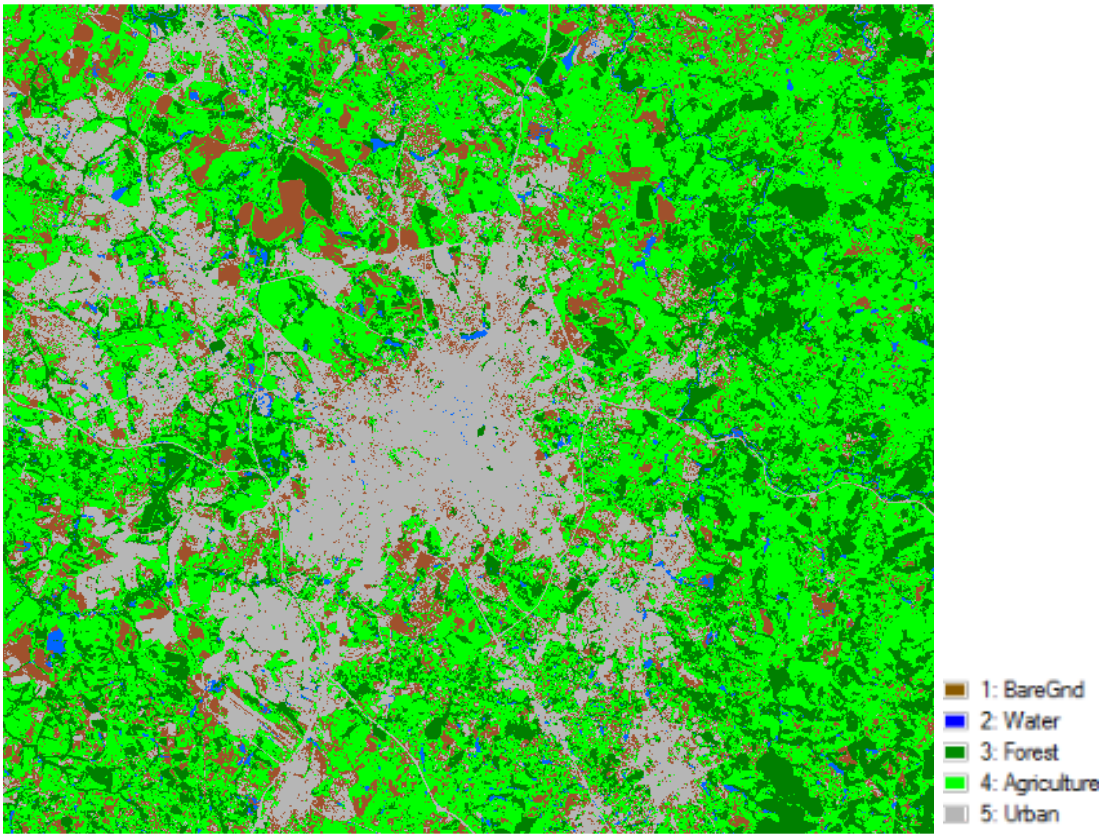

Figure 36. Classification image using only EO bands for Campinas, Brazil. Scene width ~ 55 km.

Table 39. Classification results comparison for Campinas, Brazil, using EO + SAR despeckled HH.

Producer's Accuracy							
Test	a	b	c	d	e	f	g
Class	X	C	L	X+C	X+L	C+L	X+C+L
BareGnd	69.35	67.59	74.73	76.36	76.84	72.61	77.21
Water	82.77	82.08	83.27	82.71	84.96	84.96	84.77
Forest	99.03	99.03	99.33	98.61	99.09	98.43	98.73
Agriculture	84.07	84.31	87.89	88.31	88.01	87.28	88.19
Urban	85.88	85.76	89.40	87.79	89.27	88.96	90.38
User's Accuracy							
BareGnd	81.17	80.03	85.18	84.59	86.23	84.40	87.35
Water	95.40	95.22	94.74	97.57	97.21	95.64	96.93
Forest	83.25	83.46	86.73	86.18	86.88	87.27	87.21
Agriculture	83.11	83.20	84.71	84.77	86.49	83.97	85.70
Urban	79.92	78.59	84.45	82.79	83.08	82.18	83.82
Overall Accuracy	84.22%	83.75%	86.93%	86.77%	87.64%	86.44%	87.86%
Kappa Coefficient	0.80	0.80	0.84	0.83	0.85	0.83	0.85

Table 40. Error matrix for Campinas, Brazil using EO + X, C, and L-band SAR despeckled HH.

Class	BareGnd	Water	Forest	Agriculture	Urban	Total	User's Acc
BareGnd	1277	37	0	29	119	1462	87.35%
Water	28	1358	4	2	9	1401	96.93%
Forest	3	73	1630	162	1	1869	87.21%
Agriculture	114	92	10	1456	27	1699	85.70%
Urban	232	42	7	2	1466	1749	83.82%
Total	1654	1602	1651	1651	1622	8180	
Producer's Acc	77.2%	84.8%	98.7%	88.2%	90.4%	Overall	87.86%
Overall Accuracy = (7187/8180) 87.86%							
Kappa Coefficient = 0.85							

4.2.4.1 Test Series 3 – EO + SAR-HH + Variance 21x21

With the exception of the C-band, adding SAR variance improved the overall classification accuracy compared to EO alone and EO+L-band despeckled HH (Table 41). Using C-band variance there was a minimal difference compared to EO + C-band despeckled HH. The greatest improvement in overall accuracy was from using all three SAR bands despeckled HH and variance with an overall accuracy of 87.69%, although accuracies from the X and L-bands were close. Using EO + SAR despeckled HH + SAR 21x21 variance from all three SAR bands, water was classified with a 96.7% user's accuracy; the other classes were classified with an overall accuracy of over 80% (Table 42). The greatest improvement from EO alone was in the separation of bare ground and urban areas.

Table 41. Classification results comparison for Campinas, Brazil, using EO + SAR despeckled HH + 21x21 variance.

Producer's Accuracy							
Test	a	b	c	d	e	f	g
Class	X	C	L	X+C	X+L	C+L	X+C+L
BareGnd	70.37	67.71	74.73	70.56	74.61	75.63	74.73
Water	83.83	82.08	83.15	83.77	83.77	83.08	83.90
Forest	99.15	99.03	99.39	99.15	99.33	99.33	99.33
Agriculture	84.31	84.31	87.95	84.07	88.19	87.95	88.19
Urban	89.83	85.76	89.83	90.01	91.86	89.95	92.29
User's Accuracy							
BareGnd	86.35	80.06	85.71	86.57	87.89	85.98	88.41
Water	95.59	95.22	94.67	95.58	94.91	94.67	94.78
Forest	83.48	83.46	86.69	83.31	86.68	86.63	86.73
Agriculture	83.35	83.20	84.62	83.26	84.80	84.62	84.85
Urban	81.12	78.68	84.61	81.29	85.00	85.32	85.20
Overall Accuracy	85.49%	83.78%	87.02%	85.50%	87.56%	87.20%	87.69%
Kappa Coefficient	0.82	0.80	0.84	0.82	0.84	0.84	0.85

4.2.4.1 Test Series 4 - EO+SAR-HH+SAR-21x21 GLCM

Adding GLCM entropy texture measure to EO and SAR despeckled HH improved classification accuracy more than did variance. The best result in overall accuracy (88.08%) was found using entropy from X-band SAR (Table 42). This represented an improvement of 4.3% over using EO alone. Using EO and SAR X-band imagery and entropy texture water had the highest user's accuracy; all classes were separated with greater than 80% accuracy (Table 44).

Table 42. Error matrix for Campinas, Brazil, using EO + X, C, and L-band SAR despeckled HH and variance imagery.

Ground Truth (Pixels)							
Class	BareGnd	Water	Forest	Agriculture	Urban	Total	User's Acc
BareGnd	1236	58	0	20	84	1398	88.41%
Water	57	1344	0	2	15	1418	94.78%
Forest	5	72	1640	171	3	1891	86.73%
Agriculture	155	76	6	1456	23	1716	84.85%
Urban	201	52	5	2	1497	1757	85.20%
Total	1654	1602	1651	1651	1622	8180	
Producer's Acc	74.7%	83.9%	99.3%	88.2%	92.3%	Overall	87.69%
Overall Accuracy = (7173/8180) 87.69%							
Kappa Coefficient = 0.85							

Table 43. Classification results comparison for Campinas, Brazil, using EO + SAR despeckled HH + entropy.

Producer's Accuracy							
Test	a	b	c	d	e	f	g
Class	X	C	L	X+C	X+L	C+L	X+C+L
BareGnd	84.95	72.37	74.61	89.78	81.32	77.45	82.77
Water	81.15	83.58	84.21	81.09	77.09	85.77	78.71
Forest	99.39	99.27	98.61	99.33	98.43	98.91	98.24
Agriculture	81.65	82.25	84.25	82.80	81.65	84.37	81.59
Urban	93.16	87.92	94.08	82.37	92.05	89.46	85.64
User's Accuracy							
BareGnd	87.21	85.38	91.54	84.76	87.28	90.59	86.54
Water	95.52	93.77	94.80	88.37	93.70	90.22	90.33
Forest	81.72	83.03	83.66	82.83	79.11	83.06	77.53
Agriculture	89.04	83.67	83.74	88.19	87.02	84.42	85.80
Urban	89.62	81.35	84.68	93.56	86.90	89.18	90.19
Overall Accuracy	88.08%	85.07%	87.14%	87.13%	86.14%	87.19%	85.43%
Kappa Coefficient	0.85	0.81	0.84	0.84	0.83	0.84	0.82

Table 44. Error matrix for Campinas, Brazil, using EO + X-band SAR despeckled HH + entropy.

Ground Truth (Pixels)							
Class	BareGnd	Water	Forest	Agriculture	Urban	Total	User's Acc
BareGnd	1405	113	0	13	80	1611	87.21%
Water	46	1300	1	3	11	1361	95.52%
Forest	5	88	1641	270	4	2008	81.72%
Agriculture	80	65	5	1348	16	1514	89.04%
Urban	118	36	4	17	1511	1686	89.62%
Total	1654	1602	1651	1651	1622	8180	
Producer's Acc	84.95%	81.15%	99.39%	81.65%	93.16%	Overall	88.08%
Overall Accuracy = (7205/8180) 88.08%							
Kappa Coefficient = 0.85							

Adding the GLCM correlation measure helped less than entropy although the best overall accuracy using SAR L-band correlation was 86.63%, still better than EO alone (Table 45). User's and producer's accuracies were slightly lower using correlation (Table 45) than entropy (see Table 44). Adding both entropy and correlation slightly improved the best classification accuracy using entropy with EO and SAR despeckled HH. In this case the best classification was found using the X-band GLCM texture measures (Table 47). The user's and producer's accuracies for all land cover classes were above 80%, water had the highest user's accuracy, and forest the highest producer's accuracy (Table 48).

Table 45. Classification results comparison for Campinas, Brazil, using EO + SAR despeckled HH + 21x21 correlation.

Producer's Accuracy							
Test	a	b	c	d	e	f	g
Class	X	C	L	X+C	X+L	C+L	X+C+L
BareGnd	75.39	72.19	77.57	76.78	77.75	78.78	74.61
Water	79.90	80.96	81.90	81.40	77.22	81.90	79.65
Forest	99.03	98.91	98.85	98.36	93.82	95.94	90.19
Agriculture	84.25	85.52	86.74	83.16	85.34	82.50	82.68
Urban	84.96	91.49	87.98	87.42	90.94	84.28	85.82
User's Accuracy							
BareGnd	81.34	88.58	85.59	89.06	91.99	84.61	87.83
Water	96.24	93.11	93.18	89.07	83.19	87.64	79.35
Forest	83.59	85.99	84.96	83.67	85.16	83.94	83.05
Agriculture	83.85	84.10	84.68	82.71	82.21	84.02	81.49
Urban	80.96	79.74	85.91	83.96	83.71	83.61	81.93
Overall Accuracy	84.73%	85.82%	86.63%	85.44%	85.04%	84.69%	82.59%
Kappa Coefficient	0.81	0.82	0.83	0.82	0.81	0.81	0.78

Table 46. Error matrix for Campinas, Brazil, using EO + L-band SAR despeckled HH + correlation.

Ground Truth (Pixels)							
Class	BareGnd	Water	Forest	Agriculture	Urban	Total	User's Acc
BareGnd	1283	74	0	14	128	1499	85.59%
Water	56	1312	0	0	40	1408	93.18%
Forest	4	78	1632	202	5	1921	84.96%
Agriculture	173	50	14	1432	22	1691	84.68%
Urban	138	88	5	3	1427	1661	85.91%
Total	1654	1602	1651	1651	1622	8180	
Producer's Acc	77.57%	81.90%	98.85%	86.74%	87.98%	overall	86.63%
Overall Accuracy = (7086/8180) 86.63%							
Kappa Coefficient = 0.83							

Table 47. Classification results comparison for Campinas, Brazil, using EO + SAR despeckled HH + 21x21 entropy and 21x21 correlation.

Producer's Accuracy							
Test	a	b	c	d	e	f	g
Class	X	C	L	X+C	X+L	C+L	X+C+L
BareGnd	85.67	71.70	76.84	79.93	75.09	73.34	72.43
Water	81.96	81.21	81.46	80.34	78.46	80.96	79.34
Forest	99.03	98.85	98.49	98.18	91.88	93.94	88.25
Agriculture	82.13	85.71	84.01	82.74	82.86	81.53	81.28
Urban	92.60	92.36	91.62	87.30	90.14	85.82	85.64
User's Accuracy							
BareGnd	90.54	89.11	89.89	88.25	91.59	85.79	89.14
Water	94.39	93.40	92.68	88.88	83.08	88.17	81.47
Forest	81.51	86.39	82.62	82.70	78.60	82.02	76.81
Agriculture	88.34	84.18	84.16	87.12	81.62	84.18	81.53
Urban	89.25	79.43	85.30	83.00	85.75	77.12	80.15
Overall Accuracy	88.30%	85.97%	86.49%	85.72%	83.69%	83.12%	81.38%
Kappa Coefficient	0.85	0.82	0.83	0.82	0.80	0.79	0.77

Table 48. Error Matrix for Campinas, Brazil, using EO + X-band SAR despeckled HH + entropy and correlation.

Ground Truth (Pixels)							
Class	BareGnd	Water	Forest	Agriculture	Urban	Total	User's Acc
BareGnd	1417	40	0	12	96	1565	90.54%
Water	69	1313	1	1	7	1391	94.39%
Forest	5	93	1635	270	3	2006	81.51%
Agriculture	83	72	10	1356	14	1535	88.34%
Urban	80	84	5	12	1502	1683	89.25%
Total	1654	1602	1651	1651	1622	8180	
Producer's Acc	85.67%	81.96%	99.03%	82.13%	92.60%	overall	88.30%
Overall Accuracy = (7223/8180) 88.30%							
Kappa Coefficient = 0.85							

4.2.4.2 Test Series 5– EO+SAR despeckled HH+SAR Variance & GLCM

Test series 5 added back the variance texture and combined with GLCM texture measure along with EO and SAR despeckled HH. Using GLCM entropy, the best result

was from X-band SAR with an overall accuracy of 88.03% (Table 49); this was a 4.23% improvement over EO alone. The error matrix is Table 50.

Table 49. Classification results comparison for Campinas, Brazil, using EO + SAR despeckled HH + variance and entropy.

Producer's Accuracy							
Test	a	b	c	d	e	f	g
Class	X	C	L	X+C	X+L	C+L	X+C+L
BareGnd	84.70	72.37	74.37	89.66	81.38	77.51	82.65
Water	81.46	83.58	84.33	81.15	76.40	85.83	78.40
Forest	99.33	99.27	98.67	99.27	98.43	98.91	98.36
Agriculture	81.59	82.25	84.19	82.80	81.59	84.37	81.41
Urban	92.97	87.92	94.02	82.49	91.12	89.21	85.39
User's Accuracy							
BareGnd	87.62	85.38	91.52	84.60	86.95	90.66	86.36
Water	95.33	93.77	94.81	88.44	93.58	90.28	90.17
Forest	81.51	83.03	83.54	82.78	78.09	82.89	77.37
Agriculture	88.97	83.67	83.48	88.25	86.79	84.22	85.66
Urban	89.44	81.35	84.91	93.70	87.40	89.38	90.17
Overall Accuracy	88.03%	85.07%	87.10%	87.13%	85.82%	87.16%	85.28%
Kappa Coefficient	0.85	0.81	0.84	0.84	0.82	0.84	0.82

Table 50. Error matrix for Campinas, Brazil, using EO + X-band SAR despeckled HH + variance and entropy.

Ground Truth (Pixels)							
Class	BareGnd	Water	Forest	Agriculture	Urban	Total	User's Acc
BareGnd	1401	105	0	13	80	1599	87.62%
Water	46	1305	1	3	14	1369	95.33%
Forest	5	92	1640	271	4	2012	81.51%
Agriculture	82	63	6	1347	16	1514	88.97%
Urban	120	37	4	17	1508	1686	89.44%
Total	1654	1602	1651	1651	1622	8180	
Producer's Acc	84.70%	81.46%	99.33%	81.59%	92.97%	overall	88.03%
Overall Accuracy = (7201/8180) 88.03%							
Kappa Coefficient = 0.85							

The L-band SAR resulted in the best (86.74%) classification accuracy when using variance and GLCM correlation with EO and SAR despeckled HH (Table 51); although better than using EO alone, the overall accuracy was lower than when using entropy. Bare ground was confused more with agriculture and urban areas (Table 52).

Table 51. Classification results comparison for Campinas, Brazil, using EO + SAR despeckled HH + variance and correlation.

Producer's Accuracy							
Test	a	b	c	d	e	f	g
Class	X	C	L	X+C	X+L	C+L	X+C+L
BareGnd	74.24	72.19	78.42	77.33	77.27	78.72	74.49
Water	79.96	80.96	81.71	81.15	77.53	81.65	79.59
Forest	99.09	98.91	98.85	98.43	93.76	95.03	89.76
Agriculture	84.19	85.52	86.74	83.16	85.10	82.50	82.80
Urban	88.35	91.49	87.85	88.53	91.25	85.02	85.76
User's Accuracy							
BareGnd	84.17	88.58	85.78	89.50	92.01	84.71	87.13
Water	96.17	93.11	93.17	89.41	83.41	88.26	79.14
Forest	83.68	85.99	84.82	83.59	85.05	83.77	83.16
Agriculture	83.79	84.10	84.73	83.01	81.83	84.02	82.00
Urban	80.73	79.74	86.42	84.52	83.85	82.72	81.54
Overall Accuracy	85.18%	85.82%	86.74%	85.73%	85.00%	84.60%	82.48%
Kappa Coefficient	0.81	0.82	0.83	0.82	0.81	0.81	0.78

Table 52. Error matrix for Campinas, Brazil, using EO + L-band SAR despeckled HH + variance and correlation.

Ground Truth (Pixels)							
Class	BareGnd	Water	Forest	Agriculture	Urban	Total	User's Acc
BareGnd	1297	74	0	14	127	1512	85.78%
Water	56	1309	0	0	40	1405	93.17%
Forest	4	78	1632	202	8	1924	84.82%
Agriculture	172	50	14	1432	22	1690	84.73%
Urban	125	91	5	3	1425	1649	86.42%
Total	1654	1602	1651	1651	1622	8180	
Producer's Acc	78.42%	81.71%	98.85%	86.74%	87.85%	overall	86.74%
Overall Accuracy = (7095/8180) 86.74%							
Kappa Coefficient = 0.83							

The classification accuracy using all texture measures and SAR despeckled HH with EO imagery were tested, as were combinations of the three SAR bands with the four texture measures. In this case the best land cover classification was 88.33% when using X-band data (Table 53), an improvement of 4.53% over EO alone. Classification accuracy was lower when combining multiple SAR bands. The corresponding error matrix is presented in Table 54; the classes that most benefited from the addition of X-band SAR were bare ground and urban.

Table 53. Classification results comparison for Campinas, Brazil, using EO + SAR despeckled HH + variance, entropy, and correlation.

Producer's Accuracy							
Test	a	b	c	d	e	f	g
Class	X	C	L	X+C	X+L	C+L	X+C+L
BareGnd	85.67	71.70	76.66	79.93	75.33	73.40	72.49
Water	81.77	81.21	81.21	80.34	77.90	80.77	78.71
Forest	98.91	98.85	98.49	98.12	92.00	93.94	88.25
Agriculture	82.68	85.71	84.25	82.68	82.86	81.53	81.28
Urban	92.48	92.36	91.49	87.24	90.07	85.76	85.88
User's Accuracy							
BareGnd	90.72	89.11	89.87	88.19	91.62	85.86	89.28
Water	94.04	93.40	92.60	88.70	82.54	88.15	81.35
Forest	81.85	86.39	82.50	82.65	78.58	81.72	76.40
Agriculture	88.46	84.18	84.25	87.16	81.77	84.28	81.63
Urban	88.92	79.43	85.19	83.04	85.84	77.15	80.24
Overall Accuracy	88.33%	85.97%	86.43%	85.68%	83.64%	83.08%	81.32%
Kappa Coefficient	0.85	0.82	0.83	0.82	0.80	0.79	0.77

Table 54. Error matrix for Campinas, Brazil, using EO + X-band SAR despeckled HH + variance, entropy and correlation.

Ground Truth (Pixels)							
Class	BareGnd	Water	Forest	Agriculture	Urban	Total	User's Acc
BareGnd	1417	40	0	12	93	1562	90.72%
Water	69	1310	1	1	12	1393	94.04%
Forest	4	95	1633	260	3	1995	81.85%
Agriculture	83	71	10	1365	14	1543	88.46%
Urban	81	86	7	13	1500	1687	88.92%
Total	1654	1602	1651	1651	1622	8180	
Producer's Acc	85.67%	81.77%	98.91%	82.68%	92.48%	overall	88.33%
Overall Accuracy = (7225/8180) 88.32%							
Kappa Coefficient = 0.85							

4.2.4.3 Test Series 6 –SAR Combination w/o EO

For regions with consistent cloud cover EO satellite imagery is difficult to collect and aerial missions are expensive; in those cases satellite based SAR is an excellent option. Test series 6 analyzed the land cover classification accuracy using only SAR from three different bands corresponding with three different satellites. The best single SAR band was the X-band with variance and the GLCM texture entropy and correlation measures with an overall accuracy of 57.71% (Table 55); the results from L-band with texture were close with 56.6%. Using SAR alone the overall classification accuracies ranged from 26.25% using C-band despeckled HH to 57.71% using data derived from X-band. Using all derived data from the C-band only achieved an overall accuracy of 32.30%. The error matrix using X-band SAR derived layers illustrated the greatest degree of confusion between the bare ground and agriculture classes (Table 56); this is explained by the lack of spectral information in SAR versus EO.

Table 55. Classification results comparison for Campinas, Brazil, using SAR despeckled HH + variance, entropy and correlation.

Producer's Accuracy								
Test	a	b	c	d	e	f	g	h
Class	X	C	L	X+V	C+V	L+V	X+E	C+E
BareGnd	55.44	0.00	31.44	3.02	0.00	32.53	24.79	1.03
Water	76.97	0.00	46.57	59.86	0.00	46.44	68.66	0.00
Forest	64.20	99.52	70.75	64.20	99.52	70.50	64.51	0.42
Agriculture	0.00	0.00	15.93	71.05	0.00	15.75	52.21	93.76
Urban	23.98	31.07	42.73	62.08	34.59	41.99	71.21	63.01
User's Accuracy								
BareGnd	32.45	0.00	31.34	12.76	0.00	30.41	41.88	7.39
Water	50.49	0.00	45.46	87.82	0.00	45.45	72.94	0.00
Forest	43.84	21.58	39.00	51.53	21.75	39.32	49.51	11.11
Agriculture	0.00	0.00	30.02	33.91	0.00	32.06	42.03	23.60
Urban	78.74	88.73	68.68	85.34	89.76	67.90	77.46	77.02
Overall Accuracy	44.00%	26.25%	41.44%	51.94%	26.94%	41.41%	56.14%	31.71%
Kappa Coefficient	0.30	0.08	0.27	0.40	0.09	0.27	0.45	0.15
Producer's Accuracy								
Test	i	j	k	l	m	n	o	p
Class	L+E	X+R	C+R	L+R	X+V+E+R	C+V+E+R	L+V+E+R	All SAR
BareGnd	28.17	20.56	0.00	29.63	34.22	0.00	42.02	36.09
Water	48.75	64.36	0.00	45.19	65.36	0.56	56.55	55.62
Forest	69.78	46.21	0.00	42.52	63.05	4.72	59.84	69.59
Agriculture	16.96	59.06	95.34	30.65	55.42	95.34	53.00	53.60
Urban	79.22	38.16	70.04	64.61	71.02	60.48	71.89	73.24
User's Accuracy								
BareGnd	30.18	34.45	0.00	26.81	56.26	0.00	53.63	47.53
Water	45.91	64.44	0.00	43.38	72.26	15.25	51.74	62.00
Forest	47.92	41.60	0.00	41.74	51.84	27.66	49.18	54.71
Agriculture	32.04	34.50	24.20	37.93	42.76	24.09	55.10	48.23
Urban	77.55	66.35	68.11	62.87	73.05	78.54	75.91	76.55
Overall Accuracy	48.46%	45.57%	33.13%	42.42%	57.71%	32.30%	56.60%	57.58%
Kappa Coefficient	0.36	0.32	0.16	0.28	0.47	0.15	0.46	0.47

Table 56. Error matrix for Campinas, Brazil, using SAR despeckled HH + X-band variance, entropy, and correlation.

Ground Truth (Pixels)							
Class	BareGnd	Water	Forest	Agriculture	Urban	Total	User's Acc
BareGnd	566	33	94	268	45	1006	56.26%
Water	120	1047	35	94	153	1449	72.26%
Forest	224	263	1041	278	202	2008	51.84%
Agriculture	711	178	266	915	70	2140	42.76%
Urban	33	81	215	96	1152	1577	73.05%
Total	1654	1602	1651	1651	1622	8180	57.71%
Producer's Acc	34.22%	65.36%	63.05%	55.42%	71.02%	overall	57.71%
Overall Accuracy = (4721/8180) 57.7%							
Kappa Coefficient = 0.47							

4.2.5 Best Band Combination per Class

In most cases the best band combination was not the same for the best producer's or user's accuracy (Table 57). For bare ground, EO fused with X and C-band SAR despeckled HH and entropy texture resulted in a producer's accuracy of 89.9%, while EO fused with X and L band SAR despeckled HH and the variance and correlation texture measures derived 92.0%. The common denominator was EO fusion with the X-band SAR. Without EO, the X-band SAR gave a producer's accuracy of 55.4% and with the addition of the three texture measures, resulted in a user's accuracy of 56.3%.

For the water class, EO with C and L-band SAR despeckled HH and entropy, and EO with X-band SAR despeckled HH with variance and correlation texture resulted in a producer's accuracy of 85.8% and user's accuracy of 96.2%, respectively. Using X-band SAR alone, a producer's and user's accuracy of 77.0% and 87.8% was achieved.

Both L-band and X-band SAR with a texture measure fused with EO resulted in a 99.4% producer's accuracy while EO and L, X+L, and X+C+L band SAR with variance

resulted in a user's accuracy of 86.7% for the forest class. Using SAR alone, the C-band resulted in 99.5% producer's accuracy but even using all SAR data available from the three bands, only a user's accuracy of 54.7% was achieved without EO.

Land with agriculture cover was best classified in the producer's perspective with EO and the X and L-band SAR, and variance (88.2%); the addition of the C-band did not make a difference in this case. EO with X-band SAR with variance and entropy resulted in a user's accuracy of 89.0%. Without EO, C-band SAR with variance gave a user's accuracy of 95.3%, while L-band SAR with all three texture measures only resulted in a user's accuracy of 55.1%. The greater roughness of forest cover contributed to more backscatter.

Lastly the urban class was classified best fusing EO with L-band SAR and entropy, and resulted in a producer's accuracy of 94.1%. The user's accuracy was 93.6% when EO was fused with X and C-band SAR, and the entropy texture measure. Without EO, L-band SAR with entropy resulted in a producer's accuracy of 79.2% but C-band SAR with variance had a user's accuracy of 89.8%.

All classes were classified greater than 85% when SAR was fused with EO imagery. Without EO, however, bare ground was not well classified (<60% for both producer's and user's accuracy), and from the map user's perspective, only water and urban classes could be classified with better than 85% accuracy.

Table 57. Band combinations with the best producer's or user's classification accuracy for EO+SAR (left) and SAR alone (right) tests for Campinas, Brazil.

Producer's Accuracy			Producer's Accuracy		
Class \ EO +	SAR Bands	% Acc	Class w/o EO	SAR Bands	% Acc
BareGnd	+XC+E	89.8%	BareGnd	X	55.4%
Water	+CL+E	85.8%	Water	X	77.0%
Forest	+L+V, +X+E	99.4%	Forest	C	99.5%
Agriculture	+XL+V, +XCL+V	88.2%	Agriculture	C+VER	95.3%
Urban	+L+E	94.1%	Urban	L+E	79.2%
User's Accuracy			**User's Accuracy**		
BareGnd	+XL+VR	92.0%	BareGnd	X+VER	56.3%
Water	+X+VR	96.2%	Water	X+V	87.8%
Forest	+L+V, +XL+V, +XCL+V	86.7%	Forest	All SAR Data	54.7%
Agriculture	+X+VE	89.0%	Agriculture	L+VER	55.1%
Urban	+XC+E	93.6%	Urban	C+V	89.8%

4.2.6 Summary

A comparison of the results for land cover classification overall accuracy are in Figure 37 by EO+SAR band and texture measures. In general, at least for Campinas, Brazil, EO fusion with the SAR X-band out-performed the C and L-band SAR while the C-band was the least beneficial. The only case where combining all three SAR bands was beneficial was when using the variance texture measure. However doing that requires obtaining data from three SAR satellites compared to including more measures from a single source.

Another way to synthesize these results is to compare the best results from each of the test series. The highest overall classification accuracy of 88.33% was derived when using X-band despeckled HH, variance, and both GLCM texture measures (Table 58). The addition of any SAR data represented at least an improvement of 2.88%. Figure 38 summarizes the results of the SAR-only test; the X-band produced the best overall accuracy with entropy or all texture. The L-band results were very similar with all the

texture measure. The thematic land cover classification map for Campinas, Brazil using EO+X-band despeckled HH, SAR variance, entropy, and correlation is Figure 39.

Table 58. Comparison of the best overall accuracy results from test series 1-6 with EO and fusion with SAR data for Campinas, Brazil.

Producer's Accuracy	1	2	3	4	5	6
Class \ Fusion with:	EO	+L-HH	+XCL-V	+X-ER	+X-VER	All SAR
BareGnd	67.53	74.73	74.73	85.67	85.67	36.09
Water	82.08	83.27	83.90	81.96	81.77	55.62
Forest	99.03	99.33	99.33	99.03	98.91	69.59
Agriculture	84.37	87.89	88.19	82.13	82.68	53.60
Urban	85.76	89.40	92.29	92.60	92.48	73.24
User's Accuracy						
BareGnd	80.01	85.18	88.41	90.54	90.72	47.53
Water	95.22	94.74	94.78	94.39	94.04	62.00
Forest	83.46	86.73	86.73	81.51	81.85	54.71
Agriculture	83.26	84.71	84.85	88.34	88.46	48.23
Urban	78.54	84.45	85.20	89.25	88.92	76.55
Overall Accuracy	83.75%	86.93%	87.69%	88.30%	88.33%	57.58%
Kappa Coefficient	0.80	0.84	0.85	0.85	0.85	0.47

Key to tests:	**Bands**	**Notes**
Series 1	EO	EO = electro-optical
Series 2	EO+LHH	X = X-band SAR
Series 3	EOHH+XCLV	C = C-band SAR
Series 4	EOHH+XER	L - L-band SAR
Series 5	EOHH+XVER	HH = SAR despeckled HH polarization
Series 6	All SAR	V = variance
		E = entropy
		R = correlation

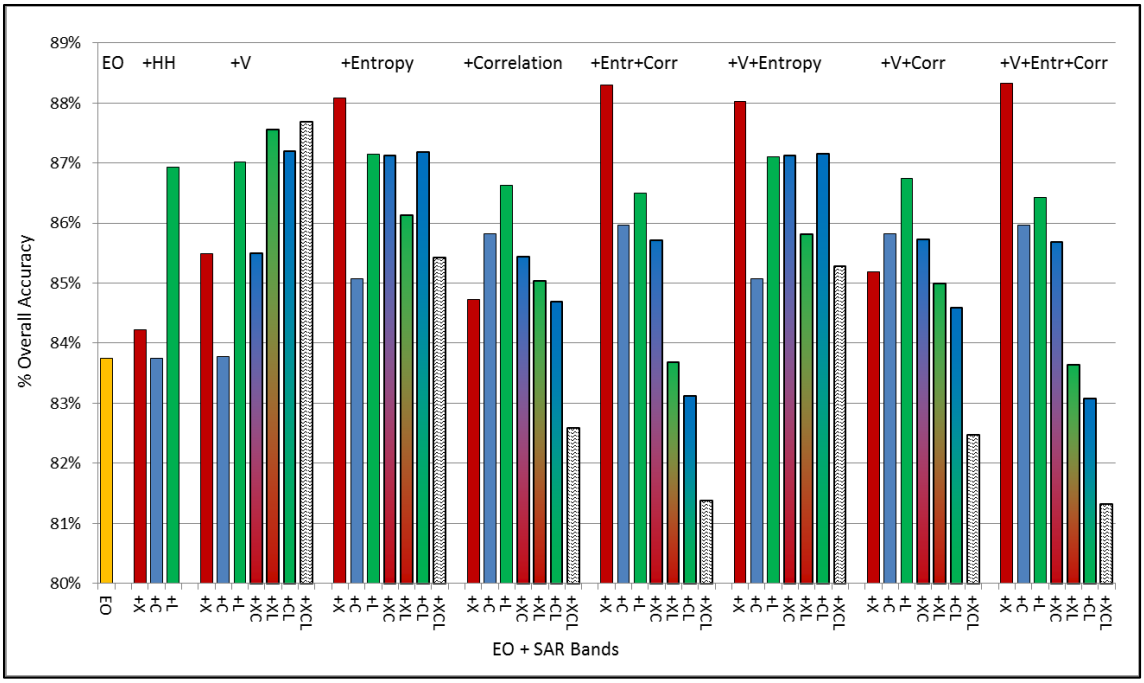

Figure 37. Overall accuracy comparison for test fusing EO bands with SAR for Campinas, Brazil.

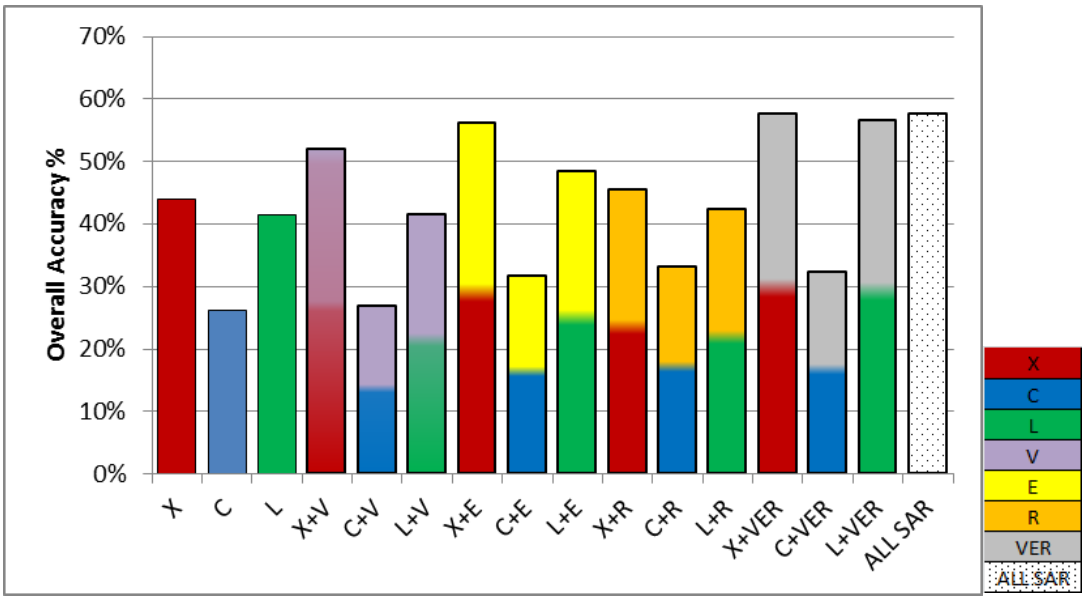

Figure 38. Overall accuracy comparison for SAR only tests for Campinas, Brazil.

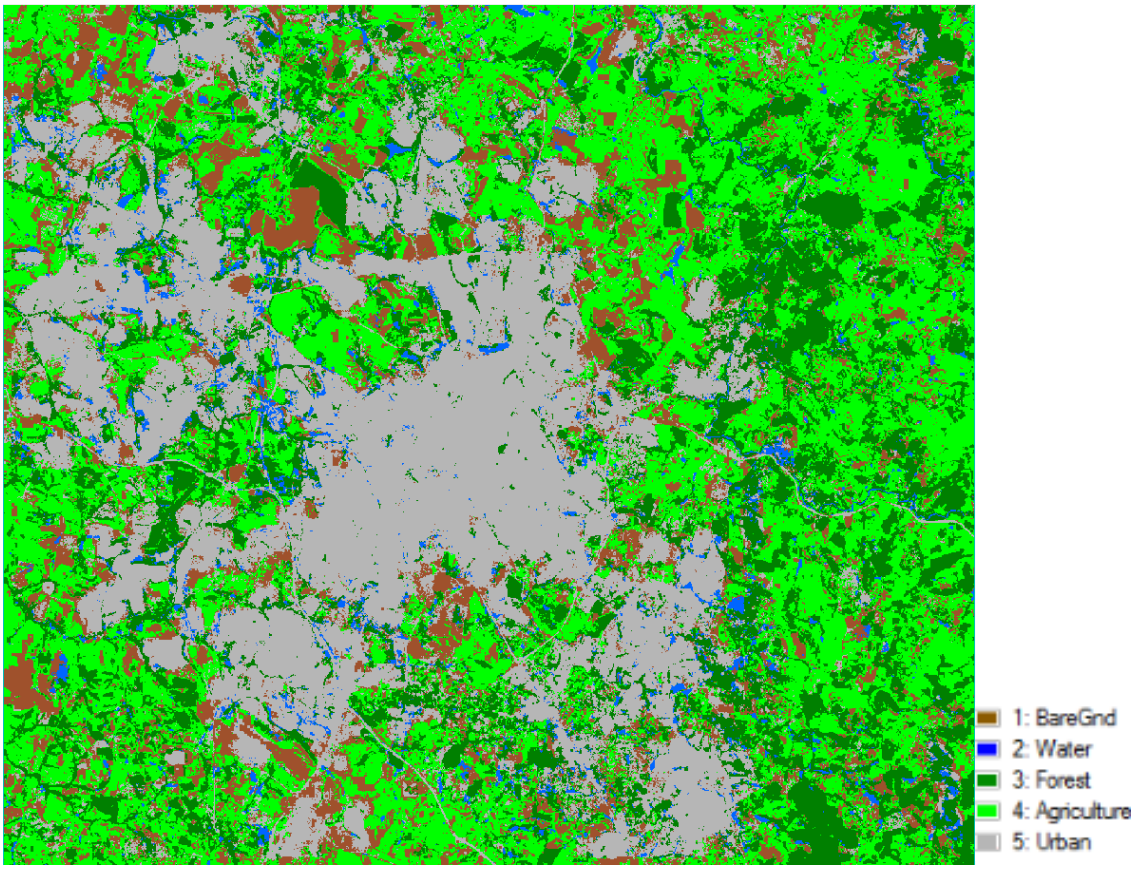

Figure 39. Classification map from EO+X-band despeckled HH, SAR variance, entropy, and correlation for Campinas, Brazil. Scene width ~ 55 km.

4.3 Fresno and Kings Counties, California, USA

4.3.1 Test Series

For Fresno-Kings Counties greater effort was placed on evaluating specific agriculture land cover leveraging the USDA 2010 CropScape – Cropland Data Layer (Boryan et al., 2011).

Various questions were investigated in six test series (Table 59). Test series 1 was to establish the baseline with EO imagery. For simplification the GLCM correlation texture measure was eliminated. Test series 2 added the three SAR band despeckled HH

data, followed by test series 3 which added the 21x21 kernel texture variance measure. Test series 4 replaced variance texture with GLCM entropy and test series 5 used both variance and GLCM entropy texture. Lastly, SAR alone was evaluated in test series 6. The test matrix of the bands used for each test is in Table 60.

Table 59. Classification tests band combinations for Fresno-Kings Counties, USA.

Test	Data	Objective	No. Tests
1	EO Bands 1-5	EO baseline	1
2	EO + SAR Despeckled HH	Test effect of adding each SAR band to EO	7
3	EO + SAR Despeckled HH +SAR variance texture 21x21 kernel per SAR satellite	Test effect of adding SAR 21x21 variance for each SAR band and combinations	7
4	EO + SAR Despeckled HH +SAR GLCM Entropy 21x21 kernel per SAR satellite	Test effect of adding SAR 21x21 GLCM entropy for each SAR band and combinations	7
5	EO + SAR Despeckled HH +SAR variance and GLCM Entropy 21x21 kernel per SAR satellite	Test effect of adding SAR 21x21 variances and GLCM entropy for each SAR band and combinations	7
6	SAR Despeckled HH +SAR 21x21Variance + GLCM Entropy & Correlation 21x21 Texture	SAR baseline with 21x21 variance & GLCM entropy for each SAR band individually and combined	16
		Total	45

Table 60. Classification test matrix for Fresno-Kings Counties, USA.

		TerraSar-X			RADARSAT-2			PALSAR		
Test	RapidEye	HH	V21	E21	HH	V21	E21	HH	V21	E21
Test 1 - EO ALONE										
1	X									
Test 2 - EO + SAR-HH										
2a	X	X								
2b	X				X					
2c	X							X		
2d	X	X			X					
2e	X	X						X		
2f	X				X			X		
g	X	X			X			X		
Test 3 - EO+SAR-HH+VAR										
3a	X	X	X							
3b	X				X	X				
3c	X							X	X	
3d	X	X	X		X	X				
3e	X	X	X					X	X	
3f	X				X	X		X	X	
3g	X	X	X		X	X		X	X	
Test 4 - EO+SAR-HH+GLCM Entropy										
4a	X	X		X						
4b	X				X		X			
4c	X							X		X
4d	X	X		X	X		X			
4e	X	X		X				X		X
4f	X				X		X	X		X
4g	X	X		X	X		X	X		X
Test 5 - EO+SAR-HH+V+GLCM Entropy										
5a	X	X	X	X						
5b	X				X	X	X			
5c	X							X	X	X
5d	X	X	X	X	X	X	X			
5e	X	X	X	X				X	X	X
5f	X				X	X	X	X	X	X
5g	X	X	X	X	X	X	X	X	X	X
Test 6 - SAR w/o EO			**TerraSar-X**			**RadarSat-2**			**PALSAR**	
Test	**RapideEye**	**HH**	**V21**	**E21**	**HH**	**V21**	**E21**	**HH**	**V21**	**E21**
6a		X								
6b					**x**					
6c								X		
6d		X	X							
6e					X	X				
6f								X	X	
6g		X		X						
6h					X		X			
6i								X		X
6j		X	X	X						
6k					X	X	X			
6l								X	X	X
6m		X	X	X	X	X	X			
6n		X	X	X				X	X	X
6o					X	X	X	X	X	X
All Sar Bands & Kernels		X	X	X	X	X	X	X	X	X

4.3.2 Spectral Signatures

The mean spectral signatures for the training pixels of the 11 land cover classes are in Figure 40; Table 61 contains the means and standard deviations.

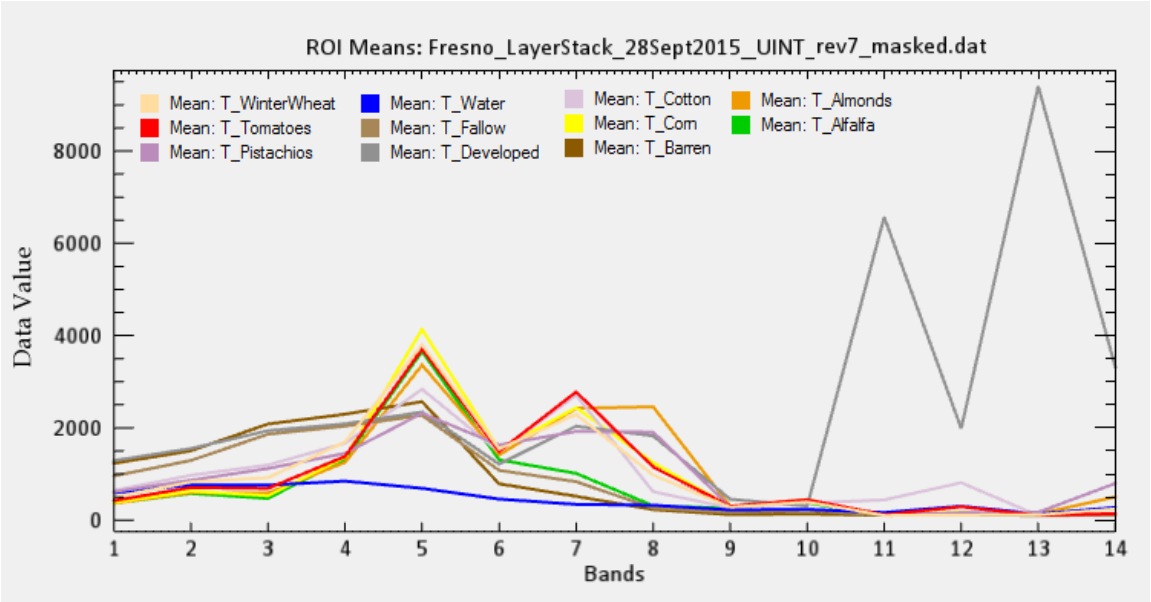

Figure 40. Mean spectral signatures for 11 classes in Fresno-Kings Counties, USA.

4.3.3 Training and Ground Truth

The training (a) and the GT (b) ROI's were distributed over the AOI assuring that there was no overlap (Figure 41). Over 3,500 pixels representing at least 0.5 sq. km were collected for each class with the exception of pistachios which was the least abundant class in the area (Table 62).

Table 61. Training ROI mean and standard deviation for Fresno-Kings Counties, USA.

		Winter Wheat		Tomatoes		Pistachios		Water		Fallow		Developed	
Bands	DataType	Mean	StdDev	Mean	StdDev	Mean	StdDev	Mean	StdDev	Mean	StdDev	Mean	StdDev
1	RapidEye_Blue	500.64	113.14	423.35	86.71	614.42	248.96	592.12	211.94	958.22	199.07	1290.19	826.69
2	RapidEye_Green	823.97	127.92	706.47	104.83	865.34	346.00	765.44	316.83	1294.31	263.71	1552.41	802.79
3	RapidEye_Red	919.89	387.63	689.03	188.26	1119.14	526.12	759.37	344.26	1862.50	392.41	1939.09	877.89
4	RapidEye_RedEdge	1694.90	289.29	1381.24	131.99	1448.03	353.69	845.84	441.47	2037.47	434.04	2086.70	813.32
5	RapidEye_NIR	3800.71	587.30	3705.85	579.44	2315.59	399.36	690.20	468.94	2271.76	494.32	2343.25	805.61
6	TerraSar-X_HH_Despeckled	1543.89	589.33	1487.89	339.79	1630.11	440.33	456.21	373.95	1079.58	267.00	1216.51	1051.99
7	RadarSat-2_HH_Despeckled	2290.75	762.20	2778.41	821.78	1923.00	353.36	342.50	393.35	834.03	351.73	2035.49	4841.37
8	Palsar_HH_Despeckled	978.48	667.42	1152.88	658.73	1908.36	1123.77	323.48	371.86	261.36	162.92	1826.31	4010.23
9	TerraSar-X_Variance_21x21	280.10	91.49	300.69	46.48	284.53	40.76	222.49	185.82	167.84	55.45	453.77	593.30
10	TerraSar-X_Entropy_21x21	394.79	135.61	441.89	81.74	412.71	67.79	233.47	108.49	215.54	95.53	304.70	175.04
11	RadarSat-2_Variance_21x21	101.87	23.69	118.14	50.35	110.89	40.78	165.27	345.76	102.63	36.28	6569.69	20613.27
12	RadarSat-2_Entropy_21x21	109.60	74.31	290.88	505.19	162.06	213.99	302.33	397.39	109.09	76.65	1987.73	3020.44
13	Palsar_Variance_21x21	114.28	49.42	103.65	16.99	169.91	112.67	134.02	113.73	100.41	4.09	9405.44	36432.63
14	Palsar_Entropy_21x21	244.61	469.55	142.68	192.98	795.96	1016.36	274.45	480.70	105.33	48.25	3322.92	5174.86

		Cotton		Corn		Barren		Almonds		Alfalfa	
Bands	DataType	Mean	StdDev	Mean	StdDev	Mean	StdDev	Mean	StdDev	Mean	StdDev
1	RapidEye_Blue	644.77	121.64	380.93	92.87	1230.49	1282.29	363.79	77.62	365.27	115.30
2	RapidEye_Green	973.13	147.31	628.73	95.72	1503.80	1261.02	593.83	113.51	578.39	127.25
3	RapidEye_Red	1195.48	240.28	528.85	170.50	2083.63	1335.21	583.63	150.66	469.92	233.01
4	RapidEye_RedEdge	1666.60	95.24	1358.10	145.63	2296.67	1274.04	1252.32	155.83	1330.11	149.12
5	RapidEye_NIR	2836.38	612.11	4132.44	734.67	2568.16	1192.81	3362.24	275.00	3654.05	576.84
6	TerraSar-X_HH_Despeckled	1481.75	588.31	1528.73	465.24	787.76	306.81	1412.97	281.38	1307.49	263.77
7	RadarSat-2_HH_Despeckled	2708.65	1894.60	2437.74	581.58	516.94	285.70	2423.97	441.17	1013.12	370.39
8	Palsar_HH_Despeckled	616.26	435.51	1246.26	473.76	227.88	127.57	2456.11	795.50	311.42	157.46
9	TerraSar-X_Variance_21x21	265.23	64.02	289.74	90.48	120.29	25.95	303.06	43.35	258.05	65.57
10	TerraSar-X_Entropy_21x21	370.07	77.62	400.71	129.67	132.89	38.64	446.50	71.05	377.78	116.96
11	RadarSat-2_Variance_21x21	438.41	1259.74	112.19	70.49	103.01	21.41	101.07	4.80	103.40	25.02
12	RadarSat-2_Entropy_21x21	811.87	1664.27	175.53	271.50	118.82	115.05	114.62	64.02	118.82	88.20
13	Palsar_Variance_21x21	100.12	2.21	106.51	59.27	101.04	8.93	134.56	44.87	100.60	3.64
14	Palsar_Entropy_21x21	101.06	20.64	127.89	213.68	114.67	107.36	502.72	451.21	108.63	50.16

4.3.4 Classification Accuracy

As in previous sections classifications were compared using their overall accuracy. Individual classes were compared by looking at their user's and producer's accuracy. To facilitate the comparison of the greater number of classes studied in the Fresno-Kings Counties region; the average of the user's and producer's accuracy was calculated as a 'Fitness Index' (FI) of the overall capability to accurately classify each specific class accounting for both the errors of omission and commission. Sorting classes by their FI provides a ranking of the classes best classified.

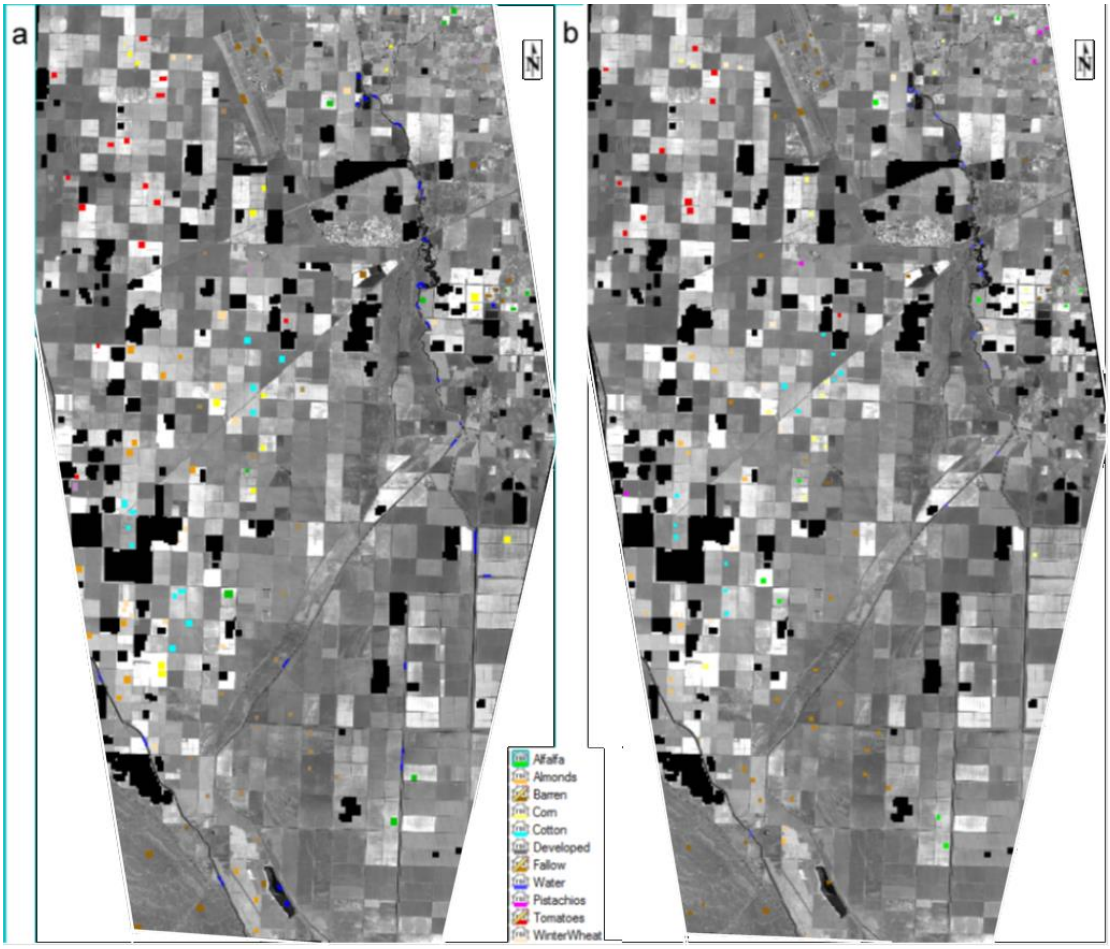

Figure 41. a) Training ROI's, and b) GT ROI's for Fresno-Kings Counties, USA. Scene width ~ 25 km.

Table 62. Number of pixels and area for training and GT polygons for each land cover class for Fresno-Kings Counties, USA

Class	Pixels	sq km
Alfalfa	3,943	0.616
Almonds	5,187	0.810
Barren	5,669	0.886
Corn	5,078	0.793
Cotton	5,096	0.796
Developed	4,246	0.663
Fallow	5,939	0.928
Water	3,674	0.574
Pistachios	1,451	0.227
Tomatoes	4,247	0.664
WinterWheat	5,064	0.791

4.3.4.1 Test 1 - EO Imagery

Using EO alone an overall accuracy of 64.4% was achieved. The user's accuracy ranged between 54.99% for barren ground and 89.6% for Alfalfa (Table 63). Producer's accuracy ranged between 44.9% for corn and 92.6% for water. Bare ground was confused with fallow and developed areas. Tomatoes were confused with winter wheat, corn, almonds, and cotton. Water had a fitness index greater than 85%, alfalfa greater than 80%; winter wheat and pistachios greater than 75%, and the remaining classes between 50-69% (Table 64). Figure 42 is the thematic map for the land cover classification using only the EO bands.

Table 63. EO baseline classification error matrix for Fresno-Kings Counties, USA.

Ground Truth (Pixels)													
Class	WinterWheat	Tomatoes	Pistachios	Water	Fallow	Developed	Cotton	Corn	Barren	Almonds	Alfalfa	Total	User's Acc
WinterWheat	3052	288	0	0	0	19	452	116	0	210	70	4207	72.5%
Tomatoes	355	2122	0	0	0	19	237	857	0	168	0	3758	56.5%
Pistachios	0	15	587	1	6	8	51	205	0	0	36	909	64.6%
Water	0	27	0	1170	0	54	0	0	197	0	0	1448	80.8%
Fallow	3	0	37	42	1878	306	61	0	750	0	0	3077	61.0%
Developed	4	0	3	50	548	2222	138	1	479	0	2	3447	64.5%
Cotton	0	352	10	0	44	94	1068	4	0	17	131	1720	74.7%
Corn	251	382	0	0	0	2	0	1284	0	0	11	1930	66.5%
Barren	56	0	1	1	965	241	0	0	1544	0	0	2808	55.0%
Almonds	140	484	0	0	0	10	249	317	0	1956	307	3463	56.5%
Alfalfa	5	1	0	0	0	0	0	73	0	97	1518	1694	89.6%
Total	3866	3671	667	1264	3441	2975	2256	2857	2970	2517	2075	28559	
Producer's Acc	78.9%	57.8%	88.0%	92.6%	54.6%	74.7%	47.3%	44.9%	52.0%	77.7%	73.2%	18401	
Overall Accuracy (18401/28559) = 64.4315%											Overall	64.43%	
Kappa Coefficient = 0.60													

Table 64. Classification fitness ranking using EO for Fresno-Kings Counties, USA.

Sorted by FI			
Class	User's	Producer's	FI
Water	80.8%	92.6%	86.7%
Alfalfa	89.6%	73.2%	81.4%
Pistachios	64.6%	88.0%	76.3%
WinterWheat	72.5%	78.9%	75.7%
Developed	64.5%	74.7%	69.6%
Almonds	56.5%	77.7%	67.1%
Cotton	74.7%	47.3%	61.0%
Fallow	61.0%	54.6%	57.8%
Tomatoes	56.5%	57.8%	57.1%
Corn	66.5%	44.9%	55.7%
Barren	55.0%	52.0%	53.5%
		Overall	64.4%

4.3.4.2 Test Series 2 - EO + SAR-HH

Test series 2 added the despeckled HH SAR bands individually to EO. The overall accuracy of the X-band resulted in 65.7%, only 1.24% better than EO alone (Table 65). The C-band plus EO had a 69.8% overall accuracy, improving the EO overall accuracy by 5.35%. With the addition of the SAR despeckled HH the class FI's changed and are compared in Table 64; the EO results are repeated for reference. Table 66 is the error matrix for this test series.

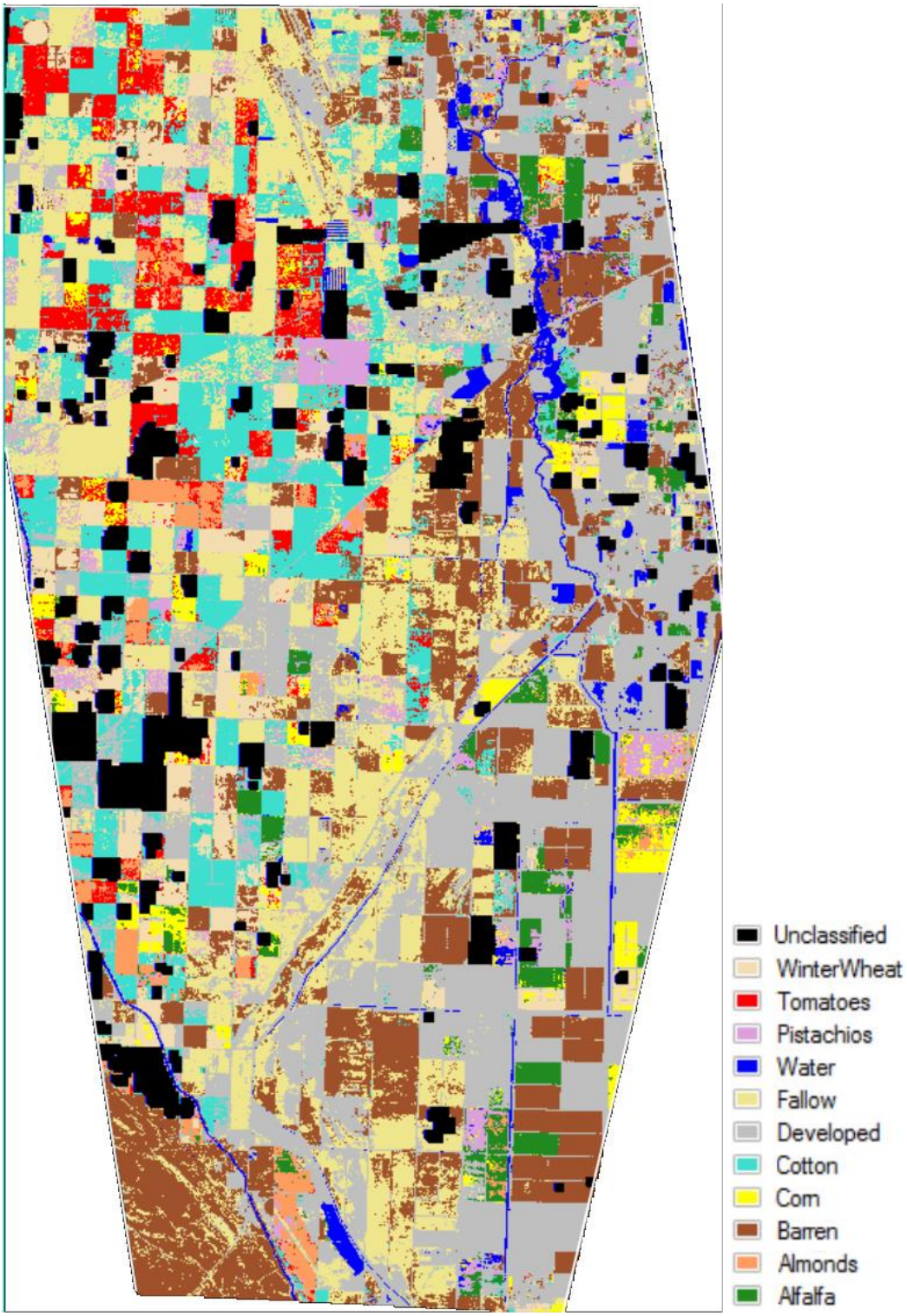

Figure 42. Land cover classification thematic map using EO imagery for Fresno-Kings Counties, USA. Overall accuracy 64.4%. Scene width ~ 25 km.

Table 65. Comparison of classification results with EO + SAR for Fresno-Kings Counties, USA.

Producer's Accuracy								
Subtest	1	a	b	c	d	e	f	g
Class / Bands	EO	X	C	L	X+C	X+L	C+L	X+C+L
WinterWheat	78.94	73.02	79.69	79.33	72.37	70.95	73.54	72.61
Tomatoes	57.80	56.12	57.12	62.41	38.35	46.64	40.32	40.04
Pistachios	88.01	91.30	79.91	88.01	86.66	65.37	79.16	87.86
Water	92.56	94.86	95.49	92.56	92.41	92.96	91.93	92.48
Fallow	54.58	53.27	60.45	54.32	68.88	65.68	67.83	68.70
Developed	74.69	80.24	77.92	74.96	59.36	57.92	60.24	59.60
Cotton	47.34	51.60	55.81	49.02	54.03	51.37	54.61	54.08
Corn	44.94	46.94	57.54	44.91	58.87	55.65	59.64	60.20
Barren	51.99	60.00	71.85	52.05	73.43	63.97	70.74	72.86
Almonds	77.71	79.54	78.35	82.72	80.45	78.19	82.84	82.96
Alfalfa	73.16	74.94	76.92	80.92	68.53	70.89	68.63	68.34
User's Accuracy								
WinterWheat	72.55	72.61	76.38	75.36	73.17	71.49	73.94	73.73
Tomatoes	56.47	52.48	54.91	55.51	47.33	48.35	47.59	47.59
Pistachios	64.58	68.50	65.80	64.72	73.82	67.70	74.58	75.71
Water	80.80	81.45	81.94	80.80	82.37	82.23	80.98	82.15
Fallow	61.03	69.80	83.37	60.98	68.38	61.05	66.48	67.97
Developed	64.46	62.36	61.86	64.53	78.87	79.51	78.70	78.94
Cotton	62.09	66.40	70.81	62.34	68.83	58.04	69.64	68.97
Corn	66.53	64.60	68.79	65.29	51.72	54.03	51.59	51.47
Barren	54.99	61.13	68.62	55.17	58.74	54.74	58.01	58.82
Almonds	56.48	62.60	61.61	68.87	57.51	63.71	61.96	62.07
Alfalfa	89.61	82.28	99.38	92.00	94.67	89.48	93.75	94.98
Overall Accuracy	64.43%	65.67%	69.75%	66.21%	65.19%	63.51%	65.43%	65.76%
Kappa Coefficient	0.60	0.62	0.66	0.62	0.61	0.59	0.62	0.62

Table 67 contains the class FI ranking for each test. With the X-band, water increased to 88.2% and three more classes passed 70% than with EO alone. Both water and alfalfa had FI's greater than 85% with the C-band, and seven classes were between 69-79%. Only tomatoes and corn were less than 65%. With EO plus the L-band, water and alfalfa had a FI greater than 85%; three classes were above 75% and the remaining classes were below 70%.

Table 66. Error matrix for Fresno-Kings Counties,, USA, using EO + SAR despeckled HH L-band.

Ground Truth (Pixels)													
Class	WinterWheat	Tomatoes	Pistachios	Water	Fallow	Developed	Cotton	Corn	Barren	Almonds	Alfalfa	Total	User's Acc
WinterWheat	3067	288	0	0	0	17	326	93	0	210	69	4070	75.4%
Tomatoes	459	2291	0	0	0	24	236	1043	0	74	0	4127	55.5%
Pistachios	0	16	587	1	5	7	56	203	0	0	32	907	64.7%
Water	0	27	0	1170	0	54	0	0	197	0	0	1448	80.8%
Fallow	3	0	37	42	1869	303	61	0	750	0	0	3065	61.0%
Developed	4	0	4	50	550	2230	138	1	477	0	2	3456	64.5%
Cotton	0	351	9	0	50	95	1106	4	0	28	131	1774	72.3%
Corn	277	385	0	0	0	2	0	1283	0	0	18	1965	65.3%
Barren	54	0	1	1	967	233	0	0	1546	0	0	2802	55.2%
Almonds	0	313	0	0	0	10	333	141	0	2082	144	3023	68.9%
Alfalfa	2	0	0	0	0	0	0	89	0	55	1679	1825	92.0%
Total	3866	3671	667	1264	3441	2975	2256	2857	2970	2517	2075	28,559	
Producer's Acc	79.3%	62.4%	88.0%	92.6%	54.3%	75.0%	49.0%	44.9%	52.1%	82.7%	80.9%	Overall	66.21%
Overall Accuracy =	66.21%												
Kappa Coefficient =	0.62												

Table 67. Comparison of FI for Fresno-Kings Counties,, USA, for classifications with EO and SAR despeckled HH. Classes are sorted by FI for each test.

EO		EO+X-band		EO+C-band		EO+L-band	
Class	FI	Class	FI	Class	FI	Class	FI
Water	86.7%	Water	88.2%	Water	88.7%	Water	86.7%
Alfalfa	81.4%	Pistachios	79.9%	Alfalfa	88.1%	Alfalfa	86.5%
Pistachios	76.3%	Alfalfa	78.6%	WinterWheat	78.0%	WinterWheat	77.3%
WinterWheat	75.7%	WinterWheat	72.8%	Cotton	74.1%	Pistachios	76.4%
Developed	69.6%	Developed	71.3%	Pistachios	72.9%	Almonds	75.8%
Almonds	67.1%	Almonds	71.1%	Fallow	71.9%	Developed	69.7%
Cotton	61.0%	Cotton	64.0%	Barren	70.2%	Cotton	60.7%
Fallow	57.8%	Fallow	61.5%	Almonds	70.0%	Tomatoes	59.0%
Tomatoes	57.1%	Barren	60.6%	Developed	69.9%	Fallow	57.6%
Corn	55.7%	Corn	55.8%	Corn	63.2%	Corn	55.1%
Barren	53.5%	Tomatoes	54.3%	Tomatoes	56.0%	Barren	53.6%

4.3.4.3 Test Series 3 – EO + SAR-HH + SAR Variance

For test series 3 the individual test results for user's and producer's accuracy for each class are compared in a single table. The addition of variance to the EO and SAR despeckled HH data improved the overall accuracy (Table 68). The C-band variance had the highest overall accuracy of 67.1%, 2.7% over EO. Using despeckled HH and variance from more than a single SAR band increased further the classification accuracy with the

exception of the combination of C-band and L-band. X-band with C-band variance raised the overall accuracy to 69.9%. Using all three SAR bands and variance only increased the overall accuracy by 0.33% so the additional cost for using more data from an additional satellite (L-band) would not be justified.

Table 68. Comparison of classification results with EO + SAR + 21x21 Variance, for Fresno-Kings Counties, USA.

EO + HH + V							
Producer's Accuracy							
sub-test	a	b	c	d	e	f	g
Class / Bands	X	C	L	X+C	X+L	C+L	X+C+L
WinterWheat	72.79	78.40	78.56	70.33	72.79	79.00	67.85
Tomatoes	55.52	35.88	46.55	60.99	59.11	48.82	63.66
Pistachios	90.85	82.16	88.01	74.06	91.15	65.07	73.31
Water	95.02	93.91	96.28	96.99	95.02	96.68	96.99
Fallow	53.01	73.35	56.18	68.00	53.33	65.53	67.51
Developed	81.21	63.36	74.15	76.94	81.85	73.01	78.66
Cotton	51.82	56.16	48.58	57.23	53.72	57.40	57.58
Corn	47.32	60.94	62.27	54.92	47.22	54.67	55.79
Barren	60.54	69.53	61.82	73.64	60.54	73.47	73.74
Almonds	79.54	82.60	79.06	78.67	82.16	80.65	79.46
Alfalfa	75.04	73.69	82.17	78.51	82.94	86.75	78.84
User's Accuracy							
WinterWheat	72.40	75.30	78.76	75.51	74.72	80.54	76.36
Tomatoes	52.16	44.95	50.18	49.37	53.12	49.23	51.50
Pistachios	68.40	88.39	64.15	63.50	68.55	59.21	63.26
Water	81.53	81.69	81.30	82.17	81.53	81.79	81.95
Fallow	70.95	68.01	67.54	78.81	71.29	74.52	79.47
Developed	62.22	79.37	68.04	69.83	62.74	71.87	70.12
Cotton	67.18	62.82	70.85	72.53	68.17	77.41	71.02
Corn	63.15	56.56	53.70	71.61	63.39	49.13	69.64
Barren	61.49	63.75	56.56	69.85	61.47	65.58	69.88
Almonds	63.41	60.95	69.27	64.35	70.63	73.15	65.10
Alfalfa	82.34	95.62	99.94	99.88	84.53	99.89	99.94
Overall Accuracy	65.75%	67.13%	66.86%	69.90%	67.27%	69.32%	70.23%
Kappa Coefficient	0.62	0.63	0.63	0.66	0.64	0.66	0.67

4.3.4.4 Test Series 4 – EO + SAR-HH + SAR Entropy

Test series 4 investigated the effect of GLCM entropy texture measure fused with EO and SAR-HH data. Again the C-band texture had the greatest improvement on the overall accuracy of 67.9% (Table 69). As was the case with variance, the combination of X-band and C-band entropy resulted in the highest overall accuracy (71.7%). Other combinations resulted about the same; using a third SAR band was not an improvement.

4.3.4.5 Test Series 5 – EO + SAR-HH + SAR Variance + SAR Entropy

Classification with variance, and GLCM entropy texture measures was tested in series 5. In general the overall accuracies from the different tests were similar to those with entropy alone (Table 70). The addition of C-band variance and entropy resulted in an overall accuracy of 69.8%, and the combination of X-band, C-band, and L-band despeckled HH, variance and entropy achieved the best overall accuracy of 71.7%. Removing the L-band, the overall accuracy was 71.4%. The highest user's accuracy was for alfalfa at 91%; the best producer's accuracy was 95.5% for water (Table 71). The thematic classification map is Figure 43.

4.3.4.6 Test Series 6 – SAR despeckled HH + Texture

SAR is especially valuable when consistent cloud cover makes collecting usable EO imagery from satellites impossible. Using SAR alone, Table 72 presents the results from 16 classification tests using different band combinations. The best overall classification achieved using a single SAR band was 33.3% using C-band despeckled HH and entropy. Combing all three SAR bands despeckled HH, variance, and entropy texture an overall accuracy of 45.69% was achieved.

Table 69. Comparison of classification results with EO + SAR + 21x21 entropy for Fresno-Kings Counties, USA.

EO + HH + E							
Producer's Accuracy							
sub-test	a	b	c	d	e	f	g
Class / Bands	X	C	L	X+C	X+L	C+L	X+C+L
WinterWheat	77.57	77.34	76.46	75.53	75.81	77.44	77.73
Tomatoes	49.09	43.67	53.06	63.25	52.33	50.80	58.87
Pistachios	86.66	62.52	57.27	90.85	79.61	61.17	71.81
Water	93.51	96.04	94.15	94.86	94.54	94.46	93.59
Fallow	67.86	73.09	71.26	72.68	72.28	71.61	70.36
Developed	64.24	69.21	69.98	73.55	71.56	74.39	80.44
Cotton	54.70	55.05	51.73	62.32	55.05	54.21	62.68
Corn	52.12	52.89	56.46	54.08	56.49	51.52	30.38
Barren	62.19	72.96	55.62	74.75	61.72	71.52	71.18
Almonds	78.63	81.88	84.35	81.68	84.27	81.33	72.31
Alfalfa	68.10	77.35	77.25	72.92	77.73	79.52	83.66
User's Accuracy							
WinterWheat	75.09	78.40	74.68	76.98	75.27	77.63	77.63
Tomatoes	50.58	48.41	50.10	55.72	49.23	51.85	56.22
Pistachios	72.43	54.16	98.71	68.71	93.32	54.69	67.18
Water	83.53	82.25	82.47	82.18	83.10	79.76	81.47
Fallow	61.94	71.63	55.85	82.81	61.64	72.30	80.41
Developed	78.06	79.07	89.20	73.77	88.86	80.47	77.14
Cotton	53.77	73.19	61.32	67.66	56.71	75.22	63.10
Corn	65.11	50.08	59.06	66.57	63.79	47.26	46.27
Barren	60.90	66.57	56.08	71.31	60.74	65.41	69.70
Almonds	60.35	63.69	75.26	67.54	73.01	73.40	72.16
Alfalfa	90.00	90.52	97.03	93.34	95.90	90.07	62.11
Overall Accuracy	65.72%	67.87%	67.12%	71.70%	68.69%	68.82%	68.61%
Kappa Coefficient	0.62	0.64	0.63	0.68	0.65	0.65	0.65

Using the C-band, the best user's accuracy was found for fallow; the developed area class showed the best producer's accuracy (Table 73). In the error matrix for the three SAR bands together, several classes had better results for user's and producer's accuracy (Table 74). The developed area class showed the highest user's accuracies

(77.66%) and the best producer's accuracy was found for the barren ground and almond classes. Figure 44 is the corresponding thematic classification map.

Table 70. Comparison of classification results with EO + SAR + 21x21 variance and entropy for Fresno-Kings Counties, USA.

EO + HH + VE							
Producer's Accuracy							
sub-test	a	b	c	d	e	f	g
Class / Bands	X	C	L	X+C	X+L	C+L	X+C+L
WinterWheat	78.32	75.97	78.38	75.50	77.73	78.19	74.47
Tomatoes	60.28	58.43	64.34	63.28	58.87	38.46	71.13
Pistachios	80.96	73.46	86.96	91.00	71.81	81.26	60.42
Water	94.22	94.94	93.20	95.17	93.59	93.91	96.52
Fallow	56.87	67.97	47.66	67.83	70.36	74.28	77.22
Developed	80.54	75.80	76.47	76.00	80.44	71.66	74.69
Cotton	55.94	55.36	49.78	61.88	62.68	55.90	60.95
Corn	31.12	56.00	46.66	54.36	30.38	61.71	39.27
Barren	69.76	72.63	61.25	74.34	71.18	69.19	74.41
Almonds	72.55	80.14	83.08	81.68	72.31	86.09	85.62
Alfalfa	77.69	74.60	84.29	73.11	83.66	68.29	78.31
User's Accuracy							
WinterWheat	77.17	74.69	75.62	76.84	77.63	75.67	84.30
Tomatoes	58.84	51.56	55.71	55.79	56.22	45.50	53.62
Pistachios	63.31	54.02	64.44	68.51	67.18	91.86	61.43
Water	81.24	81.91	80.35	82.34	81.47	82.72	82.27
Fallow	81.07	78.25	63.44	81.78	80.41	67.67	73.50
Developed	63.54	70.82	66.74	71.17	77.14	86.60	82.45
Cotton	63.26	72.36	63.05	69.14	63.10	62.86	72.14
Corn	49.06	73.29	66.55	65.47	46.27	53.96	52.65
Barren	68.77	68.67	55.09	71.00	69.70	64.99	70.40
Almonds	64.45	65.72	72.13	68.62	72.16	73.14	77.83
Alfalfa	61.55	90.63	93.48	93.30	62.11	83.50	90.99
Overall Accuracy	66.48%	69.81%	67.16%	71.35%	68.61%	68.33%	71.71%
Kappa Coefficient	0.627	0.664	0.634	0.681	0.651	0.647	0.685

Table 71. Error matrix for the classification with EO + X, C, and L-band SAR + 21x21 variance and entropy for Fresno-Kings Counties, USA.

Ground Truth (Pixels)													
Class	WinterWheat	Tomatoes	Pistachios	Water	Fallow	Developed	Cotton	Corn	Barren	Almonds	Alfalfa	Total	User's Acc
WinterWheat	2879	105	0	0	0	4	166	56	0	202	3	3415	84.30%
Tomatoes	355	2611	0	0	0	0	317	1449	0	56	81	4869	53.62%
Pistachios	0	1	403	0	0	1	65	170	0	0	16	656	61.43%
Water	0	24	0	1220	0	38	0	0	201	0	0	1483	82.27%
Fallow	10	0	200	0	2657	520	6	0	222	0	0	3615	73.50%
Developed	0	0	36	41	52	2222	7	0	337	0	0	2695	82.45%
Cotton	54	302	0	0	0	4	1375	0	0	37	134	1906	72.14%
Corn	548	355	0	0	0	0	41	1122	0	0	65	2131	52.65%
Barren	16	0	0	3	732	178	0	0	2210	0	0	3139	70.40%
Almonds	3	181	0	0	0	8	211	60	0	2155	151	2769	77.83%
Alfalfa	1	92	0	0	0	0	68	0	0	0	1625	1786	90.99%
Total	3866	3671	667	1264	3441	2975	2256	2857	2970	2517	2075	28559	
Producer's Acc	74.47%	71.13%	60.42%	96.52%	77.22%	74.69%	60.95%	39.27%	74.41%	85.62%	78.31%	Overall	71.71%
Overall Accuracy(20479/28559)= 71.71%													
Kappa Coefficient = 0.69													

Table 72. Comparison of classification results with SAR + 21x21 variance and entropy for Fresno-Kings Counties, USA.

HH + VE																
Producer's Accuracy																
sub-test	a	b	c	d	e	f	g	h	i	j	k	l	m	n	o	p
Class / Bands	X	C	L	X+V	C+V	L+V	X+E	C+E	L+E	XVE	CVE	LVE	XCVE	XLVE	CLVE	XCLVE
WinterWheat	0.00	7.17	0.00	0.00	6.23	0.00	0.00	21.75	0.57	0.00	21.75	0.57	21.44	5.30	22.01	5.59
Tomatoes	53.01	36.12	0.00	0.00	12.18	0.00	0.00	5.56	0.00	6.40	5.39	0.00	6.02	55.49	16.07	53.36
Pistachios	0.00	0.00	0.00	0.00	0.00	0.00	0.00	0.00	1.65	0.00	0.00	1.65	0.00	0.00	9.00	14.24
Water	43.35	0.00	0.00	48.81	0.87	0.00	52.37	16.61	4.03	54.51	28.64	4.03	46.68	46.76	33.15	59.41
Fallow	34.93	59.02	100.00	45.10	84.02	100.00	38.04	81.05	97.38	32.98	57.40	97.38	59.29	42.81	57.25	51.26
Developed	0.00	3.80	0.00	25.24	31.09	15.09	0.00	43.63	51.56	29.48	49.58	51.66	51.09	58.69	57.01	58.32
Cotton	18.35	8.20	0.00	23.54	17.33	0.00	40.87	14.67	0.00	41.27	14.18	0.00	15.03	30.41	13.61	28.24
Corn	0.00	0.00	0.00	26.25	0.00	0.00	9.52	1.47	0.00	4.83	1.61	0.00	19.46	16.17	34.69	22.89
Barren	70.07	89.73	0.00	68.65	74.18	0.00	80.61	71.11	0.00	77.21	85.86	0.00	84.11	80.81	86.09	80.91
Almonds	34.13	47.16	84.51	17.36	65.04	82.72	66.75	42.59	82.84	51.37	42.59	82.84	61.10	70.88	82.64	78.70
Alfalfa	0.00	0.00	0.00	47.18	0.00	0.00	0.00	2.02	0.00	14.02	2.41	0.00	39.37	26.02	0.14	41.20
User's Accuracy																
WinterWheat	0.00	8.60	0.00	0.00	8.24	0.00	0.00	13.94	4.36	0.00	13.91	4.36	27.30	37.48	17.96	32.53
Tomatoes	23.51	23.70	0.00	0.00	21.84	0.00	0.00	33.28	0.00	27.01	32.84	0.00	39.89	44.11	33.39	32.95
Pistachios	0.00	0.00	0.00	0.00	0.00	0.00	0.00	0.00	7.24	0.00	0.00	7.38	0.00	0.00	39.47	38.00
Water	41.70	0.00	0.00	44.04	55.00	0.00	57.12	43.66	22.97	54.38	56.04	22.97	68.37	69.61	70.30	66.34
Fallow	20.69	34.39	14.68	26.01	36.84	14.87	26.32	39.14	15.59	27.46	38.36	15.59	41.06	29.15	38.81	40.58
Developed	0.00	100.00	0.00	86.82	98.51	100.00	0.00	73.04	78.79	88.23	79.17	78.82	68.81	77.43	75.38	77.66
Cotton	41.99	48.18	0.00	34.73	37.03	0.00	19.01	49.70	0.00	15.53	64.65	0.00	42.27	23.92	43.24	24.49
Corn	0.00	0.00	0.00	26.39	0.00	0.00	20.39	24.00	0.00	9.08	25.56	0.00	26.77	27.03	24.83	23.12
Barren	34.01	38.88	0.00	40.05	51.86	0.00	46.99	57.07	0.00	47.95	45.00	0.00	63.99	49.58	46.33	64.03
Almonds	14.42	18.30	41.51	15.37	17.45	42.71	15.47	14.54	50.34	19.55	14.54	50.34	18.52	61.20	60.80	69.56
Alfalfa	0.00	0.00	0.00	12.40	0.00	0.00	0.00	8.12	0.00	12.89	11.31	0.00	46.90	20.19	1.23	45.97
Overall Accuracy	24.69%	27.26%	19.50%	26.81%	30.62%	20.91%	25.35%	31.31%	24.70%	27.60%	31.13%	24.71%	38.33%	41.75%	40.35%	45.69%
Kappa Coefficient	0.16	0.18	0.09	0.19	0.22	0.11	0.18	0.23	0.15	0.20	0.23	0.15	0.31	0.35	0.33	0.39

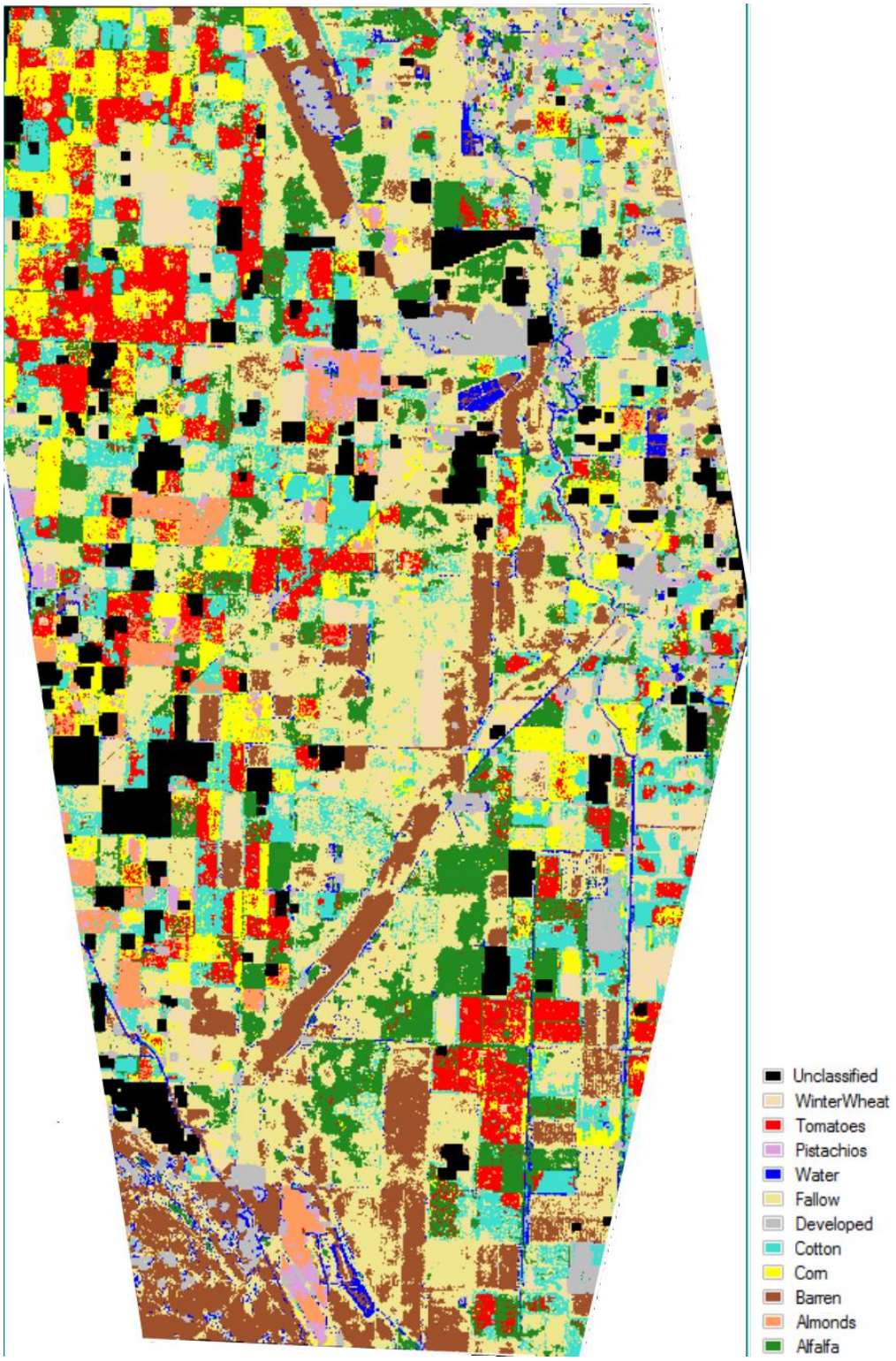

Figure 43. Land cover classification using EO, X, C, and L-band SAR and 21x21 variance and entropy texture measures for Fresno-Kings Counties, USA. Overall accuracy was 71.7%. Test 5g. Scene width ~ 25 km.

Table 73. Error matrix with C-band SAR + 21x21 entropy for Fresno-Kings Counties, USA.

Ground Truth (Pixels)													
Class	WinterWheat	Tomatoes	Pistachios	Water	Fallow	Developed	Cotton	Corn	Barren	Almonds	Alfalfa	Total	User's Acc
Unclassified	0	0	29	0	0	0	0	0	0	67	0	96	
WinterWheat	841	1427	384	12	99	77	591	875	4	1189	534	6033	13.94%
Tomatoes	16	204	0	11	0	12	156	14	0	136	64	613	33.28%
Pistachios	0	0	0	0	0	0	0	0	0	0	0	0	0.00%
Water	0	0	0	210	28	131	0	0	112	0	0	481	43.66%
Fallow	1183	13	86	78	2789	588	223	178	731	7	1250	7126	39.14%
Developed	1	73	0	352	11	1298	15	27	0	0	0	1777	73.04%
Cotton	0	2	0	68	0	232	331	0	0	0	33	666	49.70%
Corn	27	20	31	1	0	0	3	42	0	46	5	175	24.00%
Barren	0	0	0	496	451	560	0	0	2112	0	82	3701	57.07%
Almonds	1754	1889	23	6	0	1	863	1701	0	1072	65	7374	14.54%
Alfalfa	44	43	114	30	63	76	74	20	11	0	42	517	8.12%
Total	3866	3671	667	1264	3441	2975	2256	2857	2970	2517	2075	28559	
Producer's Acc	21.75%	5.56%	0.00%	16.61%	81.05%	43.63%	14.67%	1.47%	71.11%	42.59%	2.02%	Overall	31.31%
Overall Accuracy (8941/28559) = 31.31%													
Kappa Coefficient = 0.23													

Table 74. Error matrix with X, C, and L-band SAR + 21x21 variance and entropy for Fresno-Kings Counties, USA.

Ground Truth (Pixels)													
Class	WinterWheat	Tomatoes	Pistachios	Water	Fallow	Developed	Cotton	Corn	Barren	Almonds	Alfalfa	Total	User's Acc
WinterWheat	216	97	1	5	70	22	2	17	31	21	182	664	32.53%
Tomatoes	778	1959	16	2	69	5	1041	1365	0	270	440	5945	32.95%
Pistachios	51	25	95	15	2	20	0	17	0	12	13	250	38.00%
Water	0	0	0	751	1	79	0	0	301	0	0	1132	66.34%
Fallow	1068	1	23	34	1764	403	222	153	235	6	438	4347	40.58%
Developed	44	0	34	314	90	1735	0	13	0	0	4	2234	77.66%
Cotton	601	606	56	73	58	59	637	318	0	117	76	2601	24.49%
Corn	910	679	178	8	6	7	297	654	0	38	52	2829	23.12%
Barren	71	0	0	27	757	480	0	0	2403	0	15	3753	64.03%
Almonds	127	209	227	0	0	0	5	299	0	1981	0	2848	69.56%
Alfalfa	0	94	9	35	624	165	52	21	0	5	855	1860	45.97%
Total	3866	3671	667	1264	3441	2975	2256	2857	2970	2517	2075	28559	
Producer's Acc	5.59%	53.36%	14.24%	59.41%	51.26%	58.32%	28.24%	22.89%	80.91%	78.70%	41.20%	Overall	45.69%
Overall Accuracy (13050/28559) = 45.69%													
Kappa Coefficient = 0.39													

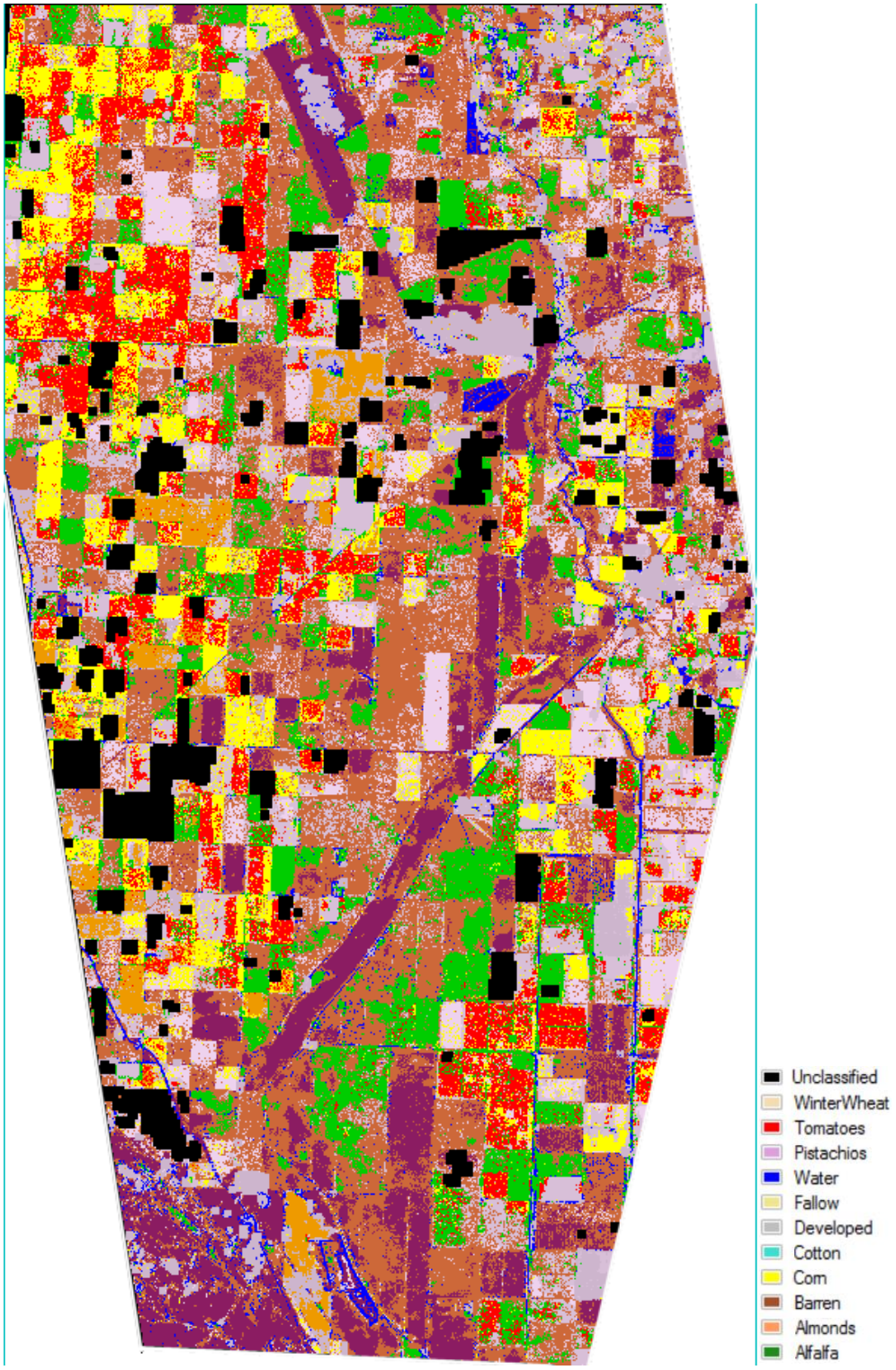

Figure 44. Land cover classification using X, C, and L-band SAR and 21x21 variance and entropy texture measures for Fresno-Kings Counties, USA. Overall accuracy was 45.7%.Test 6p. Scene width ~ 25 km.

4.3.5 Best Band Combination per Class

The FI was used to compare band combinations for each class to account for both user's and producer's accuracy, representing both errors of commission and omission. Using EO, the highest FI was 86.68% for water; the lowest FI was 53.49 for barren ground (Table 75). For EO+SAR, alfalfa had the highest FI (93.3%), followed by water, pistachios, almonds, and developed areas. Tomatoes, corn and cotton were the most difficult classes to identify using EO+SAR. Using only SAR, almonds and barren ground had the highest FI just over 74%; corn, pistachios and winter wheat, were the most difficult classes to separate using SAR alone.

Table 75. Best band combinations for each class based on the FI using EO+SAR and SAR alone for Fresno-Kings Counties, USA. The table is sorted on FI.

	EO		EO+SAR			SAR Only	
Class	FI	Class	Best Bands	FI	Class	Best Bands	FI
Water	86.68%	Alfalfa	EO+CLV	93.32	Almonds	XCLVE	74.13
Alfalfa	81.38%	Water	EO+XCVL	89.58	Barren	XCVE	74.05
Pistachios	76.29%	Pistachios	EO+CLVE	86.56	Developed	XLVE	68.06
WinterWheat	75.75%	Almonds	EO+XCLVE	81.73	Water	XCLVE	62.88
Developed	69.58%	Developed	EO+XLE	80.21	Fallow	CV	60.43
Almonds	67.10%	WinterWheat	EO+CLV	79.77	Tomatoes	XLVE	49.80
Cotton	61.00%	Fallow	EO+XCE	77.75	Alfalfa	XCLVE	43.59
Fallow	57.81%	Barren	EO+XCE	73.03	Cotton	CVE	39.42
Tomatoes	57.14%	Cotton	EO+CLV	67.41	Corn	CLVE	29.76
Corn	55.74%	Corn	EO+CVE	64.65	Pistachios	XCLVE	26.12
Barren	53.49%	Tomatoes	EO+XCVL	62.38	WinterWheat	XCVE	24.37

Alfalfa and Water

C-band despeckled HH was the best single SAR band to use individually to classify alfalfa; the combination of C and L-band with variance, however resulted, in the highest FI of 93.3% (Figure 45). Water was best classified by SAR C-band with EO; the

best band combination was X plus C-band despeckled HH and variance with a FI of 89.58% (Figure 46).

Pistachios and Almonds

For Pistachios, the X-band SAR despeckled HH was the best individual SAR contributor with EO but the C-band with variance, and the X and L band with despeckled HH and entropy was better (Figure 47). C and L-band despeckled HH, variance, and entropy, however, did slightly better with a FI of 86.56%. Almonds were best classified when fusing EO with an individual SAR by the L-band SAR despeckled HH. Entropy texture increased the FI more than variance (Figure 48). When all SAR bands despeckled HH, variance, and entropy texture were fused with EO the highest FI of 81.73% was achieved (see Table 75).

Developed Areas and Winter Wheat

The single best SAR band to identify developed areas when fused with EO was the X-band (Figure 49). Variance texture increased the FI but entropy texture did better with L-band and the best FI was found with X and L-band SAR despeckled HH and entropy with EO. For winter wheat, the C-band SAR despeckled HH was the best individual SAR band to fuse with EO but the FI increased to nearly 80% by also using the L-band and variance from both SAR bands (Figure 50).

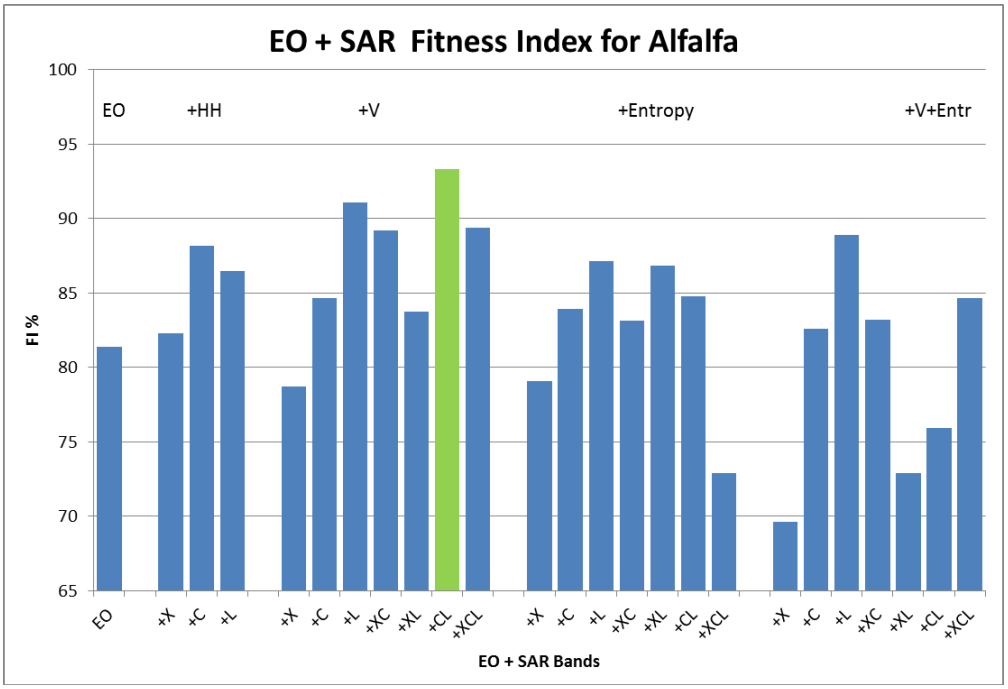

Figure 45. FI for alfalfa using different band combinations for Fresno-Kings Counties, USA.

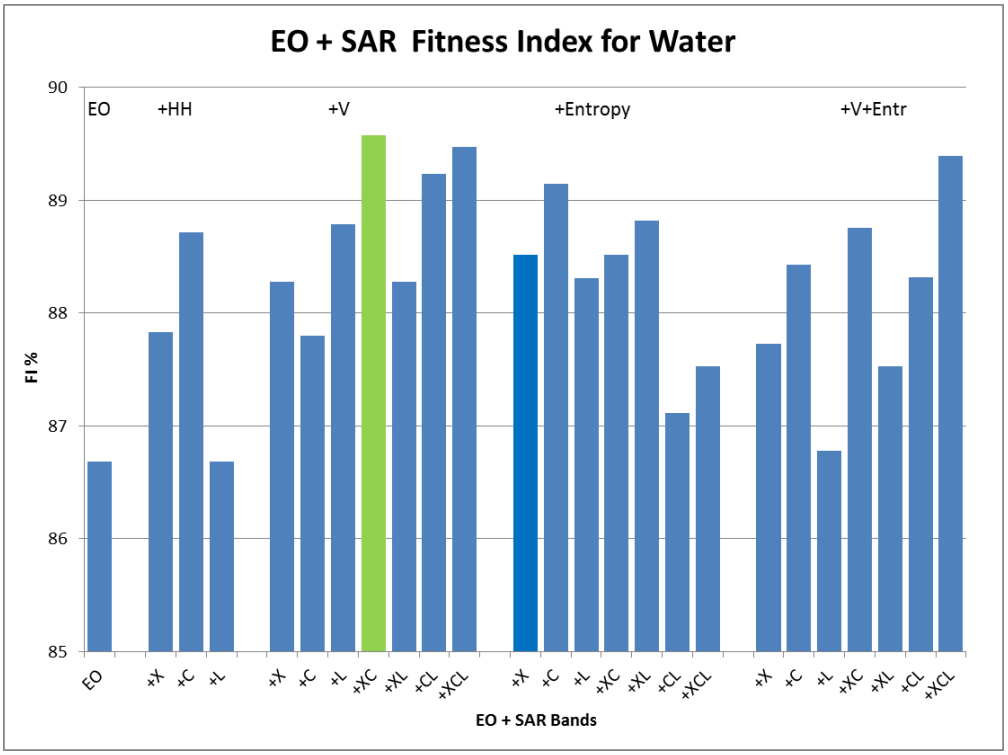

Figure 46. FI for water using different band combinations for Fresno-Kings Counties, USA.

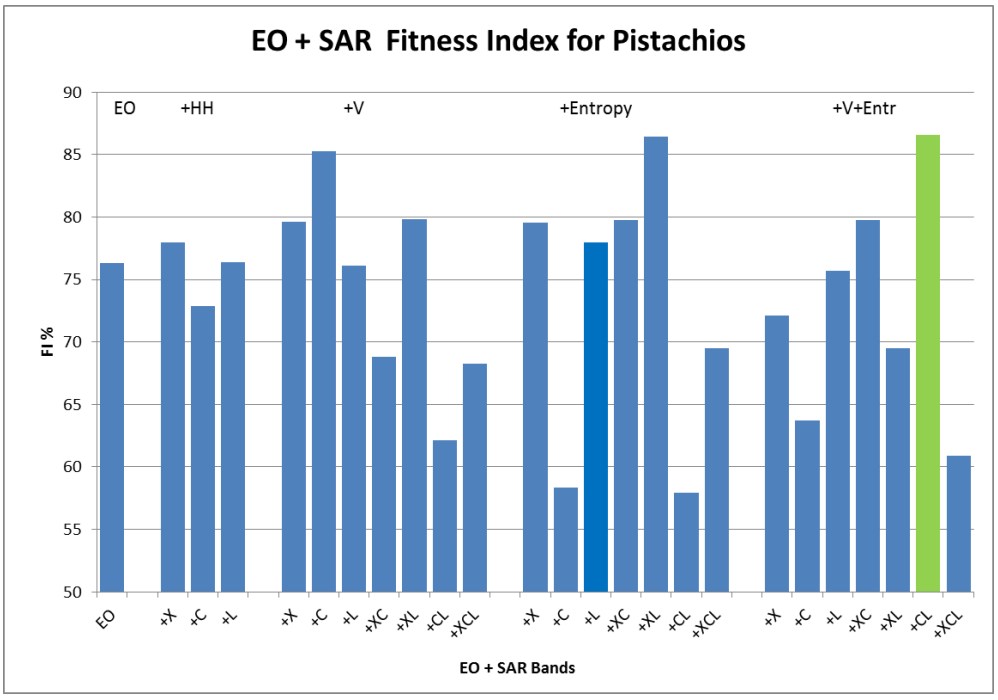

Figure 47. FI for pistachios using different band combinations for Fresno-Kings Counties, USA.

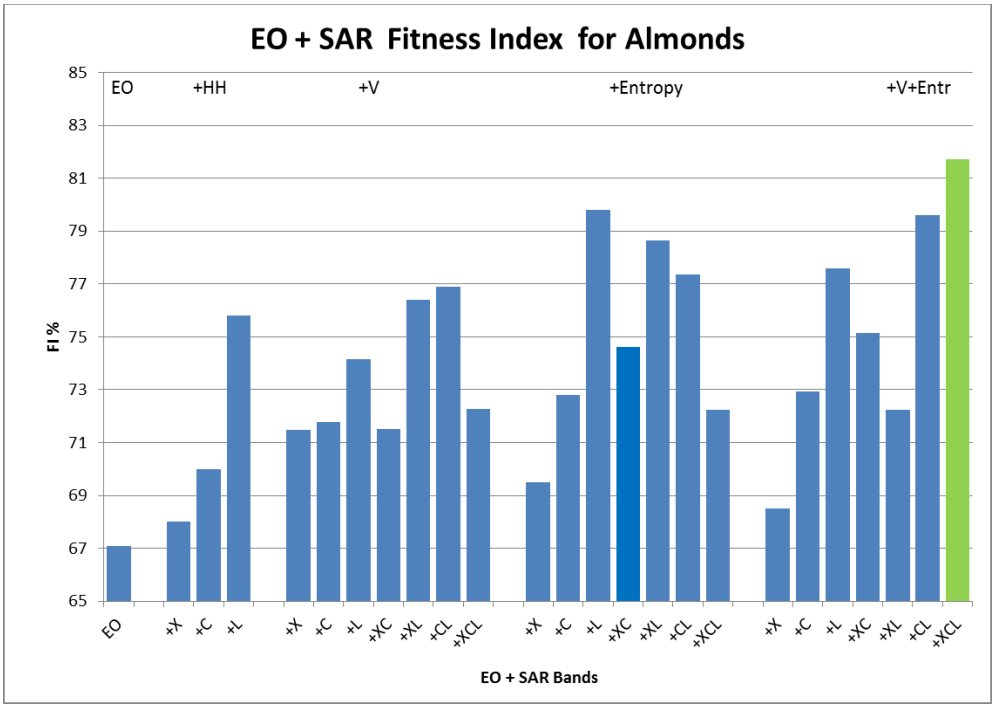

Figure 48. FI for almonds using different band combinations for Fresno-Kings Counties, USA.

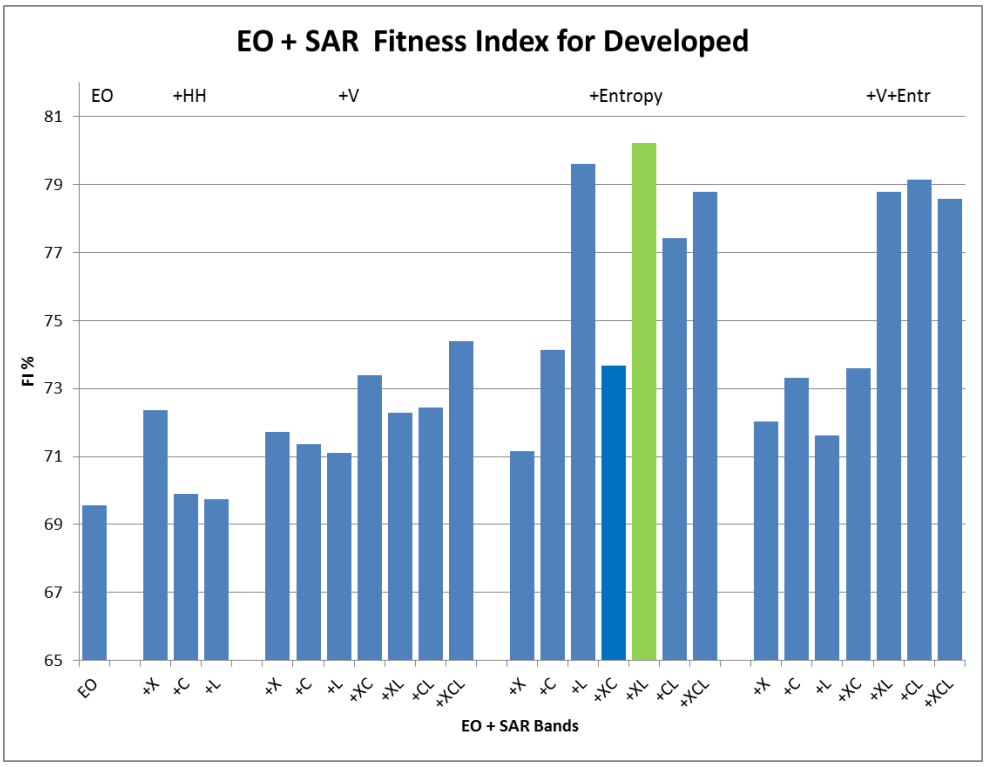

Figure 49. FI for developed areas using different band combinations for Fresno-Kings Counties, USA.

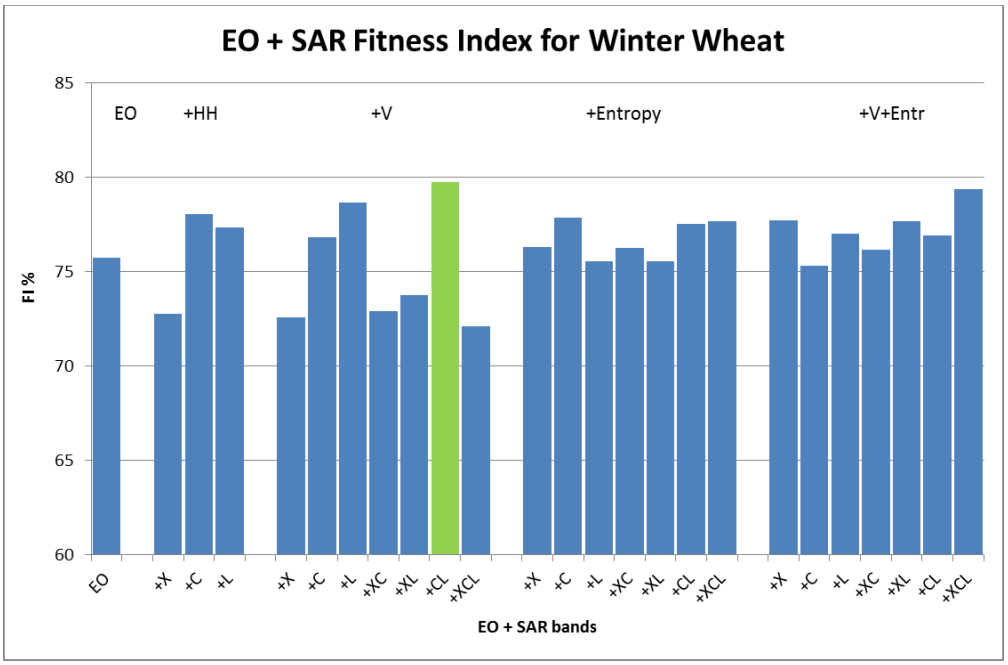

Figure 50. FI for winter wheat using different band combinations for Fresno-Kings Counties, USA.

Fallow and Barren Ground

For fallow, the C-band despeckled HH made the best individual improvement when fused with EO (Figure 51); the X and C-band despeckled HH with entropy had the highest FI of 77.75%. Barren ground was best classified by fusing EO with C-band SAR despeckled HH (Figure 52). Some combinations of EO + SAR with variance gained better FI but the best FI was with X and C-band despeckled HH and entropy with 73% (see Table 75).

Cotton and Corn

C-band SAR was also the best individual SAR band for cotton (Figure 53) and corn (Figure 54). The addition of the L-band and variance was the best band combination for cotton while C-band despeckled HH, variance and entropy texture had the best FI for corn. Tomatoes were harder to classify than the other classes; the L-band SAR despeckled HH helped the most compared to the other two SAR bands. X and C-band despeckled HH with entropy did better, but fusion with data from all three SAR bands, plus variance and entropy texture was the best classifier reaching 62.38% FI (Figure 55, see Table 75).

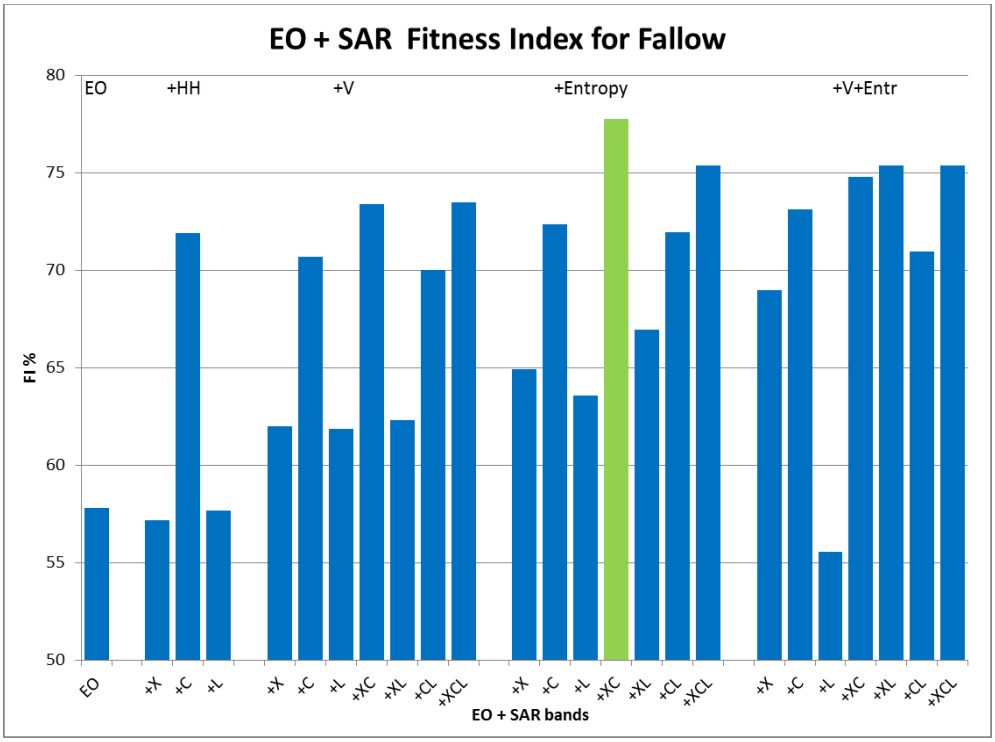

Figure 51. FI for fallow using different band combinations for Fresno-Kings Counties, USA.

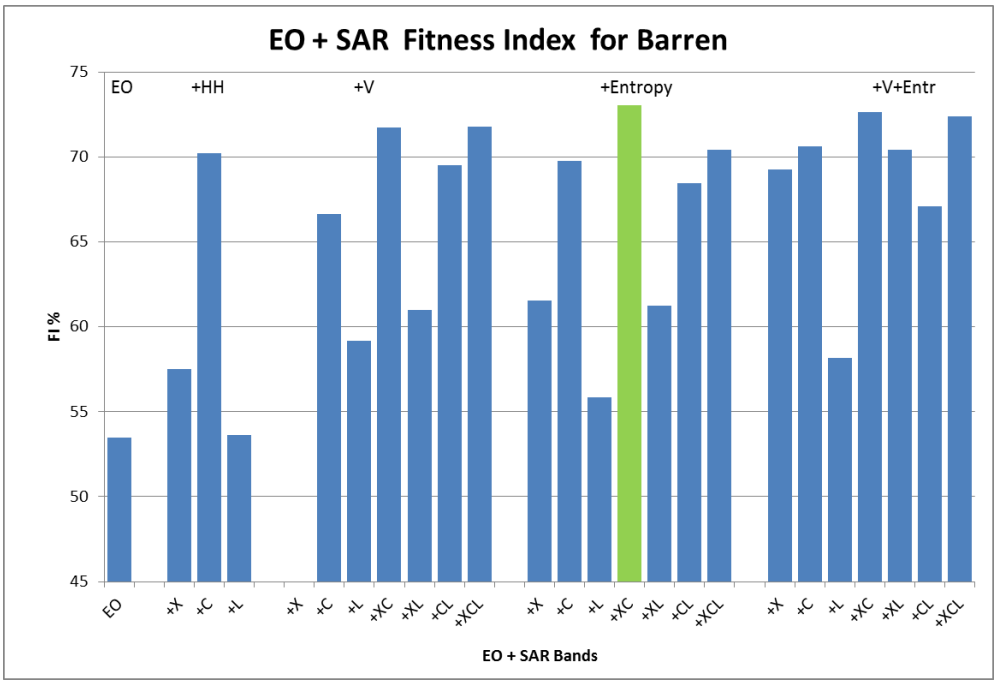

Figure 52. FI for barren ground using different band combinations for Fresno-Kings Counties, USA.

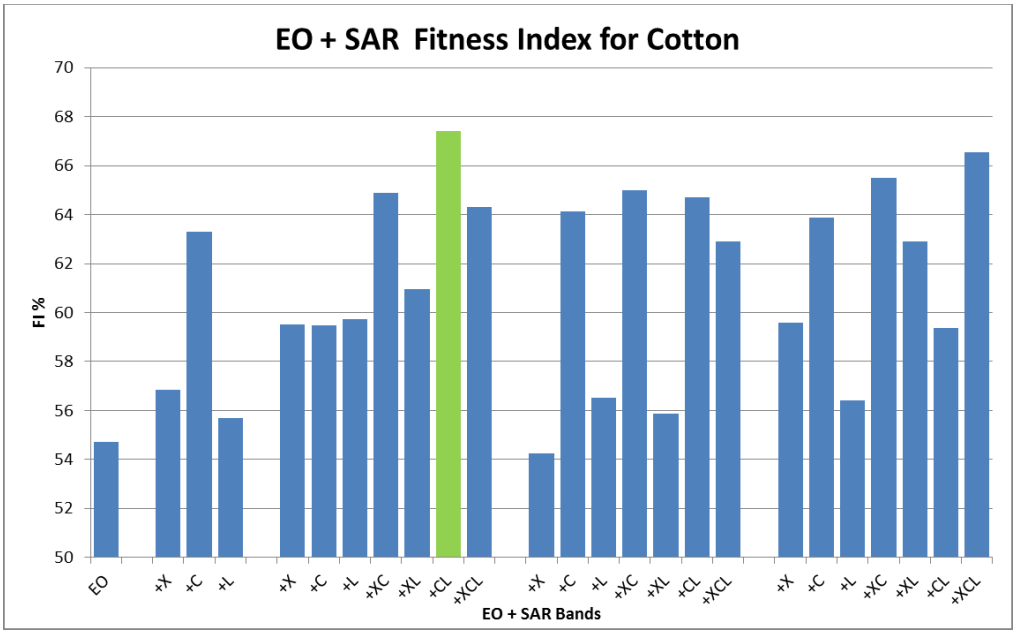

Figure 53. FI for cotton using different band combinations for Fresno-Kings Counties, USA.

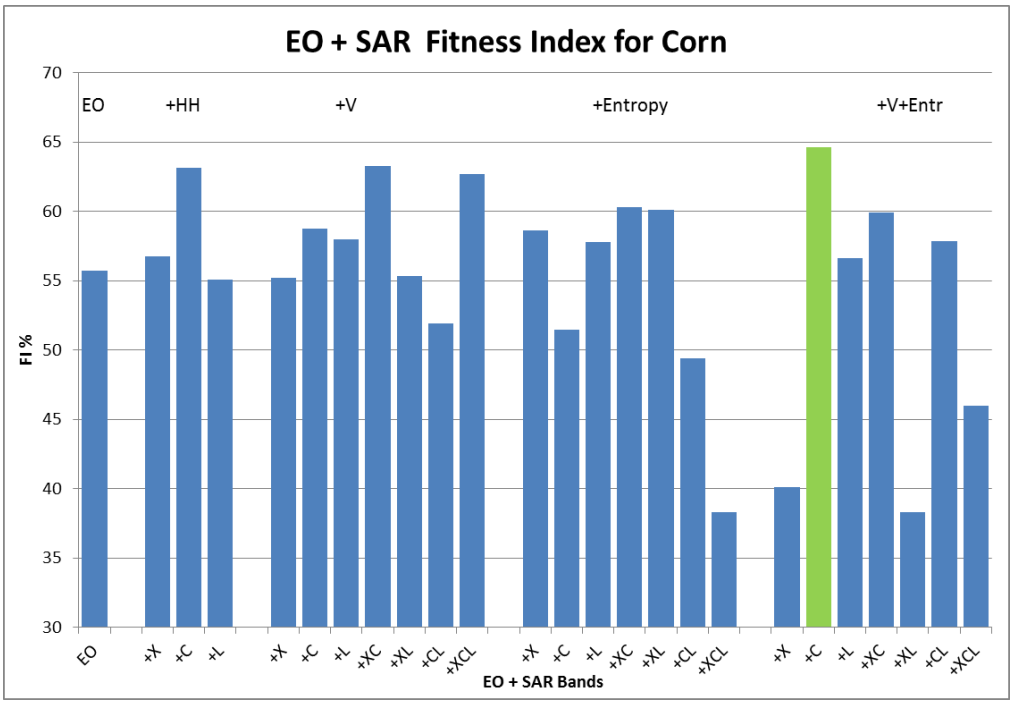

Figure 54. FI for corn using different band combinations for Fresno-Kings Counties, USA.

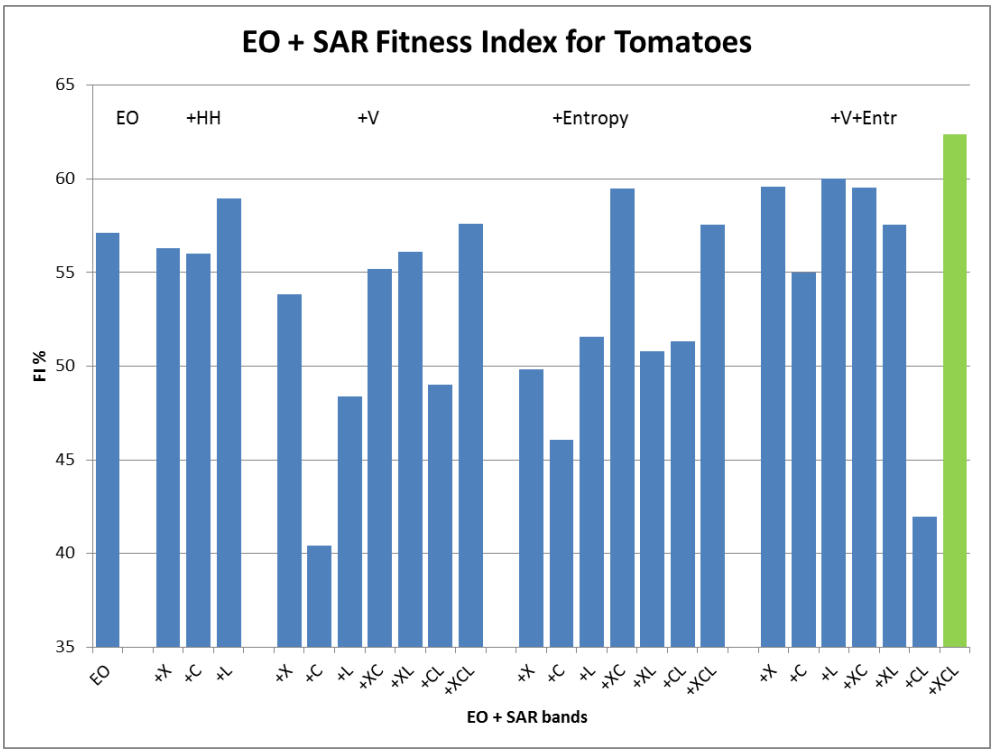

Figure 55. FI for tomatoes using different band combinations for Fresno-Kings Counties, USA.

4.3.6 Summary

SAR alone, as expected, had the lowest overall accuracy compared to EO and EO+SAR (Figure 56, Table 76). All three SAR bands despeckled HH and texture measures were necessary to reach an overall accuracy of 45.7%. EO alone had an overall accuracy of 64.4% and adding X-band SAR with variance and entropy texture increased the overall accuracy by 7.3% to 71.71%. At least for the Fresno-Kings Counties study site, the C-band had the best individual effect compared to the other two SAR bands. Of course once satellite imagery has been obtained, using derived bands represents no additional cost and should be explored.

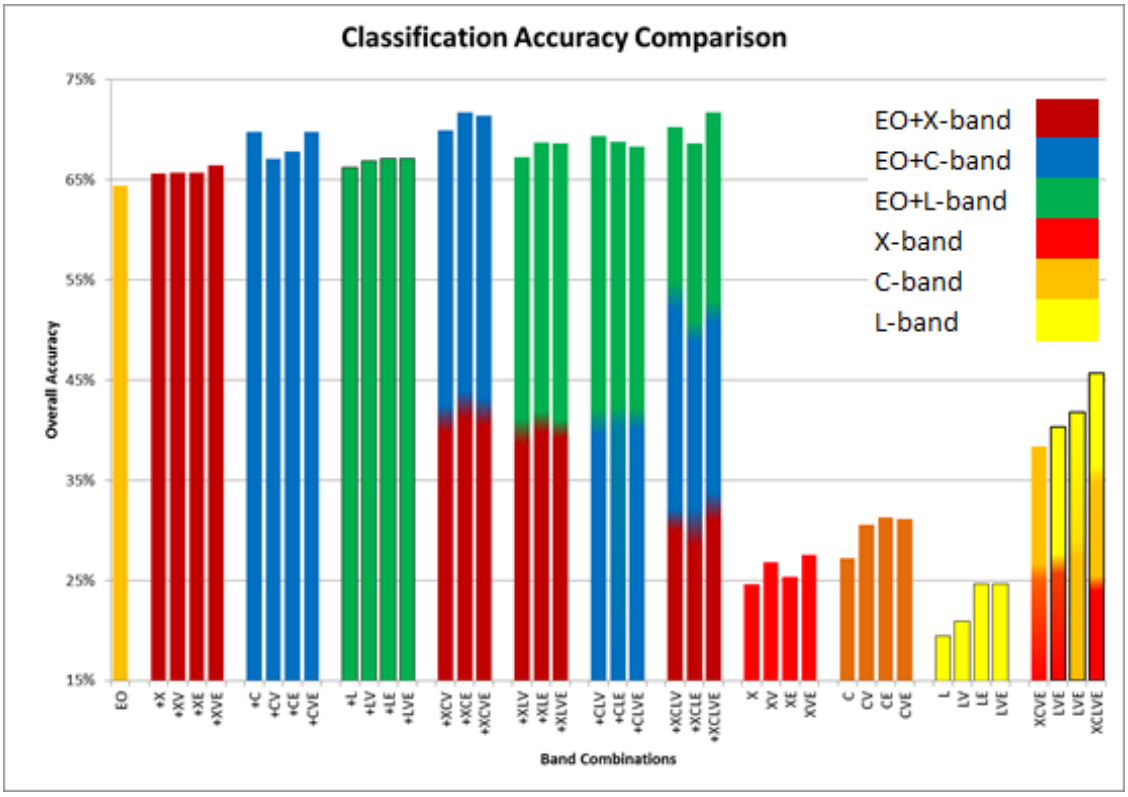

Figure 56. Overall accuracy comparison between different band combinations for Fresno-Kings Counties, USA.

Table 76. Best band combinations for each test based on the overall accuracy using EO+SAR and SAR alone for Fresno-Kings Counties, USA.

Producer's Accuracy	1	2	3	4	5	6
Class \ Fusion with:	EO	+C-HH	+XCL-V	+XC-E	XCL+VE	SAR-XCLVE
WinterWheat	78.94	79.69	67.85	75.53	74.47	5.59
Tomatoes	57.80	57.12	63.66	63.25	71.13	53.36
Pistachios	88.01	79.91	73.31	90.85	60.42	14.24
Water	92.56	95.49	96.99	94.86	96.52	59.41
Fallow	54.58	60.45	67.51	72.68	77.22	51.26
Developed	74.69	77.92	78.66	73.55	74.69	58.32
Cotton	47.34	55.81	57.58	62.32	60.95	28.24
Corn	44.94	57.54	55.79	54.08	39.27	22.89
Barren	51.99	71.85	73.74	74.75	74.41	80.91
Almonds	77.71	78.35	79.46	81.68	85.62	78.70
Alfalfa	73.16	76.92	78.84	72.92	78.31	41.20
User's Accuracy						
WinterWheat	72.55	76.38	76.36	76.98	84.30	32.53
Tomatoes	56.47	54.91	51.50	55.72	53.62	32.95
Pistachios	64.58	65.80	63.26	68.71	61.43	38.00
Water	80.80	81.94	81.95	82.18	82.27	66.34
Fallow	61.03	83.37	79.47	82.81	73.50	40.58
Developed	64.46	61.86	70.12	73.77	82.45	77.66
Cotton	62.09	70.81	71.02	67.66	72.14	24.49
Corn	66.53	68.79	69.64	66.57	52.65	23.12
Barren	54.99	68.62	69.88	71.31	70.40	64.03
Almonds	56.48	61.61	65.10	67.54	77.83	69.56
Alfalfa	89.61	99.38	99.94	93.34	90.99	45.97
Overall Accuracy	64.43%	69.75%	70.23%	71.70%	71.71%	45.69%
Kappa Coefficient	0.60	0.66	0.67	0.68	0.68	0.39
Key to tests:	Bands		Notes			
Series 1	EO		EO = electro-optical			
Series 2	EO+HH		X = X-band SAR			
Series 3	EOHH+V		C = C-band SAR			
Series 4	EOHH+E		L - L-band SAR			
Series 5	EOHH+VE		HH = SAR despeckled HH			
Series 6	SAR-XCLVE		V = variance			
			E = entropy			

5 DISCUSSION AND FUTURE RESEARCH

5.1 Discussion

As reported in the literature for other locations (Anys and He, 1995; Haack and Bechdol, 1999; Haack and Bechdol, 2000; Herold and Haack, 2002; Herold, et al., 2004; Sawaya, et al., 2010; Sheoran and Haack, 2014; Idol, et al., 2015a; Idol, et al., 2015b) the fusion of SAR data with EO increased the classification accuracy in all three of the sites investigated in this dissertation (Table 77). Additionally as more information content was added, for example different texture measures or additional SAR bands, the classification accuracy also increased. Using SAR alone, the overall accuracy was 46% in Fresno-Kings Counties using C-band; 58% and 70% using X-band in Campinas and Wad Medani, respectively. Using only EO, Campinas was classified the best (84%), then Wad Medani, and lastly Fresno-Kings Counties with 68% and 65% overall accuracies. However using all available data, the best overall classification was achieved at Wad Medani (92%), followed by Campinas with 87% and lastly an overall classification accuracy in Fresno-Kings Counties of 72%.

One concern with the present study is that only the despeckled HH polarization from each microwave wavelength was used; multiple polarizations were not available from the data sources of the three SAR bands used. Nevertheless, testing with three wavelength bands together (X, C and L) from the same location has not been done before this study.

Table 77. Study site comparison of the best band combinations for each test based on the overall accuracy using EO, EO+SAR, and SAR alone.

Best Test Results	Wad Medani, Sudan			Campinas, Brazil			Frenso & King's Counties, USA		
Data Type	Best SAR	Best Combo	Overall Acc %	Best SAR	Best Combo	Overall Acc %	Best SAR	Best Combo	Overall Acc %
SAR	X	X, VCER71121	69.61%	X	X, VER21	57.71%	C	XCL, VE21	45.69%
EO	--	--	68.02%	--	--	83.75%	--	--	64.43%
EO+HH	X	XCL	84.09%	L	XCL	86.93%	C	C	69.75%
EO+HH+V	X	X, V7	87.63%	L	XCL, V21	87.69%	C	XC, V21	69.90%
EO+HH+GLCM	L	XCL, CER721	92.69%	X	X, E21	88.08%	C	XC, E21	71.70%
EO+HH+V+GLCM	X	XCL, VCER711	92.26%	L	L, VE21	86.63%	C	XCL, VE21	71.71%
Definitions:	V = Variance								
	C = Contrast								
	E = Entropy								
	R = Correlation								

It is important to examine some differences between the data and LC classes between the study sites. The first issue is the difference in the spatial resolution for Campinas where the C-band SAR was only available from ScanSAR data with a spatial resolution of 25.0 m instead of 6.25 m as was available for the other two sites. According to the proposed methodology during the data fusion process all data was under-sampled to the lowest spatial resolution of the available data to minimize resampling errors, so for Campinas classifications were carried out with a spatial resolution of 25.0 m. Larger pixel sizes results in including more classes in the same pixels; i.e. more mixed pixels making classification more difficult.

There was also a difference between the study sites in the number of classes to be tested. For Campinas five general LC classes were analyzed; in Wad Medani, based on examination of the imagery, more specificity was investigated for urban and agriculture areas and nine classes were tested. For the Fresno-Kings Counties study site, classifications of eight specific crops were attempted given the detailed GT information from the USDA CDL (Boryan, et al., 2011). One should note however that the CDL was

based on Landsat TM imagery with 30 m spatial resolution (Boryan, et al., 2011) while the data to be classified was of 12.5 m spatial resolution. In addition to using the CDL for GT, 0.5 m spatial resolution PS imagery from Worldview-2 was utilized, but the CDL was the only information reporting the exact crops for each field. Of further concern is that CDL is a yearly report and a single crop label is assigned to fields that are used for multiple crops throughout the year. Thus the crop label for a given field might not correspond with the actual crop detected on the date of the satellite imagery (Boryan, et al., 2011). Attempts were made to account for this issue when selecting pixels for GT. The original EO imagery at 5.0 m and the 0.5 m PS WV-2 imagery were compared with the CLD information and care was taken to not select GT pixels from areas where the LC appeared to be very different than the rest of the polygons for the same LC. The increased number and specificity of classes and the difficulty of assuring accuracy in GT may explain the overall lower classification accuracy results for Fresno-Kings Counties.

Three SAR bands were tested individually and combined; X, C, and L-bands. The X-band provided the best SAR-only overall classification for Wad Medani and Campinas (Table 77), while the C-band did the best for Fresno-Kings Counties. When combined with EO, the X-band was best for Wad Medani, the L-band for Campinas, and the C-band was the best single SAR band for the Fresno-Kings Counties area. Combining all three SAR bands resulted in a better classification for Wad Medani and Campinas although only slightly better than using two bands; using two SAR bands was better than one. For Fresno-Kings Counties, however, adding other SAR bands to the C-band resulted in

lower accuracy; in this case X-band data were collected from March which was likely too early in the growth season.

Four texture measures were tested for the Wad Medani test site; the parametric 2nd order variance, and three GLCM texture measures: contrast, entropy, and correlation. For the Wad Medani test site kernel sizes of 7x7, 11x11, and 21x21 pixels were tested for all four texture measures. As described for Wad Medani, texture improved the classification accuracy but the difference between the different kernel sizes was small; for the other two test areas only the 21x21 kernel size was used. Variance texture improved the classification accuracy for all three study sites. Three GLMC measures improved classification accuracy slightly more than variance (Table 78); using both variance and GLMC showed a small improvement compared to using either measure alone. The different GLCM measures were tested individually for the Wad Medani site and it was found that contrast resulted in lower classification accuracies as well as making ROI training locations more difficult to assess. For Campinas only entropy and correlation were used, and based on those results, only entropy was used for Fresno-Kings Counties.

Table 78 also compares the results in overall accuracy for the different texture measures. Neither variance nor GLCM texture measures were consistently superior to the other, but on a case by case basis one usually resulted in better classification accuracy. There were also cases where the combination of variance with GLCM was superior to each measure alone suggesting that using both types of texture measures is important especially because there is little additional cost in creating derived image layers once a given source of data has been acquired. Although Clausi (2002) found that contrast,

entropy, and correlation together were good; ; the present research found that entropy seemed to perform the best. Inconsistent results for texture measures and kernel sizes have been reported in the literature (Haack and Bechdol, 2000; Franklin, et al., 2001; Herold, et al., 2004; Berberoglu, et al., 2007; Idol, et al., 2015a; Idol, et al., 2015b); no general rule for best practices can be determined other than on a case-by-case basis the derived data layers that contribute the most must be determined before final classifications are made.

The methodology for this research was to under-sample the higher spatial resolution data to match that of the lowest spatial resolution data in order to minimize errors due to resampling. Nevertheless much information is lost by doing so and increasing the processed pixel size increases error from mixed pixels. Given the lost information content it seems that the error from under-sampling is likely to be greater than the resampling error especially when larger pixels are broken into smaller pixels of the same value and no interpolation is used. This problem was most serious for the Campinas study area where only ScanSAR data were available for the C-band so the EO data at 5.0 m spatial resolution were under-sampled to 25.0 m spatial resolution. Even for the Fresno-Kings Counties area, increasing the amount of mixture in LC classes in the pixels degrading from 5.0 to 12.5 m may have hampered the ability to reach higher classification accuracy.

Table 78. Study site comparison of overall accuracy for different texture measures.

EO + SAR Band	Wad Medani (21x21)					
	V	Contrast	Entropy	Correlation	All GLCM	V+GLCM
EO + X	83.52%	84.03%	85.11%	88.23%	84.20%	86.28%
EO + C	72.84%	76.67%	79.13%	73.43%	80.38%	80.40%
EO + L	80.78%	80.01%	80.37%	84.10%	88.32%	83.49%
EO + X+C	84.44%	87.43%	91.38%	89.22%	89.57%	89.72%
EO + X+L	84.10%	83.66%	90.17%	85.07%	91.19%	88.07%
EO + C+L	82.34%	83.65%	84.98%	87.95%	88.55%	86.54%
EO + X+C+L	86.13%	87.39%	92.86%	89.54%	92.70%	90.87%
	Campinas (21x21)					
	V	Contrast	Entropy	Correlation	All GLCM	V+GLCM
EO + X	84.22%	--	88.08%	84.73%	88.30%	88.30%
EO + C	83.75%	--	85.07%	85.82%	85.97%	85.97%
EO + L	86.93%	--	87.14%	86.63%	86.49%	86.49%
EO + X+C	86.77%	--	87.13%	85.44%	85.72%	85.72%
EO + X+L	87.64%	--	86.14%	85.04%	83.69%	83.69%
EO + C+L	86.44%	--	87.19%	84.69%	83.12%	83.12%
EO + X+C+L	87.86%	--	85.43%	82.59%	81.38%	81.38%
	Frenso-Kings Counties (21x21)					
	V	Contrast	Entropy	Correlation	All GLCM	V+GLCM
EO + X	65.75%	--	65.72%	--	--	66.48%
EO + C	67.13%	--	67.87%	--	--	69.81%
EO + L	66.86%	--	67.12%	--	--	67.16%
EO + X+C	69.90%	--	71.70%	--	--	71.35%
EO + X+L	67.27%	--	68.69%	--	--	68.61%
EO + C+L	69.32%	--	68.82%	--	--	68.33%
EO + X+C+L	70.23%	--	68.61%	--	--	71.71%

Different LC classes were investigated in the three study sites, from generic classes of water and bare soil, to more detailed classes in developed areas and agriculture. Water, fallow, and barren ground were common to all three study sites. In Wad Medani two classes of urban areas were separated (low and medium) and orchards&trees were separated from sparse forest; an attempt was made to separate bare agricultural land from

barren ground. Due to many years operating under the Gezira irrigation scheme, agricultural land in Wad Medani has higher moisture and carbon content than unused or abandoned land and their spectral signatures are different. In Campinas, basic classes were urban and green agriculture, forest, and a general barren ground class. For simplicity sake, barren ground included uses for agriculture (bare fields) and urban areas (areas cleared for roads and urban development). In Fresno-Kings Counties, water, a single urban class, and a general barren ground classes were separated while agricultural lands were classified into fallow and five crops (cotton, tomatoes, winter wheat, alfalfa, and corn). Orchards with pistachios or almonds were also separated.

The ability to separate different classes at each study area is important. At the Wad Medani location, using EO, all SAR bands, contrast and entropy an overall accuracy of 92.79% was achieved (see Table 32, page 79). All classes were classified to about 90% in user's accuracy except for orchards&trees and green crops which were confused with each other and with sparse forest. Bare ground and bare agricultural soil were separated nicely with above 95% in both user's and producer's accuracy

For Campinas, Brazil, reported earlier (see Table 53, page 97), forest areas were confused with agriculture (81.85% and 88.46% user's accuracy), and urban areas were confused with bare ground and water. Water had a producer's accuracy of 81.77% compared to a user's accuracy of 94.04% suggesting the ROI's for the training or GT could have been improved. For California, Fresno-Kings Counties, the highest overall accuracy was found using EO with all SAR bands and the texture measures variance and entropy. Water had the best producer's accuracy of 96.5%, and alfalfa had the best user's

accuracy of 91.0%. Corn had the lowest producer's accuracy (39.3%) being confused with tomatoes, and also with winter wheat in the case of user's accuracy (see Table 70, page 119).

The selection of pixels representative of each land cover class for training and GT areas, while challenging, is foundational for land cover classification (Congalton and Green, 1999; Campbell and Wynne, 2011; Canty, 2014). Haack et al. (2015) described remote sensing as "both an art and a science" referring to the task of selecting pixels (or polygons) for class training and GT. Those authors recognized that LULC often does not result in consistent results as was the case in the present study. More iterations and refinements in the training and GT ROIs in the present study may have resulted in higher classification accuracies, especially between crops in California.

EO and SAR sensors measure energy from very different regions of the EMS and thus are capable of detecting very different phenomenology from materials within their field of view (Richards, 2013). EO systems passively detect energy reflected by materials while SAR systems actively transmit energy and measure as backscatter the energy received. EO systems measure the variations in the colors reflected by materials based on its chemistry and the absorption of different wavelengths of visible light. Materials scatter radar energy in relation to their surface roughness, dielectric constant, and shape; physical properties rather than chemical properties (Woodhouse, 2006). SAR and EO are complimentary and through data fusion a more complete picture of the ground is collected as shown in the results of the present research. EO does very well in separating

material of different colors but different materials of similar colors are very difficult to discern.

In Wad Medani SAR and EO alone performed about the same given similar proportions of bare soil and urban areas, and vegetation (69.6% and 68.0% respectively); however, the overall accuracy reached 92.3% when combined. SAR was instrumental in separating urban areas with man-made buildings and roads. Buildings scatter SAR especially well due to their corner reflector effect (Woodhouse, 2006; Richards, 2013) and in Wad Medani this allowed for the separation of low and medium urban intensity areas. Soil of different moisture content and different dielectric constant was also better separated using SAR; trees stood out with SAR because of the increased roughness compared to green fields. In Campinas green vegetation dominated the study area and soil and urban areas were different enough that EO was able to achieve good classification accuracy (83.8%). In this case the addition of SAR helped but only added 4.3%. SAR alone had only 57.7% overall accuracy. As previously discussed, accuracies were lower in Fresno-Kings Counties but EO alone out performed SAR alone (64.4% vs 45.7%). Man-made structures and orchards were separated better using SAR than with EO alone. In all three study areas the fusion of EO and SAR resulted in higher classification accuracies than either EO or SAR alone.

5.2 Future Research

This research focused on the use of three different SAR bands, X, C, and L. Because dual or quad polarization data were not available for the study sites for all three SAR bands, only the despeckled HH polarization was used. Many studies have shown the

importance and improvement in classification accuracy by using dual or quad polarization because more information is represented from the different views (Sheoran, 2005; Haack and Khatiwada, 2010; Sawaya, et al., 2010; Sheoran and Haack, 2013a; Sheoran and Haack, 2013b; Idol, et al., 2015a; Idol, et al., 2015b). It cannot be determined from the present work if using more than one SAR band provides the same or better improvement than using dual or quad polarimetric data from a single source; using a single source of satellite data however, is likely to be more cost effective in material costs and data processing effort than obtaining data from different providers. Future research should attempt to acquire dual or quad polarimetric data from multiple SAR bands to investigate this question.

Another aspect that was not included in this research is the use of derived layers from the EO data such as the Normalized Difference Vegetation Index (NDVI), band ratios, impervious surface index, and texture based on EO. Given that derived data from SAR were investigated, the best classification possible using EO alone should also be included. In that sense a large set of original and derived layers can be generated to enhance the classification decision rule process. Gounaridis and Kougloulas (2016) tested classification adding different database, vector and image layers including LC maps derived from other studies, population, road network, and an impervious surface layer. Aksoy et al. (2009) performed LC classification using EO plus the DEM, NDVI, band indices, and Gabor texture layers.

With the ever increasing availability of satellite imagery, scalable cloud-based computation power to derive multiple data layers, the number of variables and possible

combinations become unmanageable to process manually. In the present research IDL (ITT, 2010; Canty, 2014) was used to write processing scripts to automate many of the processing steps but including every possible test combinations in the script is challenging as the number of variables increases. The linear processing of so many tests becomes computationally inefficient and manually comparing and summarizing the results is difficult. Big data analytics, data mining, and machine learning (Witten et al., 2011) have become popular to extract information from large data sets. Machine learning techniques including decision trees (Aksoy et al., 2009; Sun, et al., 2011; Cervone and Haack, 2012; Kostas, 2016) and, for example random forests (Breiman, 2001; Liaw and Wiener, 2002; Gounaridis and Koukoulas, 2016; Ludwig, et al., 2016) techniques have great potential to determine the best data layer combinations in a LC classification exercise.

5.3 Conclusions

The overall conclusions from this research are:

1. The decision rule classifier Support Vector Machine was superior to Maximum Likelihood, Mahalanobis Distance, and Neural Net classifiers although processing time was greater.
2. Using more than a single SAR band improved the classification accuracy although the best SAR band alone or combined was not consistent between the three study areas or land cover classes.
3. The addition of GLCM texture to variance improved the classification accuracy more than using variance texture alone.

4. Different texture kernel sizes and combinations are useful to improve classification accuracy but not in a consistent manner.
5. Classification with SAR alone typically results in lower accuracy than when using EO; however, under cloudy conditions when no EO is available SAR provides the only satellite-based option. The addition of texture to SAR despeckled HH was important.
6. The combination of EO with SAR typically results in higher overall classification accuracies, although on a per class basis EO or SAR may be better.

REFERENCES

Aksoy, S., K. Kopersk, C. Tusk, and G. Marchisio. 2009. Land Cover Classification with Multi-Sensor Fusion of Partly Missing Data. *Photogrammetric Engineering & Remote Sensing*. 5: 577-593.

Amolins, K., Y. Zhang, and P. Dare. 2007. Wavelet based image fusion techniques – An introduction, review and comparison. *Photogrammetry & Remote Sensing*. 52: 249-263.

Anderson, J. R., E. E. Hardy, J. T. Roach, and R. E. Witmer. 1976. A land use and land cover classification system for use with remote sensor data. Washington, D.C. US Government Printing Office.US Geological Survey. Professional Paper 964.

Anys, H. and D. C. He. 1995. Evaluation of textural and multi-polarization radar features for crop classification. *IEEE Trans. Geosci. Remote Sens*. 33 (5): 1170–1181.

Array Systems Computing, Inc. 2016. http://www.array.ca/nest Last accessed 10 Oct. 2016.

Berberoglu, S., P. L. Curran, C. D. Lloyd, and P. M. Atinson. 2007. Texture classification of Mediterranean land cover. *International Journal of Applied Earth Observation and Geoinformation*. 9(3): 322-334.

Boryan, C., Z. Yang, R. Mueller, and M. Craig. 2011. Monitoring US agriculture: the US Department of Agriculture, National Agricultural Statistics Service, Cropland Data Layer Program. *Geocarto International*, 26(5): 341–358.

Breiman, L. 2001. Random forest. *Machine Learning*. 40: 5-32.

Campbell, J. B. and R. H. Wynne. 2011. Introduction to Remote Sensing. 5th Ed. The Guilford Press. 667 p.

Canty, M. J. 2014. Image analysis, classification and change detection in remote sensing. 3rd Ed. CRC Press. Fl. 527 P.

CDFA. 2015. California Agricultural Statistical Review: 2011-2012. California. Department of Food and Agriculture. Sacramento. 127 p. https://www.cdfa.ca.gov/Statistics/PDFs/ResourceDirectory_2011-2012.pdf Last accessed 20 Nov. 2016.

Cervone, G. and B. N. Haack. 2012. Supervised machine learning of fused RADAR and optical data for land cover classification. *J. Applied Remote Sensing*. 6. 18 p.

CIA World Factbook. 2013. Last accessed 15 Nov. 2016. https://www.cia.gov/library/publications/the-world-factbook/

Clausi, D. A. 2002. An analysis of co-occurrence texture statistics as a function of grey level quantization. *Canadian Journal Remote Sensing*. 28(1): 45-62.

Congalton, R. G. and K. Green. 1999. Assessing the Accuracy of Remotely Sensed Data: Principals and Practices. Lewis Publishers. Boca Raton. 137 p.

DIVA GIS. 2013. http://www.diva-gis.org/gdata/ Last accessed 20 Oct. 2016.

ENVI. 2013. ENVI Tutorial: Landsat TM and SAR Data Fusion. http://www.harrisgeospatial.com/portals/0/pdfs/envi/TM_SAR_Fusion.pdf Last accessed 20 Oct. 2016.

ERDAS. 2010. ERDAS Field Guide. ERDAS. GA. 812 p.

FAO. 2005. Aquastat Survey 205: Irrigation in Africa in Figures – Sudan. 16 p. ftp://ftp.fao.org/agl/aglw/docs/wr29_eng.pdf Last accessed 20 Oct. 2016.

Franklin, S. E., M. A. Wulder, and G. R. Gerylo. 2001. Texture analysis of IKONOS panchromatic data for Douglas-fir forest age class separability in British Columbia. *International Journal of Remote Sensing.* 22 (13): 2627-2632.

GADM, 2013. Global Administrative Areas. http://www.gadm.org/ Last accessed 20 Oct. 2016.

Gounaridis, D. and S. Koukoulas. 2016. Urban land cover thematic disaggregation, employing datasets from multiple sources and Random Forests Modeling. *International Journal of Applied Earth Observation and Geoinformation.* 51:1-10.

Haack, B. N. 2007. A comparison of Land Use/Cover Mapping with Varies Radar Incident Angles and Seasons. *GIScience & Remote Sensing*. 44 (4): 305-319.

Haack, B. N. 2016. Remote Sensing Information Extraction. ATI Course Sampler. http://www.aticourses.com/sampler/RemoteSensingInformationExtraction_CourseSampler.pdf Last accessed 10 Oct. 2016.

Haack, B. N. and M. Bechdol. 1999. Multisensor remote sensing data for land use/cover mapping. Computers. *Environment and Urban Systems*. 23 :53-69.

Haack, B. N. and M. Bechdol. 2000. Integrating multisensor data and RADAR texture measurements for land cover mapping. *Computers & Geosciences*. 26: 411-421.

Haack, B. N., Herold and M. Bechdol. 2000. Radar and optical data integration of land-use/land-cover mapping. *Photogrammetric Engineering and Remote Sensing*. 66(6): 709-716.

Haack, B. N. and G. Khatiwada. 2010. Comparison and integration of optical and quad polarization radar imagery for land cover/use delineation. *Journal of Applied Remote Sensing*. 4(1): 043507.

Haack, B. N., R. Mahibir and J. Kerkering. 2015. Remote sensing-derived national land cover land use maps: a comparison for Malawi. *Geocarto International*. 30(3): 270-292.

Haack, B. N., E. Solomon, M. Bechdol, and N. Herold. 2002. Radar and optical data comparison/integration for urban delineation: a case study. *Photogrammetric Engineering and Remote Sensing*. 68 (12): 1289-1296.

Halounová, L. 2009. Light SAR 1, Radar Basics. ESA Advanced Training Course on Land Remote Sensing. 29 June 2009. Prague. D1La1. Last accessed 15 Nov. 2016. http://earth.esa.int/landtraining09/D1La1_Halounova_SARBasics.pdf

Hammann, M. G. 2011. Urban Growth in Campinas, Brazil, 1989-2010, As Estimated from Landsat Imagery. Proceedings from ASPRS Pecora 18 – Forty Years of Earth Observation…Understanding a Changing World. ASPRS – Pecora 18 Symposium. November 14 - 17, 2011. Herndon, Virginia. Last accessed 20 Oct. 2016. http://www.asprs.org/pecora18/proceedings/Hammann.pdf

Han, W., Z. Yang, L. Di, and R. Mueller. 2012. CropScape: A Web service based application for exploring and disseminating US conterminous geospatial cropland data products for decision support. *Computers and Electronics in Agriculture*. 84: 111–123.

Herold, N. D and B. N. Haack. 2002. Fusion of Radar and Optical Data for Land Cover Mapping. *Geocarto International*. 17 (2): 21-30.

Herold, N. D., B. N. Haack, and E. Solomon. 2004. An evaluation of radar texture for land use/cover extraction in varied landscapes. *International Journal of Applied Earth Observation and Geoinformation.* 5: 113–128.

Herold, N., B. N. Haack, and E. Solomon. 2005. Radar spatial considerations for land cover extraction. *International Journal of Remote Sensing*. 26(7): 1383-1401.

IBGE. 2012. Censo Demográfico 2010: Características Urbanísicas do Entorno dos Domicíluos. Insitututo Brasileiro de Geografia e Estatística – IBGE. Rio de Janeiro. 171 p. Last accessed 20 Nov.2016

http://biblioteca.ibge.gov.br/visualizacao/periodicos/96/cd_2010_entorno_domicilios.pdf

Idol, T. A. 2012. Analysis of Techniques Used to Generate Land Cover/Use Classification Using Multi-Wavelength Quad-Polarized Radar. George Mason University Dissertation. GGS. 216 p.

Idol, T., B. N. Haack, and R. Mahabir. 2015a. Radar and optical remote sensing data evaluation and fusion; a case study for Washington, DC, USA. *International Journal of Image and Data Fusion.* 6:2, 138-154.

Idol, T, B. N. Haack, and R. Mahabir. 2015b. Comparison and integration of spaceborne optical and radar data for mapping in Sudan. *International Journal of Remote Sensing.* 36:6: 1551-1569.

Infoterra. 2009. TerraSAR-X Services – Image Product Guide. Issue 1.00. 28 p.

Instituto Agronômico de Campinas. 2007. Classificação Climática de Köppen e ee Thornthwaite e Sua Aplicabilidade na Determinação de Zonas Agroclimáticas Para o Estado de São Paulo. Bragantia, Campinas. 66(4): 711-720.

ITT. 2009. Atmospheric Correction Modules: QUAC and FLAASH User's Guide. ITT Visual Information Solutions. V4.7. 44 p.

ITT. 2010. Image Processing. ITT Visual Information Solutions. June 2010. 300 p.

Jain, R., R. Kasturi, and B. S. Schunck. 1995. Machine Vision. Ch. 7. Texture. McGraw-Hill. ISBN 0-07-032018-7.

Japan Space Systems. 2012. PALSAR Reference Guide. 6st Edition. 73 p.

JAXA. 2008. ALOS Data Users Handbook. Revision C. 158 p.

Jensen, J. R. 2005. Introductory Digital Image Processing: A Remote Sensing Perspective. 3rd Ed. Prentice Hall. New Jersey. 526 p.

Jensen, J. R. 2007. Remote Sensing of the Environment: An Earth Resource Perspective. 2nd Ed. Prentice Hall. New Jersey. 592 p.

Klein, L. A. 2013. Sensor and Data Fusion: A Tool for Information Assessment and Decision Making. 2nd Ed. SPIE Press. Bellingham. 474 p.

Kostas, S. 2016. Using crowdsourcing and machine learning to locate swimming pools in Australia http://blog.tomnod.com/crowd-and-machine-combo Last accessed 9 Oct. 2016.

Kottek, M., J. Grieser, C. Beck, B. Rudolf, and F. Rubel. 2006. World Map of the Köppen-Geiger climate classification updated. *Meteorol. Z.* 15: 259-263.

LandInfo. 2016a. GeoEye-1 High-Resolution Satellite Imagery. http://www.landinfo.com/geo.htm Last accessed 17 Aug. 2016.

LandInfo. 2016b. WorldView-2 50 cm Global High-Resolution Satellite Imagery. http://www.landinfo.com/WorldView2.htm Last accessed 17 Aug. 2016.

Lewis, A. J. and F. H. Henderson. 1998. Introduction. Ch. 1. In: Principals and Applications of Imaging Radar. Manual of Remote Sensing, Third Ed. Vol. 2. Edited by: F. L. Henderson and A. J. Lewis. John Wiley & Sons, Inc. 866 p.

Liang, S. 2004. Quantitative Remote Sensing of Land Surfaces. John Wiley & Sons. New Jersey. 534 p.

Liaw, D. and M. Wiener. 2002. Classification and regression by random Forest. *R News*. 2(3): 18-22.

Ludwig, A., H. Mayer and T. Nauss. 2016. Automatic classification of Google Earth images for a larger scale monitoring of bush encroachment in South Africa. *International Journal of Applied Earth Observation and Geoinformation*. 50: 89-94.

MDA. 2011. RADARSAT-2 Product Description. RN-SP-52-1238. MacDonald, Detwiller, and Associates. B.C. Canada. 6o p. Last accessed 20 Oct. 2016. http://mdacorporation.com/docs/default-source/technical-documents/geospatial-services/52-1238_rs2_product_description.pdf?sfvrsn=10

Metz, H. C. 1992. Sudan: A Country Study. Washington: GPO for the Library of Congress.336 p.

Mohamedzein, Y. E-A., M. G. Mohamed, and A. M. El Sharief. 1999. Finite element analysis of short piles in expansive soils. *Computers and Geotechnics*. 24: 231-243.

Moskal, L. M., S. E. Franklin. 2004. Relationship between airborne multispectral image texture and aspen defoliation. *International Journal of Remote Sensing*. 25 (14): 2701-2711.

Nyoungui, , E. Tonye, and A. Alono. 2002. Evaluation of speckle filtering and texture analysis methods for land cover classification from SAR images. *International Journal of Remote Sensing*. 23: 1895-1925.

Ojala, T. A, M. Pietikainen, and D. Harwood. 1996. A comparative study of texture measures with classification based on featured distributions. *Pattern Recognition*. 29 (1): 51-59.

Ojala, T., M. Pietikainen, and T. Maenpaa, 2002. Multiresolution gray-scale and rotation invariant texture classification with local binary patterns. *IEEE Transactions on Pattern Analysis and Machine Intelligence*. 24(7): 971-987.

Pajares, G. and J. M. de la Cruz. 2004. A wavelet-based image fusion tutorial. *Pattern Recognition.* 37:1855-1872.

Pal, S., T. Majumdar, and A. Bhattachrya. 2007. ERS-2, SAR and IRS-IC LISS III data fusion: A PCA approach to improve remote sensing based geological interpretation. *Journal of Photogrammetry and Remote Sensing*. 60: 281-297 .

Palma, Jose L. 2011. InSAR: Deformation, Mapping and Modeling. https://vhub.org/resources/817 Last accessed 20 Oct. 2016.

Planet. 2016. RapidEye Satellite Imagery Product Specifications. Planet. V6.1. 50 p. https://www.planet.com/products/satellite-imagery/files/160625-RapidEye%20Image-Product-Specifications.pdf Last accessed 20 Oct. 2016.

Pohl, C. and J. L. Van Genderen. 1998. Multisensor image fusion in remote sensing: concepts, methods and applications. *International Journal of Remote Sensing*. 19(5): 823-854.

Puissant, A, J. Hirsch, and C. Weber. 2005. The utility of texture analysis to improve per-pixel classification for high to very high spatial resolution imagery. *International Journal of Remote Sensing*. 26 (4): 733-745.

Raney, R. K. 1998. Radar Fundamentals: Technical Perspective. Ch. 2. In: Principals and Applications of Imaging Radar. Manual of Remote Sensing, Third Ed. Vol. 2. Edited by: F. L. Henderson and A. J. Lewis. John Wiley & Sons, Inc. 866 p.

Richards, J. A. 2013. Remote Sensing Digital Analysis: An Introduction. 5th Ed. Springer-Verlag. Berlin. 494 p.

Ryerson. B. and S. Aronoff. 2010. Why 'where' matters: understanding and profiting from GPS, GIS and remote sensing. Kim Geomatics Corp. Ontario. 379 p.

Ryerson, R. and B. N. Haack. 2016. The Role of Remote Sensing in Assisted Development: Experience Drawn from Work in Over 40 Countries. *Canadian Journal of Remote Sensing*. 42:4, 324-331.

Sawaya, S., B. N. Haack, T. Idol, and A. Sheoran. 2010. Land Use/Cover Mapping with Quad-polarization Radar and Derived Texture Measures near Wad Madani, Sudan. *GIScience & Remote Sensing*. 47:3, 398-411.

Schott, J. R. 2007. Remote Sensing: The Image Chain Approach. 2nd Ed. Oxford Univ. Press. 666 p.

Sheoran, A. 2005. Land Cover/Use Classification Using Optical and Quad Polarization Radar Imagery. MS Thesis. George Mason University. 130 p.

Sheoran, A. and B. N. Haack. 2013a. Comparison and integration of Landsat optical and PALSAR quad polarization radar: a case study in Bangladesh. *Journal of Applied Remote Sensing.* 7(1) 073545.

Sheoran, A. and B. N. Haack. 2013b. Classification of California agriculture using quad polarization radar data and Landsat Thematic Mapper data. *GIScience & Remote Sensing.* 50:1, 50-63.

Sheoran, A. and B. N. Haack. 2014. Optical and radar data comparison and integration: Kenya example. *Geocarto International*. 29(4): 370-382.

Shettigara, V. K. 1992. A generalized component substitution technique for spatial enhancement of multispectral images using a higher resolution data set. *Photogrammetric Engineering and Remote Sensing*. 58(5): 561-567.

Solbreg, A., H. S., A. K. Jain, and T. Taxt. 1994. Multisource classification of remotely sensed data: fusion of Landsat TM and SAR images. *IEEE Transactions on Geoscience and Remote Sensing*. 32, 768-778.

Strahorn, A. T., J. W. Nelson, L. C. Holmes, and E. C. Eckmann. 1914. Soil Survey of the Fresno Area, California. USDA. Washington D. C. GPO. 82 p.

Sun, D., Y. Yu, and M. D. Golberg. 2011. Deriving Water Fraction and Flood Maps from MODIS Images Using a Decision Tree Approach. *IEEE J. Selected Topics in Applied Earth Observation and Remote Sensing.* 4(4): 814-825.

UNEP. 2007. Sudan: Post-Conflict Environmental Assessment. United Nations Environmental Programme. Geneva. 356 p. ISBN: 978-92-807-2702-9 http://www.unep.org/sudan/post-conflict/PDF/UNEP_Sudan.pdf Last accessed 20 Nov 2016.

USDA. 2013. National Agricultural Statistics Service Cropland Data Layer. Published crop-specific data layer [Online]. USDA-NASS, Washington, DC. http://nassgeodata.gmu.edu/CropScape/ Last accessed 20 Oct. 2016.

USGS. 2013. Landsat Project Description. Last accessed 20 Oct. 2016. http://landsat.usgs.gov/about_project_descriptions.php

Valladares, G. S., M. G. Pereira, and L. H. Cunja dos Anjos. 2007. Humic substance fractions and attributes of histosols and related high-organic-matter soils from Brazil. *Communications in Soil Science and Plant Analysis*. 38: 763–777.

Villiger, E. 2008. Radar and Multispectral Image Fusion Options for Improved Land Cover Classification. George Mason University Dissertation. 220 p.

Weather.com . 2016. Data for Fresno, CA. Last accessed 20 Oct. 2016. https://weather.com/weather/monthly/l/USCA0406:1:US

Weather-and-Climate.com. 2016. Data for Campinas, Brazil and Wad Medani, Sudan. Last accessed 20 Oct. 2016. https://weather-and-climate.com/

Witten, I. H., E. Frank and M. A. Hall. 2011. Data Mining: Practical Machine Learning Tools and Techniques. 3rd Ed. Elsevier-Morgan Kaufmann. 629 p.

Woodhouse, I. H. 2006. Introduction to Microwave Remote Sensing. CRC Taylor & Francis. NY. 370 p.

Wulder, M. A., R. J. Hall, N. C. Coops, and S. E. Franklin. 2004. High spatial resolution remotely sensed data for ecosystem characterization. *Bioscience*. 54(6): 511-521.

BIOGRAPHY

Mark Gregory Hammann earned his Bachelor of Art in Biology with a minor in Chemistry from Whittier College in 1978. He continued his studies and received a Master in Science in Biological Oceanography from Oregon State University in 1981, after which Greg accepted a teaching position at the University of Baja California, School of Marine Sciences in Ensenada, Baja California, Mexico (USBC). In 1985 he entered a graduate teaching and research position at the Center for Advanced Studies and Scientific Research of Ensenada (CICESE) and founded the Fisheries Ecology research group. With the 1997 launch of the OrbView-2 satellite carrying the SeaWiFS instrument, Greg was honored to be the first chief oceanographer at Orbital Imaging Corporation, and was responsible for the development and operations of the marine commercial products and services from that satellite. GeoEye combined with DigitalGlobe Inc. in 2013 and Greg was assigned to the Next Generation Product team for WorldView-3. In 2014 Greg founded the consulting company EarthSightful Solutions LLC and is currently the Director of Strategic Business Development for Marine Instruments, S. A. Greg is a member of Phi Kappa Phi, an Eagle Scout, and a Knight of Columbus.